Models of radiative neutrino mass and lepton-flavour non-universality

John Gargalionis

Submitted in total fulfilment
of the requirements of the degree of

Doctor of Philosophy

School of Physics
The University of Melbourne

September 2020

Abstract

This is a summary of what we did. We did x and y.

Draft compiled on 2020/11/12 at 19:18:00

Publications

Refs. [1–5] below are the journal publications, and preprints authored or co-authored during my PhD candidature. The authors are listed alphabetically in all of the titles.

Journal papers and preprints

[1] R. Foot and J. Gargalionis, *Explaining the 750 GeV diphoton excess with a colored scalar charged under a new confining gauge interaction*, *Phys. Rev. D* **94** (2016), no. 1 011703, [arXiv:1604.06180].

[2] Y. Cai, J. Gargalionis, M. A. Schmidt, and R. R. Volkas, *Reconsidering the One Leptoquark solution: flavor anomalies and neutrino mass*, *JHEP* **10** (2017) 047, [arXiv:1704.05849].

[3] I. Bigaran, J. Gargalionis, and R. R. Volkas, *A near-minimal leptoquark model for reconciling flavour anomalies and generating radiative neutrino masses*, *JHEP* **10** (2019) 106, [arXiv:1906.01870].

[4] J. Gargalionis, I. Popa-Mateiu, and R. R. Volkas, *Radiative neutrino mass model from a mass dimension-11 $\Delta L = 2$ effective operator*, *JHEP* **03** (2020) 150, [arXiv:1912.12386].

[5] J. Gargalionis and R. R. Volkas, *Exploding operators for Majorana neutrino masses and beyond*, [arXiv:2009.13537].

Draft compiled on 2020/11/12 at 19:18:00

Declaration

This is to certify that

1. the thesis comprises only my original work towards the PhD except where indicated clearly,
2. due acknowledgement has been made in the text to all other material used,
3. the thesis is less than 100,000 words in length, exclusive of tables, maps, bibliographies and appendices.

John Gargalionis, September 2020

Draft compiled on 2020/11/12 at 19:18:00

Statement of contribution

I did x and someone else did y.

Draft compiled on 2020/11/12 at 19:18:00

Preface

Particle physics currently finds itself in a strange or exciting place, depending on who you ask. The discovery of a Higgs-like boson at close to 125 GeV has meant both the completion of the Standard Model (SM), and the end of clear signs of new particles at the electroweak scale. Although the Large Hadron Collider (LHC) will continue to collect data well into the next few decades, the mass reach will not increase significantly. The community waits for a new machine, for which there are many candidates and promises, that will continue to push the energy frontier and test theories addressing the many shortcomings of the SM. Time frames for many of these see data taking beginning at the end of my career. If progress is driven by experiment, where do we go from here?

Thankfully, there are already clear signs of new physics in the neutrino sector. The observation of neutrino oscillations, and therefore neutrino masses, is by far the strongest terrestrial evidence demanding an extension of the SM. It is no surprise that a full understanding of the neutrinos has alluded us so far; they are, with the possible exception of the Higgs boson, the most elusive particles currently under laboratory scrutiny. As we move into an era of precision neutrino measurements, now is the right time to take stock of the phenomenologically viable and economic models that explain the pattern of neutrino masses and mixings observed. Armed with the list of possible mechanisms, we can make progress in probing those that are testable and, given that these models are falsified, build circumstantial evidence in favour of those that are not.

Even on the collider front, it is unclear yet that the LHC has left us with the so-called 'nightmare scenario' of a lonely Higgs. Perhaps unexpectedly, the most interesting signs of new physics from CERN have come from the LHC*b* experiment. The now famous 'flavour anomalies' are a collection of theoretically consistent anomalous measurements indicating a departure from the lepton-flavour universality present in the SM. Are these related to the growing evidence for deviations in leptonic anomalous magnetic moments? Might they be clues to a deeper theory of flavour and mass? The Belle II experiment has only just begun taking data, and we wait eagerly for what it has to say on these matters. LHC*b* too will continue to improve its measurements with more collisions; if the anomalies persist, these will be undeniable evidence of physics beyond the SM accessible to the next generation of hadron colliders.

These measurements are tantalising because of their consistency and breadth, but it would not be the first time that physicists have been lead astray, should they disappear

with more statistics. Even so, what is perhaps the central result of my doctoral work will remain unchanged: that deviations from lepton-flavour universality in four-fermion operators may be intimately connected to mass generation in the neutrino sector.

Acknowledgements

I would like to thank x and y.

Draft compiled on 2020/11/12 at 19:18:00

For x and y.

Draft compiled on 2020/11/12 at 19:18:00

Contents

List of Figures

Draft compiled on 2020/11/12 at 19:18:00

List of Tables

Draft compiled on 2020/11/12 at 19:18:00

1 Introduction

The following is a general introduction to the background topics referred to and assumed in subsequent chapters. This includes a review of popular theories of neutrino mass, the current status of neutrino-oscillation parameters, a general introduction to Effective Field Theory (EFT), the experimental situation relevant to the flavour anomalies, and topics peripheral to all of these.

1.1 The Standard Model and neutrinos

Laboratory experiments to date have firmly established the predictive power of the Standard Model (SM) of particle physics, a combined theory of the electroweak and strong interactions described by the gauge group $G_{\text{SM}} = \text{SU}(3)_c \otimes \text{SU}(2)_L \otimes \text{U}(1)_Y$. It is a model whose probes and predictions span at least 33 orders of magnitude[1] with varying degrees of precision, and these are consistent with almost all known experiments. Although it displays a number of arbitrary features, the dynamics of the theory are mostly fixed by the fundamental principles of gauge theory and Lorentz invariance. Most of this arbitrariness resides in the matter sector of the theory, whose properties (masses, coupling constants, quantum numbers, *etc.*) are not predicted, but are instead motivated on phenomenological grounds. We show the fields of the SM and their defining properties in Table 1.1, according to the mathematical conventions of Appendix A.

[1] The interval given is from the distance scales probed at the LHC (roughly 10^{-17} cm) to the size of the solar system (roughly 10^{16} cm).

Field	$\mathrm{SU}(3)_c \otimes \mathrm{SU}(2)_L \otimes \mathrm{U}(1)_Y$	$\mathrm{SU}(2)_+ \otimes \mathrm{SU}(2)_-$
$Q^{\alpha a i}$	$(\mathbf{3}, \mathbf{2}, \frac{1}{6})$	$(\mathbf{2}, \mathbf{1})$
$L^{\alpha i}$	$(\mathbf{1}, \mathbf{2}, -\frac{1}{2})$	$(\mathbf{2}, \mathbf{1})$
$\bar{u}_a^\alpha$	$(\bar{\mathbf{3}}, \mathbf{1}, -\frac{2}{3})$	$(\mathbf{2}, \mathbf{1})$
$\bar{d}_a^\alpha$	$(\bar{\mathbf{3}}, \mathbf{1}, \frac{1}{3})$	$(\mathbf{2}, \mathbf{1})$
$\bar{e}^\alpha$	$(\mathbf{1}, \mathbf{1}, 1)$	$(\mathbf{2}, \mathbf{1})$
$(G_{\alpha\beta})^a{}_b$	$(\mathbf{8}, \mathbf{1}, 0)$	$(\mathbf{3}, \mathbf{1})$
$(W_{\alpha\beta})^i{}_j$	$(\mathbf{1}, \mathbf{3}, 0)$	$(\mathbf{3}, \mathbf{1})$
$B_{\alpha\beta}$	$(\mathbf{1}, \mathbf{1}, 0)$	$(\mathbf{3}, \mathbf{1})$
H^i	$(\mathbf{1}, \mathbf{2}, \frac{1}{2})$	$(\mathbf{1}, \mathbf{1})$

Table 1.1: The SM fields and their transformation properties under the SM gauge group G_{SM} and the Lorentz group written as $\mathrm{SU}(2)_+ \otimes \mathrm{SU}(2)_-$. The final unbolded number in the 3-tuples of the G_{SM} column represents the $\mathrm{U}(1)_Y$ charge of the field, normalised such that $Q = I_3 + Y$. For the fermions a generational index has been suppressed. See Appendix A for details about the mathematical notation used here and throughout this work.

The SM inherits the experimental success of the $\mathrm{SU}(2) \otimes \mathrm{U}(1)$ theory of the weak interactions, first proposed by Glashow [24] in 1961 as a possible underlying structure for Fermi's theory of beta decay. Before the end of the same decade, Weinberg [25] and Salam [26] had constructed the modern theory of leptons based on the spontaneous breaking of $\mathrm{SU}(2)_L \otimes \mathrm{U}(1)_Y$ to the electromagnetic symmetry. Interestingly, it seems that these seminal papers went mostly unnoticed (see Fig. 1.1) until the early 1970s, when 't Hooft proved the renormalisability of spontaneously broken gauge theories [27] as a graduate student working under the supervision of Veltman. By the mid 1970s the framework had been extended to include the quarks [28] and the unbroken chromodynamic group, which was successfully shown to reproduce the Bjorken scaling seen in deep-inelastic-scattering experiments through asymptotic freedom [29].

Despite its successes, the SM cannot be the complete theory of fundamental particles and their interactions. It does not explain phenomena such as the baryon asymmetry present, and the particle spectrum contains no viable candidate for dark matter. The SM cannot explain why the electric dipole moment of the neutron is so small, why there are three generations of matter or, notably in our case, the origin of neutrino oscillations and the implied small but non-zero neutrino masses.

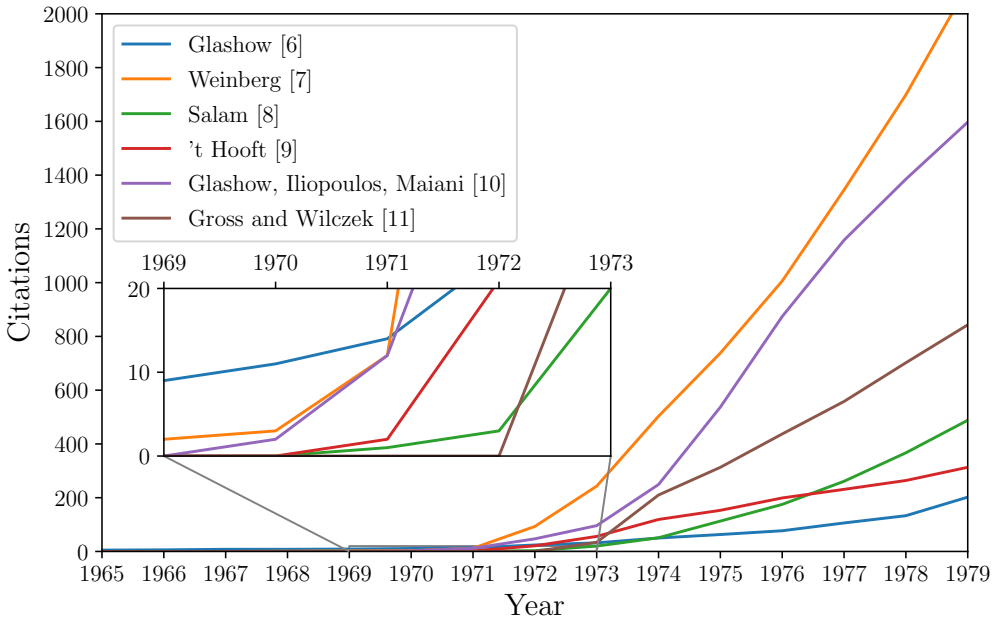

Figure 1.1: The cumulative citation graph for a selection of papers presenting foundational results relevant to the SM. Weinberg's seminal paper 'A model of leptons' (1967) saw an explosion of citations following 't Hooft's work on the renormalisability of gauge theories (1971).

1.2 Massive neutrinos in experiment and theory

The minimal SM predicts massless neutrinos, a prediction that today sits in contradiction to a wealth of empirical evidence. This evidence could in principle have come from many kinds of experiments, but currently only neutrino oscillations provide strong signs that the masses are non-zero. Below we discuss the phenomenon of neutrino oscillations in the context of the outstandingly successful three-flavour mixing paradigm. We then move on to other probes of neutrino masses, which currently only provide limits on the mass scale. On the theory side, we summarise some popular and motivated extensions of the SM that accommodate massive neutrinos, placing particular emphasis on the direction we have followed in the novel work presented in this thesis. This includes an overview of tree- and loop-level models of Majorana neutrino mass.

1.2.1 Neutrino oscillations

The neutrino flavour eigenstates $\check{\nu}_i = (\nu_e, \nu_\mu, \nu_\tau)$ are defined as the states that couple at charged-current interaction vertices with the corresponding charged lepton. These

are the states in which the neutrinos are almost always produced in experiments, and certainly always measured. If neutrinos are massive there is no reason to expect these to coincide with the mass eigenstates $\nu_i = (\nu_1, \nu_2, \nu_3)$. In general, the flavour eigenstates will be an admixture of the propagating fields

$$\check{\nu}_i = U_i{}^j \nu_j \,, \tag{1.1}$$

where the $U_i{}^j$ are elements of the unitary Pontecorvo–Maki–Nakagawa–Sakata (PMNS) neutrino mixing matrix [30, 31]. The PMNS matrix is defined such that it diagonalises the neutrino mass matrix:

$$\mathbf{U}^\dagger \mathbf{m}_\nu \mathbf{U}^* = \mathrm{diag}(m_1, m_2, m_3), \tag{1.2}$$

where the m_i are the neutrino masses. Being a 3×3 unitary matrix, $\mathbf{U}$ is in general parametrised by three mixing angles and six phases. Not all of the phases are physical, since the neutrino and charged-lepton fields can be redefined in such a way that five of the phases are removed in the case of Dirac neutrinos. In the presence of a Majorana mass term, only the charged leptons can be rephased. This leaves three physical phases with the two additional ones termed *Majorana phases*. In general

$$\mathbf{U} = \begin{bmatrix} c_{12}c_{13} & s_{12}c_{13} & s_{13}e^{-i\delta_{\mathrm{CP}}} \\ -s_{12}c_{23} - c_{12}s_{23}s_{13}e^{i\delta_{\mathrm{CP}}} & c_{12}c_{23} - s_{12}s_{23}s_{13}e^{i\delta_{\mathrm{CP}}} & s_{23}c_{13} \\ s_{12}s_{23} - c_{12}c_{23}s_{13}e^{i\delta_{\mathrm{CP}}} & -c_{12}s_{23} - s_{12}c_{23}s_{13}e^{i\delta_{\mathrm{CP}}} & c_{23}c_{13} \end{bmatrix} \mathbf{P} \,, \tag{1.3}$$

where $c_{ij} = \cos\theta_{ij}$, $s_{ij} = \sin\theta_{ij}$ and

$$\mathbf{P} = \begin{cases} \mathrm{diag}(e^{i\alpha_1}, e^{i\alpha_2}, 1) & \text{for Majorana neutrinos} \\ \mathbf{1}_{3\times 3} & \text{for Dirac neutrinos} \end{cases} . \tag{1.4}$$

The phase δ_{CP} is often called the *Dirac phase*, while $\alpha_{1,2}$ are the Majorana phases discussed above.

Neutrino oscillation experiments typically involve the production of neutrino flavour states from charged-current processes, *e.g.* leptonic pion decays. Each mass eigenstate evolves in time independently according to the Schrödinger equation: *i.e.* $|\nu_i(t)\rangle = \exp(-iE_i t)|\nu_i(0)\rangle$, for evolution *in vacuo*. This alters the initial superposition away from being a pure flavour eigenstate:

$$|\check{\nu}_i(t)\rangle = \sum_j U_i^{*j} e^{-iE_j t} |\nu_j\rangle \tag{1.5}$$

$$= \sum_{j,k} U_i^{*j} e^{-iE_j t} U_j{}^k |\check{\nu}_k\rangle \,. \tag{1.6}$$

The probability of measuring a specific flavour through the charged-current interaction then oscillates with time:

$$\mathrm{P}(\check{\nu}_m \to \check{\nu}_n) = |\langle \check{\nu}_n | \check{\nu}_m(t) \rangle|^2 = \left| \sum_i U_m^{*i} U_i{}^n e^{-iE_i t} \right|^2 . \tag{1.7}$$

The expression can be expanded and the kinematic factors simplified from the fact that the neutrinos are ultra-relativistic. We follow the usual convention and take $E_i = \sqrt{\mathbf{p}^2 + m_i^2} \approx |\mathbf{p}| + m_i^2/(2E)$ with $E = |\mathbf{p}|$. This gives

$$\begin{aligned} \mathrm{P}(\check{\nu}_m \to \check{\nu}_n) = \delta_{mn} &- 4 \sum_{i<j} \mathrm{Re}\left(U_m^{\ i} U_m^{*j} U_n^{*i} U_n{}^j \right) \sin^2 \frac{\Delta m_{ij}^2 L}{4E} \\ &+ 2 \sum_{i<j} \mathrm{Im}\left(U_m^{\ i} U_m^{*j} U_n^{*i} U_n{}^j \right) \sin \frac{\Delta m_{ji}^2 L}{2E} , \end{aligned} \tag{1.8}$$

where $\Delta m_{ij}^2 \equiv m_j^2 - m_i^2$ are the squared neutrino mass differences and $L = ct$, sometimes called the baseline, is the approximate distance travelled by the particles. To interpret the results of many experiments, it is often sufficient to consider an effective two-flavour oscillation paradigm. In this case, the neutrino-oscillation probabilities are governed by by a single squared mass difference Δm^2 and a single angle θ. Interestingly, the CP-violating phase is completely absent from the two flavour formula:

$$\mathrm{P}(\check{\nu}_m \to \check{\nu}_n)_{n_f=2} = \sin^2(2\theta) \sin^2 \frac{\Delta m^2 L}{4E} . \tag{1.9}$$

From the expressions in Eqs. (1.8) and (1.9) a number of properties of the vacuum neutrino oscillations become clear.

1. The neutrino oscillation probabilities depend on the neutrino mass differences, and not on the absolute mass scale. For three flavours, there are only two independent squared mass differences. Typically chosen to be Δm_{21}^2 and Δm_{31}^2, although often they are refereed to with the historical names $\Delta m_{\mathrm{sol}}^2$ and $\Delta m_{\mathrm{atm}}^2$, discussed in detail below.

2. From Eq. (1.8) it is clear that the oscillations only occur if the neutrinos are non-degenerate and the neutrino mixing is non-trivial, *i.e.* if $\Delta m_{ij} \neq 0$ and $\mathbf{U} \neq \mathbf{1}$.

3. The PMNS matrix elements only appear in the combination $U_m^{\ i} U_m^{*j}$, to which the Majorana phases contained within the matrix $\mathbf{P}$ do not contribute. This implies that oscillation experiments cannot comment on the Dirac or Majorana nature[2] of the neutrinos. Oscillations can however probe δ_{CP}.

[2] Of course, this is already clear from the fact that neutrino oscillations conserve total lepton number, despite breaking the individual familial lepton-number symmetries $L_{e,\mu,\tau}$.

4. In the effective two-flavour mixing paradigm, both θ and Δm^2 appear in such a way that neither the sign of Δm^2 nor the octant of θ can be uniquely determined.

Thus, neutrino oscillations imply that the neutrino masses of at least two of the mass eigenstates are non-degenerate, and therefore only one neutrino could potentially be massless. The largest squared mass difference can therefore be translated into an lower bound on the mass of the heaviest neutrino, which we present later with modern data.

Historically, the effective two-flavour mixing paradigm has provided a good framework for interpreting early indications of neutrino oscillations. Specifically, the solar and atmospheric neutrino puzzles have approximate descriptions in terms of a two-flavour picture. Oscillations $\nu_e \to \nu_{\text{active}}$, where ν_{active} is a coherent superposition of ν_μ and ν_τ, in both matter and vacuum account for the deficit of electron neutrinos measured from the sun, and $\nu_\mu \to \nu_\tau$ oscillations *in vacuo* explain the shortage of muon neutrinos from cosmic-ray-induced production in the upper atmosphere.

The measurement and resolution of these puzzles is an interesting and exciting chapter in the recent history of physics. Experiments as early as the 1960s had noticed a shortage of electron neutrinos coming from the sun relative to the predictions of solar models [32–35], which themselves were subject to much uncertainty [36]. For detection there were three main approaches: Raymond Davis and collaborators [37] pioneered experiments that measured the solar electron-neutrino flux using Chlorine, the Kamiokande and later Super-Kamiokande collaborations [38, 39] used water Cherenkov detectors, and the experiments GALLEX [40] and SAGE [41] had Gallium as the detecting material. All of these experiments showed a deficit of solar electron neutrinos, although they were sensitive to neutrinos of different energies. The Sudbury Neutrino Observatory gave the final word on the oscillation solution to the solar neutrino puzzle with accurate confirmation of the electron-neutrino deficit, along with a measurement of the *total* neutrino flux which was found to be in agreement with the solar models [42, 43].

Atmospheric neutrinos were known to come about from helicity-suppressed kaon and pion decays to muons and muon neutrinos. A zenith-angle and energy-dependent suppression in the flux of atmospheric muon neutrinos was measured by the Kamiokande and Irvine–Michigan–Brookhaven experiments [44, 45] in the early 1990s, and after the upgrade to Super-Kamiokande the deficit was confirmed to high precision with results presented at the 'Neutrino 1998' conference [46–49].

The pairs of mixing parameters associated with these two classes of measurements are usually dubbed $\theta_{\text{sol}}, \Delta m^2_{\text{sol}}$ and $\theta_{\text{atm}}, \Delta m^2_{\text{atm}}$. Experimental results find $\Delta m^2_{\text{sol}} \ll \Delta m^2_{\text{atm}}$ and that both θ_{sol} and θ_{atm} are large compared to any angles found in the CKM matrix, the quark mixing matrix. Interpreted in terms of three-flavour mixing, common convention identifies Δm^2_{sol} with the squared mass difference between ν_2 and ν_1, which is known to be positive[3] (*i.e.* $\Delta m^2_{21} > 0$). The solar mixing angle θ_{sol} is then

[3] We note that the sign of Δm^2_{21} can be known since oscillations in matter are also relevant for the

associated with θ_{12}. The atmospheric mixing parameters are identified with $|\Delta m^2_{31}|$ or $|\Delta m^2_{32}|$ and θ_{23}. Of course, three-flavour effects alter the simplistic picture presented here and must be included to interpret measurements of θ_{13} and δ_{CP}, see *e.g.* Ref. [50] and references therein for a more detailed discussion. The picture that emerges from these experiments is then

$$\Delta m^2_{\text{sol}} \approx \Delta m^2_{21} \ll |\Delta m^2_{31}| \approx |\Delta m^2_{32}| \approx |\Delta m^2_{\text{atm}}| \,, \tag{1.10}$$

with which both the *normal mass ordering* $m_1 < m_2 < m_3$ and the *inverted mass ordering* $m_3 < m_1 < m_2$ are consistent.

Neutrino oscillation experiments have continued to probe the squared mass differences and mixing parameters with impressively high precision, see *e.g.* Refs. [6, 51]. Reactor neutrino experiments like KamLAND [52] and long-baseline accelerators, *e.g.* T2K [53] and NOνA [54], are sensitive to all of these parameters, although Δm^2_{atm} and θ_{13} are best measured at short-baseline reactors like Double Chooz [55], RENO [56] and Daya Bay [57]. Today the octant of θ_{12} is certainly known, while θ_{13} is constrained to be close to 0.15. The sign of the atmospheric squared mass difference is still unknown, and therefore so is the mass ordering for the neutrinos. The value of the CP-violating Dirac phase δ_{CP} is less clear, although there is a preference for a value somewhere between π and $3\pi/2$. The extent of CP-violation in the neutrino sector can be represented in a rephasing-invariant way with the leptonic Jarlskog invariant

$$J_{CP} = \frac{1}{8} \cos\theta_{13} \sin 2\theta_{12} \sin 2\theta_{13} \sin 2\theta_{23} \sin\delta_{\text{CP}} \,, \tag{1.11}$$

so a value of π would imply no CP-violating effects, while $\delta_{\text{CP}} = 3\pi/2$ would make these maximal. For this work we take the results of the most recent fit to neutrino oscillation data by the NuFit collaboration [6, 7] in the context of the three-flavour paradigm. These results are summarised in Fig. 1.2 separately for the cases of normal and inverted mass ordering. Results including atmospheric neutrino oscillation data from Super-Kamiokande and those not are also distinguished. Two-dimensional projections of the χ^2 fit for the same parameters are shown in Fig. 1.3. These data suggest a leptonic mixing matrix that has a very different form to the CKM matrix, which we call **V**. We represent this qualitatively by using boxes whose side lengths are scaled to the magnitude of the best-fit values of the parameters in the matrices, the textures are

$$\mathbf{U} \sim \begin{pmatrix} \blacksquare & \blacksquare & \cdot \\ \cdot & \blacksquare & \blacksquare \\ \blacksquare & \blacksquare & \blacksquare \end{pmatrix}, \qquad \mathbf{V} \sim \begin{pmatrix} \blacksquare & \cdot & \\ \cdot & \blacksquare & \\ & & \blacksquare \end{pmatrix}. \tag{1.12}$$

For the PMNS matrix we take the best fit values for the normal mass ordering including the Super-Kamiokande results, *i.e.* the numbers in the top-left quadrant of Fig. 1.2. The

solar squared mass difference, which depart from the simple formula of Eq. (1.9).

same numbers also imply an upper bound on the mass of the heaviest neutrino at

$$m_{\text{heaviest}} \leq \sqrt{|\Delta m^2_{\text{atm}}|} \approx 0.05\,\text{eV}\,. \tag{1.13}$$

1.2.2 Other experimental probes

Although neutrino oscillations provide a wealth of evidence for non-zero masses for at least two of the neutrino fields, they do not probe the absolute mass scale. There are however kinematic and cosmological probes which bound the neutrino masses, and some of these are mentioned here.

Beta decay

A study of the kinematics of beta-decay experiments shows that differences in the energy distribution of the emitted electron are expected for different values of the neutrino mass. Currently these experiments only provide upper bounds on the effective neutrino mass [58]

$$m_\beta \equiv \sqrt{\sum_i |U_1{}^i|^2 m_i^2}\,. \tag{1.14}$$

The best results come from tritium experiments which probe $^3\text{H} \to {}^3\text{He} + e + \bar{\nu}_e$. The KATRIN experiment recently presented the most stringent upper bound [59, 60]

$$m_\beta < 1.1\,\text{eV}\,, \tag{1.15}$$

at 90% confidence, with a projected limit of $m_\beta < 0.2\,\text{eV}$ with the full dataset.

Another process with the potential to probe the absolute scale of the neutrino masses, as well as the Majorana phases, is neutrinoless double beta decay ($0\nu\beta\beta$). The process requires the violation of lepton-number by two units, and is therefore intimately tied to the neutrinos' possible Majorana nature. If double-beta decay is seen, the *black box theorem* [61–63] guarantees that the neutrinos pick up a radiative Majorana mass, even if the neutrino masses vanish at tree level. Graphically this is easy to understand: a $0\nu\beta\beta$ operator can always be turned into a neutrino self-energy graph with four loops. The amplitude for the process is proportional to

$$\langle m_\nu \rangle_{\beta\beta} = \sum_i (U_1{}^i)^2 m_i\,, \tag{1.16}$$

which features both the neutrino masses and the Majorana phases. (Of course it may be that the four-loop contribution to the neutrino mass implied by the double-beta-decay operator represents only a small correction to the neutrino masses, which could

NuFIT 5.0 (2020)

		Normal Ordering (best fit)		Inverted Ordering ($\Delta\chi^2 = 2.7$)	
		bfp $\pm 1\sigma$	3σ range	bfp $\pm 1\sigma$	3σ range
without SK atmospheric data	$\sin^2\theta_{12}$	$0.304^{+0.013}_{-0.012}$	$0.269 \to 0.343$	$0.304^{+0.013}_{-0.012}$	$0.269 \to 0.343$
	$\theta_{12}/^\circ$	$33.44^{+0.78}_{-0.75}$	$31.27 \to 35.86$	$33.45^{+0.78}_{-0.75}$	$31.27 \to 35.87$
	$\sin^2\theta_{23}$	$0.570^{+0.018}_{-0.024}$	$0.407 \to 0.618$	$0.575^{+0.017}_{-0.021}$	$0.411 \to 0.621$
	$\theta_{23}/^\circ$	$49.0^{+1.1}_{-1.4}$	$39.6 \to 51.8$	$49.3^{+1.0}_{-1.2}$	$39.9 \to 52.0$
	$\sin^2\theta_{13}$	$0.02221^{+0.00068}_{-0.00062}$	$0.02034 \to 0.02430$	$0.02240^{+0.00062}_{-0.00062}$	$0.02053 \to 0.02436$
	$\theta_{13}/^\circ$	$8.57^{+0.13}_{-0.12}$	$8.20 \to 8.97$	$8.61^{+0.12}_{-0.12}$	$8.24 \to 8.98$
	$\delta_{\rm CP}/^\circ$	195^{+51}_{-25}	$107 \to 403$	286^{+27}_{-32}	$192 \to 360$
	$\frac{\Delta m^2_{21}}{10^{-5}\ {\rm eV}^2}$	$7.42^{+0.21}_{-0.20}$	$6.82 \to 8.04$	$7.42^{+0.21}_{-0.20}$	$6.82 \to 8.04$
	$\frac{\Delta m^2_{3\ell}}{10^{-3}\ {\rm eV}^2}$	$+2.514^{+0.028}_{-0.027}$	$+2.431 \to +2.598$	$-2.497^{+0.028}_{-0.028}$	$-2.583 \to -2.412$
		Normal Ordering (best fit)		Inverted Ordering ($\Delta\chi^2 = 7.1$)	
		bfp $\pm 1\sigma$	3σ range	bfp $\pm 1\sigma$	3σ range
with SK atmospheric data	$\sin^2\theta_{12}$	$0.304^{+0.012}_{-0.012}$	$0.269 \to 0.343$	$0.304^{+0.013}_{-0.012}$	$0.269 \to 0.343$
	$\theta_{12}/^\circ$	$33.44^{+0.77}_{-0.74}$	$31.27 \to 35.86$	$33.45^{+0.78}_{-0.75}$	$31.27 \to 35.87$
	$\sin^2\theta_{23}$	$0.573^{+0.016}_{-0.020}$	$0.415 \to 0.616$	$0.575^{+0.016}_{-0.019}$	$0.419 \to 0.617$
	$\theta_{23}/^\circ$	$49.2^{+0.9}_{-1.2}$	$40.1 \to 51.7$	$49.3^{+0.9}_{-1.1}$	$40.3 \to 51.8$
	$\sin^2\theta_{13}$	$0.02219^{+0.00062}_{-0.00063}$	$0.02032 \to 0.02410$	$0.02238^{+0.00063}_{-0.00062}$	$0.02052 \to 0.02428$
	$\theta_{13}/^\circ$	$8.57^{+0.12}_{-0.12}$	$8.20 \to 8.93$	$8.60^{+0.12}_{-0.12}$	$8.24 \to 8.96$
	$\delta_{\rm CP}/^\circ$	197^{+27}_{-24}	$120 \to 369$	282^{+26}_{-30}	$193 \to 352$
	$\frac{\Delta m^2_{21}}{10^{-5}\ {\rm eV}^2}$	$7.42^{+0.21}_{-0.20}$	$6.82 \to 8.04$	$7.42^{+0.21}_{-0.20}$	$6.82 \to 8.04$
	$\frac{\Delta m^2_{3\ell}}{10^{-3}\ {\rm eV}^2}$	$+2.517^{+0.026}_{-0.028}$	$+2.435 \to +2.598$	$-2.498^{+0.028}_{-0.028}$	$-2.581 \to -2.414$

Figure 1.2: The figure shows a table taken from the latest global fit to neutrino mass and mixing parameters by the NuFit collaboration [6, 7] in the three-flavour picture. The results presented in the upper (lower) panel are obtained by excluding (including) the χ^2 data on atmospheric neutrinos provided by the Super-Kamiokande collaboration (SK). The numbers in the 1st (2nd) column are obtained assuming normal (inverted) neutrino mass ordering. See Ref. [7] for more information.

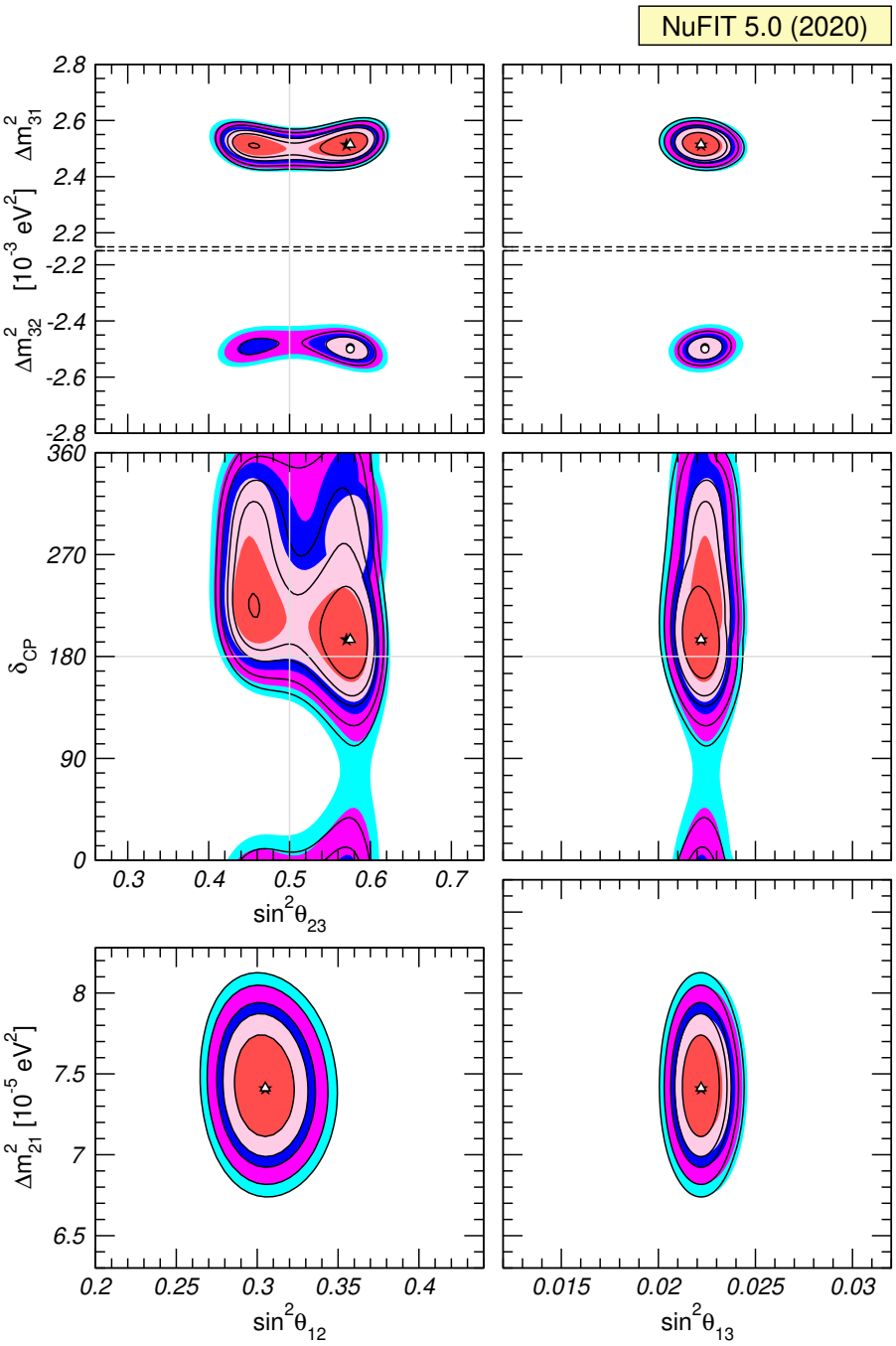

Figure 1.3: The figure shows the two-dimensional allowed regions obtained by the latest fit to the neutrino mass and mixing parameters by the NuFit collaboration [6, 7]. Each plot shows the two-dimensional projection of the allowed region after marginalising with respect to the other parameters. The coloured regions (black contour curves) are obtained by excluding (including) the Super-Kamiomande χ^2 data. The different contours correspond to the two-dimensional allowed regions at 1σ, 90%, 2σ, 99%, 3σ confidence. See Ref. [7] for more information.

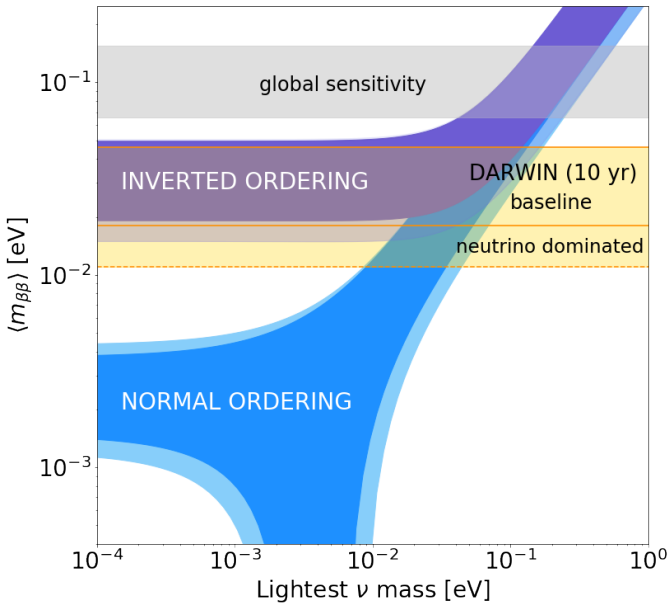

Figure 1.4: The figure shows limits on the effective neutrino mass for different values of m_{lightest} for both normal and inverted mass ordering. The grey region represents the combined sensitivity from a number of leading experiments [8]. The yellow regions are projections for the DARWIN experiment under different background hypotheses. The figure is taken from Ref. [9], and we point the reader there for more information.

arise at lower order.) Current limits on $\langle m_\nu \rangle_{\beta\beta}$ are around 0.2 eV, see *e.g.* Ref. [64] for a recent review of the experimental status and prospects. Constraints on $\langle m_\nu \rangle_{\beta\beta}$ are usually presented against the mass of the lightest neutrino mass eigenstate. The behaviour of $\langle m_\nu \rangle_{\beta\beta}$ is very sensitive to the neutrino mass ordering, in such a way that the inverted scenario implies a minimum allowed value of $\langle m_\nu \rangle_{\beta\beta}$, which will begin to be probed by the next generation of experiments. A combined global limit and the projected sensitivity of the DARWIN experiment [9] are shown in Fig. 1.4, which also illustrates the different behaviour of the inverted and normal neutrino mass orderings in the $\langle m_\nu \rangle_{\beta\beta}$ vs. m_{lightest} plane.

Cosmological limits

The most stringent limits on the sum of the neutrino masses come from cosmology, although they are model-dependent. In the minimal ΛCDM model adjusted for massive

neutrinos, the limit implied by the most recent Planck data release [65] is

$$\sum_i m_i < 0.12\,\text{eV}\,, \tag{1.17}$$

at 95% confidence. This is impressively small, and puts pressure on the inverted-ordering scenario, for which $\sum_i m_i \gtrsim 0.1\,\text{eV}$. Excitingly, future cosmological probes will likely make a measurement of the sum of the neutrino masses.

1.2.3 Models of neutrino masses

In the SM the neutrino fields appear only within the lepton doublet L, and one cannot write down—in analogy to the up-type Yukawa—a renormalisable operator that leads to neutrino masses because of the absence of the right-handed fields. A simple model of neutrino mass then involves introducing right-handed neutrino fields $\bar{\nu} \sim (\mathbf{1}, \mathbf{1}, 0)_{(\mathbf{1},2)}$, extending the Yukawa sector of the SM accordingly to

$$-\mathscr{L}_Y \supset y_e \bar{e} L H^\dagger + y_d \bar{d} Q H^\dagger + y_u \bar{u} Q H + y_\nu \bar{\nu} L H\,, \tag{1.18}$$

in a simplified one-flavour picture. This implies Dirac neutrinos with a mass $m_\nu \approx y_\nu v$, and makes mass generation symmetric between the quarks and leptons.

There are a number of problems with this simplistic scenario. First, it is perhaps uncomfortable to suppose that the neutrinos are many orders of magnitude lighter than the charged fermions only because y_ν is a very small number. Indeed, the posited large hierarchy between y_ν and y_u seems to spoil any aesthetic arguments for quark–lepton symmetry in favour of this hypothesis. Although the Yukawa couplings for the other SM fermions span six orders of magnitude, couplings within any one generation are all of similar order. We illustrate this in Fig. 1.5, where the fermion masses are plotted by generation. Whereas one could consider that some underlying theory of flavour may explain, for example, the disparity in scale between the masses of the electron and the top quark, the large mass difference between the electron and the lightest neutrino, although technically natural, seems to cry out for its own explanation.

A second point of criticism with the simple scenario presented above is that it ignores the Majorana mass term for $\bar{\nu}$

$$\mathscr{L} \supset -\tfrac{1}{2}\mu \bar{\nu}\bar{\nu} + \text{h.c.} \tag{1.19}$$

In order to maintain the Dirac neutrino mass with the relation $m_\nu \approx y_\nu v$, the Majorana mass must be forbidden or else chosen to be negligibly small, assumptions adding additional layers of contrivance to the theory. A sensible choice for the scale μ is some high scale Λ associated with the breaking of $\mathrm{U}(1)_{B-L}$. Taking $\mu \gg y_\nu v$, the neutrino-mass matrix takes on the form

$$\mathbf{m}_\nu = \begin{pmatrix} 0 & y_\nu v \\ y_\nu v & \mu \end{pmatrix}\,, \tag{1.20}$$

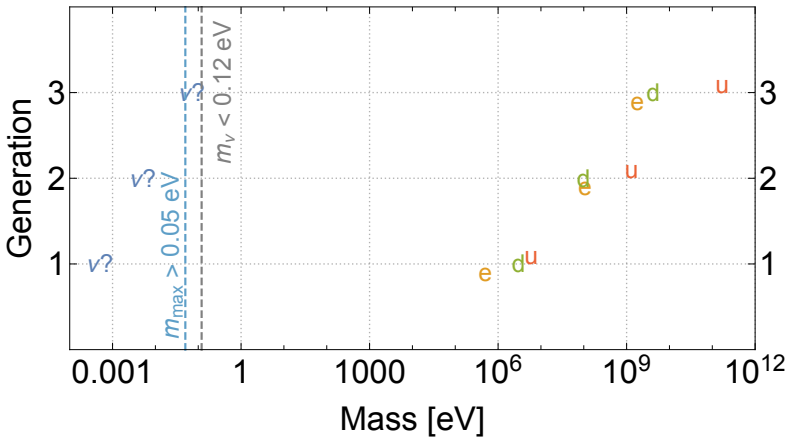

Figure 1.5: The masses of the SM fermions grouped by generation. While the SM Yukawa couplings span a wide range of values, within any specific generation they are all of similar order. The tiny masses of the neutrinos seem to suggest an alternate mass-generation mechanism.

with eigenvalues

$$m_l \approx \frac{y_\nu^2 v^2}{\mu}, \quad m_h \approx \mu \,. \tag{1.21}$$

The assumption $\mu \gg y_\nu v$ implies that $m_l \ll y_\nu v$, and the neutrino is successfully arranged to be much lighter than $y_\nu v$, which can now be taken to be on the order of the charged fermion masses. The theory also leaves us with a neutrino whose mass must be significantly larger than the electroweak scale: $m_h \gtrsim 10^{14}$ GeV, assuming $m_l = 0.05$ eV and $y_\nu = 1$. After transforming into the mass-diagonal basis, the physical fields ν_l and ν_h correspond to Majorana particles. Thus, in the most motivated region of parameter space, the phenomenology of the light neutrinos in even the SM + $\bar{\nu}$ scenario is Majorana. This toy scenario illustrates the mechanism commonly called the *seesaw mechanism*: making the neutrinos very light at the expense of making other fields very heavy. This is discussed more broadly below.

Tree-level models of neutrino mass

The toy seesaw scenario discussed above can be understood more generally by studying the effective theory valid below the scale μ, which does not contain the field $\bar{\nu}$. The leading-order lepton-number-violating (LNV) effects appear at dimension five in the operator

$$\mathscr{L} \supset \frac{\kappa}{\Lambda}(L^i L^j) H^k H^l \cdot \epsilon_{ik}\epsilon_{jl} \,, \tag{1.22}$$

with κ a dimensionless coefficient. This operator is commonly called the *Weinberg operator*. In the broken phase it gives rise to a Majorana mass for the neutrinos consistent with the seesaw formula:

$$\mathscr{L} \supset \frac{v^2\kappa}{\Lambda}\nu\nu\,. \tag{1.23}$$

The SM + $\bar{\nu}$ scenario is not the only simplified model that generates the Weinberg operator at tree-level. A simple diagram-topology analysis suggests there are another two seesaw mechanisms in the UV: a model with a scalar isotriplet field $\Xi_1 \sim (\mathbf{1},\mathbf{3},1)_S$, called the type-II mechanism, and another with an isotriplet Majorana fermion $\Sigma \sim (\mathbf{1},\mathbf{3},0)_F$, called type-III. Along with the type-I heavy $\bar{\nu}$ model, these are collectively referred to as the canonical seesaw mechanisms [66–76] and have been studied at length in the literature. They are simple models in that they introduce only very few exotic degrees of freedom and free parameters. However, the high seesaw scale makes these models practically untestable at current and future collider experiments.

Models of Majorana neutrino mass can be made more testable if, instead of the suppression of the neutrino masses coming from a large Λ in Eq. (1.23), the coefficient κ were somehow arranged to be small. Although there are a number of mechanisms to achieve this, we concentrate below on radiative models of Majorana neutrino mass, in which κ is made small through loop and coupling suppression.

Radiative models and their classification

It may be the case that the field content of whatever high-energy theory describes the neutrino masses is such that no neutrino self-energy diagram can be drawn at the tree level. Indeed, this will be the case if there is lepton-number violation by two units ($\Delta L = 2$) from interactions other than those present in the canonical seesaw models. Such models are called radiative, since the neutrino masses arise through loop graphs. The historically important Zee [77] and Zee–Babu [78, 79] models have come to be archetypal radiative scenarios in which the neutrinos gain masses through $\Delta L = 2$ the interactions of exotic scalars at one and two loops respectively. In the Zee model, an additional Higgs doublet $\varphi \sim (\mathbf{1},\mathbf{2},\frac{1}{2})$ and a charged scalar $\mathcal{S}_1 \sim (\mathbf{1},\mathbf{1},1)$ are introduced, while the Zee–Babu model contains $\mathcal{S}_1$ and the doubly-charged scalar $\mathcal{S}_2 \sim (\mathbf{1},\mathbf{1},2)$. The neutrino self-energy diagrams for these models are shown in Fig. 1.6 as examples. The corresponding neutrino-mass matrices are

$$[\mathbf{m}_\nu^{\text{Zee}}]_{rs} = \frac{\mu v^2}{16\pi^2}\sum_t x_{[rt]} I_t [\mathbf{m}_e]_t y_{ts} + (r \leftrightarrow s)\,, \tag{1.24}$$

$$[\mathbf{m}_\nu^{\text{Zee–Babu}}]_{rs} = \frac{\mu' v^2}{(16\pi^2)^2}\sum_{t,u} x_{[rt]}[\mathbf{m}_e]_t z_{\{tu\}}[\mathbf{m}_e]_u x_{[us]} I'_{tu} + (r \leftrightarrow s)\,, \tag{1.25}$$

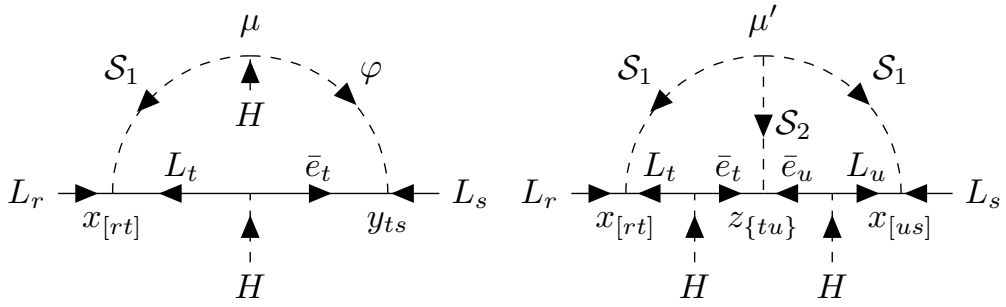

Figure 1.6: The neutrino self-energy diagrams relevant to the Zee (left) and Zee–Babu (right) models.

written in terms of the couplings $x, y, z \in \mathbb{C}$ as shown in Fig. 1.6, and the associated loop functions I and I'. One can see that in these models, the coefficient of the Weinberg operator κ is naturally suppressed with respect to the seesaw formula by SM-fermion masses (charged-lepton masses in this case), exotic couplings, and loop factors.

Such models are economic, since they do not require the imposition of *ad hoc* symmetries, and in many cases make a connection to other unsolved problems of the SM such as the nature of dark matter or the matter–antimatter asymmetry of the Universe. They are also elegant, since the smallness of the neutrino masses emerges as a natural consequence, rather than through the imposed requirement of exceedingly small coupling constants. Radiative models are easier to probe experimentally since the additional loop suppression and products of couplings bring down the allowed scale of the new physics, in some cases to LHC-accessible energy ranges [80]. The Zee–Babu model, for example, is non-trivially constrained by same-sign dilepton searches performed by ATLAS [81–83] and CMS [84–86]. Additionally, the predicted dependence of the neutrino-mass matrix on SM parameters, as is clear from Eqs. (1.24) and (1.25), can make these models very predictive as far as neutrino phenomenology is concerned. For example, the minimal version of the Zee model has the charged-lepton masses arising from couplings to φ, allowing for a simplification of the expression Eq. (1.24) such that the leptonic flavour index t is identified with s. The antisymmetry in the leptonic flavour indices implied by $x_{[rs]}$ must be accounted for by an antisymmetry in the loop integral such that $I \sim I_r - I_s$. The flavour structure then becomes [87]

$$[\mathbf{m}_\nu^{\text{Min. Zee}}]_{rs} \propto x_{[rs]}([\mathbf{m}_e]_r^2 - [\mathbf{m}_e]_s^2)\,, \tag{1.26}$$

which makes clear predictions relevant to neutrino oscillations that in this case rule out the model. For recent reviews of radiative models see Refs. [88, 89].

The Zee and Zee–Babu scenarios are only two of a very large number of radiative models, none of which are *a priori* more likely to be true than any other. In the context of such a large theory-space, it is useful to have an organising principle to aid in the

study and classification of these models, and beginning with $\Delta L = 2$ effective operators has been shown to be an effective strategy.

One approach to this model taxonomy involves studying loop-level completions of the Weinberg operator, and its dimension-$(5 + 2n)$ generalisations

$$\mathcal{O}_1^{\prime\cdots\prime} = (LL)HH(H^\dagger H)^n \,.$$

Here, models can be systematically written down by studying the various topologies able to be accommodated by the operator with increasing number of loops. This is done in such a way that models implying lower-order contributions to the neutrino mass can be discarded [90]. Such an approach has been applied to the Weinberg operator up to three loops [91–93] and to its dimension-seven generalisation at one loop [94]. An alternative and complementary method begins by considering all of the gauge-invariant $\Delta L = 2$ operators in the SM effective field theory (SMEFT), first listed in this context by Babu and Leung [95] and extended by de Gouvêa and Jenkins [80]. Supposing that the tree-level coefficient of one of these is non-zero at the high scale, neutrino masses will be generated from loop graphs contributing to the mixing of this operator and the Weinberg-like operators $\mathcal{O}_1^{\prime\cdots\prime}$. The process of expanding the operator into a series of UV-complete, renormalisable models that generate the parent operator at tree-level is called *opening up* or *exploding* the operator. The remaining external fields must be looped-off, with additional loops of SM gauge bosons or Higgs fields added as necessary in order to obtain a neutrino self-energy diagram. A model-building formula along these lines has been formulated in Ref. [96], and it has been used to write down all of the minimal, tree-level UV-completions of $\Delta L = 2$ operators at dimension seven [97] corresponding to tree-level and radiative neutrino-mass models. The tree-level completions of the Weinberg-like operators have been written down up to dimension eleven [97–99]. The $\Delta L = 2$ operators in the SM EFT are discussed in more detail in Sec. 1.3.2.

We note that an economic classification scheme, separate from an EFT framework, was presented in Ref. [100] based on the number of exotic degrees of freedom by which the SM is extended. There, the method is applied to the case of radiative models with two exotics[4], and has also been used to study minimal neutrino-mass models compatible with SU(5) unification [101].

1.3 Effective field theory

In the following we introduce EFT in general, and then specialise to those built out of SM fields: the Standard Model EFT (SMEFT) and the Weak Effective Theory (WET). We place particular emphasis on the operators appearing at dimension-six, since these play an important role in phenomenological analyses. Much of the focus of this work is the

[4]Including models with one scalar and one Dirac fermion.

operators of odd mass-dimension up to dimension eleven, which organise the building of neutrino-mass models in the tradition of Refs. [80, 95–97]. Many of the principles introduced here for the dimension-six SMEFT will be directly relevant there. We begin with prefatory comments on the process of tree-level matching, then move on to discuss the SMEFT and some of the intricacies associated with redundancies among operators.

1.3.1 Tree-level matching

Suppose one has a theory with light particle states described by fields π_i and heavy states described by Π_i with a Lagrangian of the form

$$\begin{aligned} \mathscr{L}_{\mathrm{UV}}[\pi,\Pi] &= \mathscr{L}_{\mathrm{kin}}[\pi,\Pi] + \mathscr{L}_{\mathrm{int}}[\pi,\Pi], \text{ with} \\ \mathscr{L}_{\mathrm{int}}[\pi,\Pi] &= \mathscr{L}^{l}[\pi] + \mathscr{L}^{h}[\Pi] + \mathscr{L}^{lh}[\pi,\Pi]. \end{aligned} \tag{1.27}$$

Below the threshold for Π_i production, an effective description of the theory can be used that involves interactions only between the light fields. This effective theory is described by a Lagrangian $\mathscr{L}_{\mathrm{eff}}[\pi]$ involving interactions between the π_i that correspond to diagrams in the full theory containing only heavy internal propagators and light external states. At the classical level, $\mathscr{L}_{\mathrm{eff}}$ can be written down by integrating out the Π_i. Perturbatively this corresponds to expanding the heavy propagators Δ in powers of momenta on the heavy mass scale[5] Λ, such that

$$\Delta = \begin{cases} -\dfrac{1}{\Lambda^2}\left(1+\dfrac{p^2}{\Lambda^2}+\cdots\right) & \text{for} \quad \text{- - - - - - - - - - -} \\[2ex] -\dfrac{\delta_{\alpha}^{\ \beta}}{\Lambda}\left(1+\dfrac{p^2}{\Lambda^2}+\cdots\right) & \text{for} \quad \beta \longleftarrow\!\!\!\longrightarrow \alpha \\[2ex] -\dfrac{ip\cdot\bar{\sigma}^{\dot{\alpha}\beta}}{\Lambda^2}\left(1+\dfrac{p^2}{\Lambda^2}+\cdots\right) & \text{for} \quad \beta \longleftarrow \dot{\alpha} \end{cases} . \tag{1.28}$$

In this notation, the arrow-preserving propagator corresponds to the part of the regular four-component fermion propagator proportional to momentum, while the arrow-violating one is the part proportional to the fermion mass. Expressions for the fermion propagators with reversed arrows follow from $\bar{\sigma}^{\mu} \to \sigma^{\mu}$ and interchanging dotted and undotted indices (see Ref. [102] Sec. 4.2 for the Lorentz structure).

Equivalently, the integration can be performed using the classical EOM of the Π_i. For some heavy field Π, the linearised solution to its classical EOM can be used to remove it from the Lagrangian completely. This procedure is mildly different for scalars

[5]We note that some UV scenarios may have more than one characteristic scale. In this case Λ can be understood as an effective scale which may not necessarily correspond to the mass of a specific particle.

and fermions, and we briefly outline these separately below. In both cases, we begin with a Lagrangian $\mathscr{L}_{\rm UV}$ for which we imagine that kinetic and mass mixing terms between heavy and light fields have been removed.

There are tree-level contributions to $\mathscr{L}^{\rm eff}$ as long as there are interaction terms linear in Π. For scalar Π, the UV Lagrangian contains the terms

$$\mathscr{L}_{\rm UV}[\Pi,\pi] \supset \Pi^\dagger(-D^2 - m_\Pi^2)\Pi + \left(\Pi\frac{\partial\mathscr{L}^{lh}}{\partial\Pi} + \text{h.c.}\right), \tag{1.29}$$

where $\partial\mathscr{L}^{lh}/\partial\Pi$ is a function only of light fields, and we are neglecting interactions of the form $\Pi^\dagger\Pi f(\pi)$ for the sake of conciseness. The EOM are

$$(-D^2 - m_\Pi^2)\Pi = -\frac{\partial\mathscr{L}^{lh}}{\partial\Pi^\dagger} + \mathcal{O}(\Pi^2)\,, \tag{1.30}$$

which can be solved for $\Pi^{\rm cl}$, the classical field configuration, by inverting the differential operator on the LHS of Eq. (1.30) and expanding in D^2/m_Π^2:

$$\Pi^{\rm cl} = -\frac{1}{m_\Pi^2}\left(1 - \frac{D^2}{m_\Pi^2} + \cdots\right)\frac{\partial\mathscr{L}^{lh}}{\partial\Pi^\dagger}\,. \tag{1.31}$$

This solution can be substituted back into Eq. (1.29) to give interactions between light fields in the tree-level effective Lagrangian:

$$\mathscr{L}_{\rm eff}[\pi] \supset -\frac{\partial\mathscr{L}^{lh}}{\partial\Pi}\frac{1}{m_\Pi^2}\left(1 - \frac{D^2}{m_\Pi^2} + \cdots\right)\frac{\partial\mathscr{L}^{lh}}{\partial\Pi^\dagger}\,. \tag{1.32}$$

Many concrete examples of this procedure can be found in the literature, see *e.g.* Ref. [103]. The expansion in D^2/m_Π^2 corresponds to the expansion in p^2/Λ^2 in the first case of Eq. (1.28), showing the expansion of the scalar propagator.

Next we sketch out the procedure for a Dirac fermion $\Pi + \bar\Pi^\dagger$, where Π and $\bar\Pi$ are separate two-component spin-$\frac{1}{2}$ fields transforming oppositely under $G_{\rm SM}$. In this case, the UV theory is described by a Lagrangian like

$$\mathscr{L}_{\rm UV}[\Pi,\pi] \supset i\Pi^\dagger\bar\sigma^\mu D_\mu\Pi + i\bar\Pi^\dagger\bar\sigma^\mu D_\mu\bar\Pi + \left(\Pi\frac{\partial\mathscr{L}^{lh}}{\partial\Pi} + \bar\Pi\frac{\partial\mathscr{L}^{lh}}{\partial\bar\Pi} - m_\Pi\bar\Pi\Pi + \text{h.c.}\right) \tag{1.33}$$

Varying the action with respect to the heavy fields gives two coupled EOM:

$$i\bar\sigma^\mu D_\mu\Pi - m\bar\Pi^\dagger + \frac{\partial\mathscr{L}^{lh}}{\partial\Pi^\dagger} = 0\,, \tag{1.34}$$

$$i\bar\sigma^\mu D_\mu\bar\Pi - m\Pi^\dagger + \frac{\partial\mathscr{L}^{lh}}{\partial\bar\Pi^\dagger} = 0\,. \tag{1.35}$$

Substituting Eq. (1.34) into Eq. (1.35) gives a second-order partial differential equation in Π, analogous to Eq. (1.30). Inverting the differential operator in a similar way gives

$$\Pi_\beta^{\rm cl} = \frac{1}{m_\Pi^2}\left(\epsilon_{\alpha\beta} + \frac{\frac{1}{2}X_{\alpha\beta} - D^2\epsilon_{\alpha\beta}}{m_\Pi^2} + \cdots\right)\left(iD^{\alpha\dot\alpha}\frac{\partial\mathscr{L}^{lh}}{\partial\Pi^\dagger_{\dot\beta}}\epsilon_{\dot\alpha\dot\beta} + m_\Pi\frac{\partial\mathscr{L}^{lh}}{\partial\bar\Pi_\alpha}\right), \tag{1.36}$$

where the field-strength tensor comes about from a structure like

$$[\sigma^\mu\bar\sigma^\nu]_\alpha^{\ \beta} D_\mu D_\nu = \eta^{\mu\nu} D_\mu D_\nu \delta_\alpha^{\ \beta} - 2i[\sigma^{\mu\nu}]_\alpha^{\ \beta} D_\mu D_\nu \tag{1.37}$$

$$= D^2\delta_\alpha^{\ \beta} - \tfrac{1}{2}X_\alpha^{\ \beta}\,. \tag{1.38}$$

Here, and later in this section, the replacement $\bar\Pi \to \Pi$ should be understood for Majorana Π. Each contribution corresponds to a particular kind of propagator in the perturbative picture. The first term in the last parenthesis of Eq. (1.36) results from the fermion propagator proportional to momentum: the arrow-preserving fermion propagator shown as the last case of Eq. (1.28). The second term in the same parentheses stems from the fermion propagator proportional to the mass, corresponding to the arrow-violating propagator shown in the middle case of Eq. (1.28). Replacing Π in Eq. (1.33) gives the tree-level effective Lagrangian with the heavy fermion integrated out:

$$\begin{aligned}\mathscr{L}_{\rm eff}[\pi] \supset\ & \frac{\partial\mathscr{L}^{lh}}{\partial\Pi_\beta}\frac{1}{m_\Pi^2}\left(\epsilon_{\alpha\beta} + \frac{\frac{1}{2}X_{\alpha\beta} - D^2\epsilon_{\alpha\beta}}{m_\Pi^2} + \cdots\right) iD^{\alpha\dot\alpha}\frac{\partial\mathscr{L}^{lh}}{\partial\Pi^\dagger_{\dot\beta}}\epsilon_{\dot\alpha\dot\beta} \\ & + \frac{\partial\mathscr{L}^{lh}}{\partial\Pi_\beta}\frac{1}{m_\Pi^2}\left(\epsilon_{\alpha\beta} + \frac{\frac{1}{2}X_{\alpha\beta} - D^2\epsilon_{\alpha\beta}}{m_\Pi^2} + \cdots\right)\frac{\partial\mathscr{L}^{lh}}{\partial\bar\Pi_\alpha}\,.\end{aligned} \tag{1.39}$$

As shown in Eqs. (1.32) and (1.39), expanding in powers of derivatives on heavy masses leads to a tower of local operators of increasing mass dimension d_i organised as a power series in the inverse heavy scale:

$$\mathscr{L}_{\rm eff}[\pi] = \mathscr{L}^l[\pi] + \sum_i \frac{C_i}{\Lambda^{d_i-4}}\mathcal{O}_i[\pi]. \tag{1.40}$$

The C_i are dimensionless coefficients which are in general calculable if one knows the high-energy theory.

1.3.2 Effective field theories of the SM

Below we discuss EFTs constructed from SM fields and invariant under SM symmetries. The main theory of study is the SMEFT: the gauge- and Lorentz-invariant EFT built

from the fields listed in Table 1.1. We also mention the WET, also known as the LEFT (Low-energy Effective Field Theory), for which invariance under $\mathrm{SU}(2)_+ \otimes \mathrm{SU}(2)_- \otimes \mathrm{SU}(3)_c \otimes \mathrm{U}(1)_{\mathrm{EM}}$ is required.

The SMEFT at dimension six

Given the broad experimental success of the SM, it is perhaps a sensible assumption that there should be a sizeable mass gap between the electroweak scale and the mass-scale characterising any new physics. In this context, the SMEFT can be a powerful tool for constraining how this new physics might look in a model-independent way. Indeed, the SMEFT operators at dimension six are already coming to play an increasingly important role in particle phenomenology, and they have become the *de facto* framework for interpreting low-energy constraints on theoretical models and experimental deviations from SM predictions. For an extensive review, we point the reader to Ref. [104].

It has not been easy to write down a complete basis of operators in the SMEFT [22, 23], although this is now a mostly solved problem [105–109]. The lowest-dimensional operator appearing in the EFT is also the only dimension-five operator:

$$\mathscr{L}^{(5)} = [C_5]_{\{rs\}}(L_r^i L_s^j)H^k H^l \epsilon_{ik}\epsilon_{jl} + \text{h.c.}\,, \tag{1.41}$$

already discussed briefly in Sec. 1.2.3. The matrix of operator coefficients is necessarily symmetric by Fermi–Dirac statistics. The operator violates lepton-number by two units, and usually gives the dominant contribution to the neutrino mass in Majorana models. Ref. [110] shows that operators in the SMEFT of mass-dimension d satisfy

$$\frac{1}{2}(\Delta B - \Delta L) = d \mod 2\,, \tag{1.42}$$

and thus odd mass-dimension operators must violate $B-L$ by two units, while operators of even mass-dimension cannot violate $B-L$. So, aside from lepton-number-violating effects, the leading-order deviations from the SM appear at dimension six, where there are many more operators.

The dimension-six operators come in eight general classes: X^3, H^6, H^4D^2, X^2H^2, ψ^2H^3, ψ^2XH, ψ^2H^2D and ψ^4. (Here, X represents a general field-strength tensor, D is a covariant derivative and ψ is a fermion field.) The ψ^4-type operators illustrate some of the difficulties encountered when writing down a complete basis of operators, since they can be simplified by Fierz and Schouten identities relating to the spinor, isospin and colour structure. The most common basis found in the literature is the Warsaw basis [22, 23], which tends to prefer vector currents for fermions. Thus, for example, the four-fermion operators with field content L^4 written in this way are

$$[\mathcal{O}_{ll}]_{rstu} = (L_r^\dagger \bar{\sigma}_\mu L_s)(L_t^\dagger \bar{\sigma}_\mu L_u)\,, \tag{1.43}$$

$$[\mathcal{O}_{ll}^{(3)}]_{rstu} = (L_r^\dagger \bar{\sigma}_\mu \tau^I L_s)(L_t^\dagger \bar{\sigma}_\mu \tau^I L_u)\,. \tag{1.44}$$

Here $\mathcal{O}_{ll}^{(3)}$ contracts the $\bar{\mathbf{2}} \otimes \mathbf{2}$ of the $L^\dagger$ and L into the triplet representation. Naively there seem to be two operators, however $\mathcal{O}_{ll}^{(3)}$ can be rewritten using the SU(2) Fierz identity

$$[\tau^I]^i{}_j[\tau^I]^k_l = 2\delta^i{}_m\delta^k_j - \delta^i{}_j\delta^k_l \tag{1.45}$$

and the related identity acting on the spinor structure

$$(\psi_1^\dagger \bar{\sigma}^\mu \psi_2)(\psi_3^\dagger \bar{\sigma}^\mu \psi_4) = (\psi_1^\dagger \bar{\sigma}^\mu \psi_4)(\psi_3^\dagger \bar{\sigma}^\mu \psi_2) \tag{1.46}$$

such that

$$[\mathcal{O}_{ll}^{(3)}]_{rstu} = 2[\mathcal{O}_{ll}]_{ruts} - [\mathcal{O}_{ll}]_{rstu} \,. \tag{1.47}$$

Thus, the operators $[\mathcal{O}_{ll}^{(3)}]_{rstu}$ can be expressed as linear combinations of the $[\mathcal{O}_{ll}]_{rstu}$, and both operators should not be included in a genuine basis. The situation is slightly more complicated for the four-quark operators, since there is an additional space of indices to handle. In the case of operators with field content Q^4, there seem to naively be four invariants, which can be written as vector currents

$$(Q^\dagger \bar{\sigma}_\mu \Gamma Q)(Q^\dagger \bar{\sigma}_\mu \Gamma Q) \,, \tag{1.48}$$

where the possible structures $\Gamma \otimes \Gamma$ can be expressed schematically as

$$1 \otimes 1, \quad \tau^I \otimes \tau^I, \quad \lambda^A \otimes \lambda^A, \quad \tau^I\lambda^A \otimes \tau^I\lambda^A \,. \tag{1.49}$$

The $\mathrm{SU}(2)_L$ and $\mathrm{SU}(3)_c$ index contraction can either be internal to the fermion current, or it may connect fermions in adjacent currents. For example, the $\mathrm{SU}(2)_L$ contraction is internal for the structures $1 \otimes 1$ and $\lambda^A \otimes \lambda^A$, but external for $\tau^I \otimes \tau^I$ and $\tau^I\lambda^A \otimes \tau^I\lambda^A$. The spinor identity Eq. (1.46) exchanges the Q fields, so it interchanges the isospin and colour indices so that

$$\text{both internal} \leftrightarrow \text{both external}, \quad \mathrm{SU}(2)_L \text{ external} \leftrightarrow \mathrm{SU}(3)_c \text{ external} \,. \tag{1.50}$$

This means only two of the four invariants are independent. These are chosen to be $1 \otimes 1$ and $\tau^I \otimes \tau^I$ in the Warsaw basis.

The operators in the Warsaw basis are listed in Tables 1.2 and 1.3. This is the form in which we use the operators throughout the rest of this work. Each operator is given in four-component spinor notation, as is usual in the literature. We refer the reader to Appendix **??** for the correspondence to the two-component notation we use elsewhere, along with other relevant mathematical notation used in the tables. Our conventions are chosen to comply with those of Ref. [111].

	Operator	Label	Operator	Label
$(\bar{L}L)(\bar{L}L)$	$(\bar{L}\gamma_\mu L)(\bar{L}\gamma^\mu L)$	$\mathcal{O}_{ll}$		
	$(\bar{Q}\gamma_\mu Q)(\bar{Q}\gamma^\mu Q)$	$\mathcal{O}_{qq}^{(1)}$	$(\bar{Q}\gamma_\mu \tau^I Q)(\bar{Q}\gamma^\mu \sigma^I Q)$	$\mathcal{O}_{qq}^{(3)}$
	$(\bar{L}\gamma_\mu L)(\bar{Q}\gamma^\mu Q)$	$\mathcal{O}_{lq}^{(1)}$	$(\bar{L}\gamma_\mu \sigma^I L)(\bar{Q}\gamma^\mu \sigma^I Q)$	$\mathcal{O}_{lq}^{(3)}$
$(\bar{R}R)(\bar{R}R)$	$(\bar{e}_R\gamma_\mu e_R)(\bar{e}_R\gamma^\mu e_R)$	$\mathcal{O}_{ee}$		
	$(\bar{u}_R\gamma_\mu u_R)(\bar{u}_R\gamma^\mu u_R)$	$\mathcal{O}_{uu}$	$(\bar{d}_R\gamma_\mu d_R)(\bar{d}_R\gamma^\mu d_R)$	$\mathcal{O}_{dd}$
	$(\bar{u}_R\gamma_\mu u_R)(\bar{d}_R\gamma^\mu d_R)$	$\mathcal{O}_{ud}^{(1)}$	$(\bar{u}_R\gamma_\mu \lambda^A u_R)(\bar{d}_R\gamma^\mu \lambda^A d_R)$	$\mathcal{O}_{ud}^{(8)}$
	$(\bar{e}_R\gamma_\mu e_R)(\bar{u}_R\gamma^\mu u_R)$	$\mathcal{O}_{eu}$	$(\bar{e}_R\gamma_\mu e_R)(\bar{d}_R\gamma^\mu d_R)$	$\mathcal{O}_{ed}$
$(\bar{L}L)(\bar{R}R)$	$(\bar{L}\gamma_\mu L)(\bar{e}_R\gamma^\mu e_R)$	$\mathcal{O}_{le}$	$(\bar{Q}\gamma_\mu Q)(\bar{e}_R\gamma^\mu e_R)$	$\mathcal{O}_{qe}$
	$(\bar{L}\gamma_\mu L)(\bar{u}_R\gamma^\mu u_R)$	$\mathcal{O}_{lu}$	$(\bar{L}\gamma_\mu L)(\bar{d}_R\gamma^\mu d_R)$	$\mathcal{O}_{ld}$
	$(\bar{Q}\gamma_\mu Q)(\bar{u}_R\gamma^\mu u_R)$	$\mathcal{O}_{qu}^{(1)}$	$(\bar{Q}\gamma_\mu \lambda^A Q_L)(\bar{u}_R\gamma^\mu \lambda^A u_R)$	$\mathcal{O}_{qu}^{(8)}$
	$(\bar{Q}\gamma_\mu Q)(\bar{d}_R\gamma^\mu d_R)$	$\mathcal{O}_{qd}^{(1)}$	$(\bar{Q}\gamma_\mu \lambda^A Q_L)(\bar{d}_R\gamma^\mu \lambda^A d_R)$	$\mathcal{O}_{qd}^{(8)}$
$(\bar{L}R)(\bar{R}L)$	$(\bar{L}e_R)(\bar{d}_R Q)$	$\mathcal{O}_{ledq}$		
$(\bar{L}R)(\bar{L}R)$	$(\bar{Q}_i u_R)(\bar{Q}_j d_R)\epsilon^{ij}$	$\mathcal{O}_{quqd}^{(1)}$	$(\bar{Q}_i \lambda^A u_R)(\bar{Q}_j \lambda^A d_R)\epsilon^{ij}$	$\mathcal{O}_{quqd}^{(8)}$
	$(\bar{L}_i e_R)(\bar{Q}_j u_R)\epsilon^{ij}$	$\mathcal{O}_{lequ}^{(1)}$	$(\bar{L}_i \sigma_{\mu\nu} e_R)(\bar{Q}_j \sigma^{\mu\nu} u_R)\epsilon^{ij}$	$\mathcal{O}_{lequ}^{(3)}$
$\Delta B = 1$			$(d_R^a u_R^b)(Q^{ci} L^j)\epsilon_{abc}\epsilon_{ij}$	$\mathcal{O}_{duq}$
			$(Q^{ai} Q^{bj})(u_R^c e_R)\epsilon_{abc}\epsilon_{ij}$	$\mathcal{O}_{qqu}$
			$(d_R^a u_R^b)(u_R^c e_R)\epsilon_{abc}$	$\mathcal{O}_{duu}$
			$(Q^{ai} Q^{bk})(Q^{cl} L^j)\epsilon_{abc}\epsilon_{ij}\epsilon_{kl}$	$\mathcal{O}_{qqq}$

Table 1.2: The table shows the four-fermion operators in the dimension-six SMEFT in the Warsaw basis [22, 23]. The operators are listed in four-component spinor notation, and a full correspondence to the two-component notation we use elsewhere can be found in Appendix ??. We remind the reader that combinations like (QQ) stand for $(\bar{Q}^C Q)$, where Q^C is the charge-conjugated spinor. Flavor indices are omitted, and should be understood to label the fermions in the order $\{r, s, t, u\}$ as they appear.

	Operator	Notation	Operator	Notation
X^3	$W_\mu^{I\nu}W_\nu^{J\rho}W_\rho^{K\mu}\epsilon_{IJK}$	$\mathcal{O}_W$	$\tilde{W}_\mu^{I\nu}W_\nu^{J\rho}W_\rho^{K\mu}\epsilon_{IJK}$	$\mathcal{O}_{\tilde{W}}$
	$G_\mu^{A\nu}G_\nu^{B\rho}G_\rho^{C\mu}f_{ABC}$	$\mathcal{O}_G$	$\tilde{G}_\mu^{A\nu}G_\nu^{B\rho}G_\rho^{C\mu}f_{ABC}$	$\mathcal{O}_{\tilde{G}}$
H^6	$(H^\dagger H)^3$	$\mathcal{O}_H$		
H^4D^2	$(H^\dagger H)\Box(H^\dagger H)$	$\mathcal{O}_{H\Box}$	$H_i^\dagger(D_\mu H)^i\cdot(D^\mu H)_j^\dagger H^j$	$\mathcal{O}_{HD}$
ψ^2H^2	$(H^\dagger H)(\bar{L}He_R)$	$\mathcal{O}_{eH}$		
	$(H^\dagger H)(\bar{Q}Hd_R)$	$\mathcal{O}_{dH}$	$(H^\dagger H)(\bar{Q}\tilde{H}u_R)$	$\mathcal{O}_{uH}$
X^2H^2	$(H^\dagger H)B_{\mu\nu}B^{\mu\nu}$	$\mathcal{O}_{HB}$	$(H^\dagger H)\tilde{B}_{\mu\nu}B^{\mu\nu}$	$\mathcal{O}_{H\tilde{B}}$
	$(H^\dagger H)W_{\mu\nu}^IW^{I\mu\nu}$	$\mathcal{O}_{HW}$	$(H^\dagger H)\tilde{W}_{\mu\nu}^IW^{I\mu\nu}$	$\mathcal{O}_{H\tilde{W}}$
	$(H^\dagger\tau^IH)W_{\mu\nu}^IB^{\mu\nu}$	$\mathcal{O}_{HWB}$	$(H^\dagger\tau^IH)\tilde{W}_{\mu\nu}^IB^{\mu\nu}$	$\mathcal{O}_{H\tilde{W}B}$
	$(H^\dagger H)G_{\mu\nu}^AG^{A\mu\nu}$	$\mathcal{O}_{HG}$	$(H^\dagger H)\tilde{G}_{\mu\nu}^AG^{A\mu\nu}$	$\mathcal{O}_{H\tilde{G}}$
ψ^2XH	$(\bar{L}\sigma^{\mu\nu}e_R)HB_{\mu\nu}$	$\mathcal{O}_{eB}$	$(\bar{L}\sigma^{\mu\nu}e_R)\tau^IHW_{\mu\nu}^I$	$\mathcal{O}_{eW}$
	$(\bar{Q}\sigma^{\mu\nu}u_R)\tilde{H}B_{\mu\nu}$	$\mathcal{O}_{uB}$	$(\bar{Q}\sigma^{\mu\nu}u_R)\tau^I\tilde{H}W_{\mu\nu}^I$	$\mathcal{O}_{uW}$
	$(\bar{Q}\sigma^{\mu\nu}d_R)HB_{\mu\nu}$	$\mathcal{O}_{dB}$	$(\bar{Q}\sigma^{\mu\nu}d_R)\tau^IHW_{\mu\nu}^I$	$\mathcal{O}_{dW}$
	$(\bar{Q}\sigma^{\mu\nu}\lambda^Au_R)\tilde{H}G_{\mu\nu}^A$	$\mathcal{O}_{uG}$	$(\bar{Q}\sigma^{\mu\nu}\lambda^Ad_R)HG_{\mu\nu}^A$	$\mathcal{O}_{dG}$
ψ^2H^2D	$(H^\dagger i\bar{D}_\mu H)(\bar{L}\gamma^\mu L)$	$\mathcal{O}_{Hl}^{(1)}$	$(H^\dagger i\bar{D}_\mu^I H)(\bar{L}\gamma^\mu\tau^IL)$	$\mathcal{O}_{Hl}^{(3)}$
	$(H^\dagger i\bar{D}_\mu H)(\bar{e}_R\gamma^\mu e_R)$	$\mathcal{O}_{He}$		
	$(H^\dagger i\bar{D}_\mu H)(\bar{Q}\gamma^\mu Q)$	$\mathcal{O}_{Hq}^{(1)}$	$(H^\dagger i\bar{D}_\mu^I H)(\bar{Q}\gamma^\mu\tau^IQ)$	$\mathcal{O}_{Hq}^{(3)}$
	$(H^\dagger i\bar{D}_\mu H)(\bar{u}_R\gamma^\mu u_R)$	$\mathcal{O}_{Hu}$	$(H^\dagger i\bar{D}_\mu H)(\bar{d}_R\gamma^\mu d_R)$	$\mathcal{O}_{Hd}$
	$H^i(iD_\mu H)^j\epsilon_{ij}\cdot(\bar{u}_R\gamma^\mu d_R)$	$\mathcal{O}_{Hud}$		

Table 1.3: The table shows the operators featuring in the Warsaw basis [22, 23] of the dimension-six SMEFT that are not four-fermion operators. We point the reader to Appendix ?? for the correspondence between the four-component notation used here and the two-component notation used elsewhere in this work for spinors, along with the definition of $\bar{D}^\mu$. Flavor indices are omitted and should be understood to act on fermions in the order $\{r, s\}$ as they appear in each operator.

The Low-energy or Weak Effective Theory

Many experimental constraints on the SM and its extensions come from low-energy flavour-changing process involving four fermions. These can be accurately described using an effective theory, similar to the Fermi theory of the Weak interactions, in which the electroweak gauge bosons, the physical higgs and the top quark have been integrated out. The dimension six operators in this low-energy EFT [112–115] have been extensively applied to B, K and D meson decays, meson–anti-meson oscillations and leptonic decays, *e.g.* [116]. They are also an invaluable tool for studying deviations from the SM in a way independent from many of the assumptions underlying SMEFT. The symmetries of the theory are only those of QCD and electromagnetism, and the fermions are the usual quarks and leptons with the top quark excluded from the theory. At dimension six there are 3,631 $\Delta B = \Delta L = 0$ operators [112], and we do not list them all here. Rather, we introduce the pertinent operators within the discussion of each specific phenomenological process we study in this work.

1.3.3 Operator redundancy and the Hilbert series

The previous section introduced some of the difficulties involved with writing down a basis of four-fermion operators for a complex EFT like the SMEFT. Additional redundancy can occur once operators with (covariant) derivatives are included. These include operator relations through integration by parts (IBP) and field redefinitions involving the classical equations of motion (EOM) [22, 117, 118]. At mass-dimensions larger than six, these come to be a large source of the difficulty in writing down a complete operator basis, but the problem can be addressed through Hilbert-series methods [105–109]. Below, we motivate how the EOM can be used to simplify effective operator bases, and explain how these redundancies can be accounted for through Hilbert series techniques.

Field redefinitions and the equations of motion

It is clear that operators can be simplified using the EOM at lowest order [22, 119–121], since the external legs are put on-shell in the Feynman rules. That is, an operator like

$$(H^\dagger H)(\bar{e}_R i \not{D} e_R) \tag{1.51}$$

can be simplified when it appears in calculations with all legs external. So, any leading-order amplitude involving the operator can be reduced through

$$i \not{D} e_R = y_e H^\dagger L \,, \tag{1.52}$$

(or equivalently $\mathscr{M} \sim \not{p} u_e = m_e u_e$ by the momentum-space Dirac equation) to $\mathcal{O}_{eH}$. Surprisingly, this useful result can be extended even to cases involving propagators and

loops by performing field redefinitions. Specifically, field redefinitions that preserve the symmetries of the theory and contain a term linear in the original field allow the EOM to simplify a local effective Lagrangian without affecting the S-matrix [122–128]. We illustrate this with a toy ϕ^4 theory:

$$\mathscr{L} = \frac{1}{2}(\partial_\mu\phi)(\partial^\mu\phi) - \frac{1}{2}m^2\phi^2 - \frac{\lambda}{4!}\phi^4 + \frac{c_1}{\Lambda^2}\phi^6 + \frac{c_2}{\Lambda^2}\phi^3\Box\phi + \mathcal{O}(\Lambda^{-4})\,. \tag{1.53}$$

Under the field redefinition

$$\phi \to \phi + \frac{c_2}{\Lambda^2}\phi^3\,, \tag{1.54}$$

the kinetic term becomes

$$\frac{1}{2}(\partial_\mu\phi)(\partial^\mu\phi) \to \frac{1}{2}(\partial_\mu\phi)(\partial^\mu\phi) - \frac{c_2}{\Lambda^2}\phi^3\Box\phi + \mathcal{O}(\Lambda^{-4})\,, \tag{1.55}$$

where the second term comes from integrating $c_2\Lambda^{-2}(\partial_\mu\phi)(\partial^\mu\phi^3)$ by parts. This term cancels the last term in Eq. (1.53), for which the additional operators induced by the field redefinition are all $\mathcal{O}(\Lambda^{-4})$ terms. Performing the field redefinition on the other interaction terms in the Lagrangian leads to an effective redefinition of λ and c_1, with all other induced operators suppressed by four powers of Λ. Concretely,

$$\begin{aligned}\mathscr{L} \to{}& \frac{1}{2}(\partial_\mu\phi)(\partial^\mu\phi) - \frac{1}{2}m^2\phi^2 - \frac{\lambda}{4!}\phi^4 + \frac{c_1}{\Lambda^2}\phi^6 + \frac{c_2}{\Lambda^2}\phi^3\Box\phi \\ &+ \frac{c_2}{\Lambda^2}\phi^3\underbrace{\left(-\Box\phi - m^2\phi - \frac{\lambda}{3!}\phi^3\right)}_{\equiv E[\phi]} + \cdots \\ ={}& \frac{1}{2}(\partial_\mu\phi)(\partial^\mu\phi) - \frac{1}{2}m^2\phi^2 - \underbrace{\left(\frac{\lambda}{4!} + \frac{c_2}{\Lambda^2}m^2\right)}_{\equiv\lambda'/4!}\phi^4 + \underbrace{\left(\frac{c_1}{\Lambda^2} - \frac{c_2}{\Lambda^2}\frac{\lambda}{3!}\right)}_{\equiv c_1'/\Lambda^2}\phi^6 + \mathcal{O}(\Lambda^{-4})\,.\end{aligned} \tag{1.56}$$

This is guaranteed since in the effective theory all of the operators consistent with the symmetries are already present, so the effects of the additional terms are exclusively to shift the coefficients of the theory around. The appearance of the EOM operator $E[\phi]$ above can be understood on the basis of the nature of the field redefinition Eq. (1.54). The additional terms induced by the field redefinition up to $\mathcal{O}(\Lambda^{-2})$ will be those in which a ϕ or its derivative has been replaced with $c_2\Lambda^{-2}\phi^3$. That is,

$$\begin{aligned}\Delta\mathscr{L} &= \frac{c_2}{\Lambda^2}\phi^3\frac{\partial\mathscr{L}}{\partial\phi} + \frac{c_2}{\Lambda^2}(\partial_\mu\phi^3)\frac{\partial\mathscr{L}}{\partial(\partial_\mu\phi)} + \mathcal{O}(\Lambda^{-4}) \\ &= \frac{c_2}{\Lambda^2}\phi^3\left[\frac{\partial\mathscr{L}}{\partial\phi} - \partial_\mu\frac{\partial\mathscr{L}}{\partial(\partial_\mu\phi)}\right] + \mathcal{O}(\Lambda^{-4})\,,\end{aligned} \tag{1.57}$$

where we have integrated the second term by parts in the last step. In order to show that the S-matrix is unaffected, it is not sufficient to show only that the Lagrangian has not changed form (up to order Λ^{-2}). In the path integral picture, the field redefinition Eq. (1.54) will also change the measure of the path integral and the sources $\mathcal{J}_i$ for each of the fields, whose effects we have not considered. These additional changes can be dealt with generically [117]. In short, the Jacobian can be written as a Lagrangian involving ghost fields, similar to the Fadeev–Popov approach taken in Gauge Theory. In this case the ghost fields acquire a mass of order Λ, and are therefore not relevant to the effective theory. The change to the source $\mathcal{J}_\phi$ does lead to a change in the Green's functions of the theory, although the S-matrix remains unchanged. We can see this easily in our toy theory. The LSZ reduction formula [129]

$$G^{(n+m)}(q_1,\dots,q_m;p_1,\dots,p_n) \underset{\substack{p_j^2\to m^2\\ q_k^2\to m^2}}{\sim} \left(\prod_{j=1}^{m}\frac{i\sqrt{Z_j}}{p_j^2-m^2+i\epsilon}\right)\left(\prod_{k=1}^{n}\frac{i\sqrt{Z_k}}{q_k^2-m^2+i\epsilon}\right)\langle q_1,\dots,q_m|S|p_1,\dots,p_n\rangle\,, \tag{1.58}$$

relates the poles in the $(m+n)$-point Green's function to the S-matrix, up to wavefunction renormalisation factors Z_i. Here momenta p_i label the m incoming particles and q_i label the n outgoing particles. Consider, for example, the four-point Green's function with all particles taken to be incoming for simplicity:

$$G^{(4)}(p_1,p_2,p_3,p_4) = \left(\prod_{i=1}^{4}\int d^4x_i\cdot e^{-ip_i\cdot x_i}\right)\langle 0|T\{\phi(x_1)\phi(x_2)\phi(x_3)\phi(x_4)\}|0\rangle\,. \tag{1.59}$$

The effect of the term $c_1\Lambda^{-2}\mathcal{J}_\phi\phi^3$ is to alter the momentum-space Green's function to

$$\begin{aligned}&\langle 0|T\{[\phi(x_1)+c_1\Lambda^{-2}\phi(x_1)^3]\cdots[\phi(x_4)+c_1\Lambda^{-2}\phi(x_4)^3]\}|0\rangle\\ &\quad=\langle 0|T\{\phi(x_1)\phi(x_2)\phi(x_3)\phi(x_4)\}|0\rangle+\langle 0|T\{c_1\Lambda^{-2}\phi(x_1)^3\phi(x_2)\phi(x_3)\phi(x_4)\}|0\rangle\\ &\qquad+\sum_{i=2}^{4}(1\leftrightarrow i)+\mathcal{O}(\Lambda^{-4})\,,\end{aligned} \tag{1.60}$$

which differs only by the terms like $\langle 0|T\{c_1\Lambda^{-2}\phi(x_1)^3\phi(x_2)\phi(x_3)\phi(x_4)\}|0\rangle$ to order Λ^{-2}. These matrix elements do not affect the S-matrix, since the singularity structure is different. In this case, there is no single-particle pole at x_1, and so there is no contribution to scattering.

In the context of this toy ϕ^4 theory we have motivated that terms in the effective Lagrangian $\mathscr{L}$ that are connected by the EOM are redundant when working to a fixed order in Λ. Such field redefinitions are a powerful tool for simplifying operator bases, and they are often used to eliminate as many operators with derivatives as possible. We proceed to illustrate how such redundancies, along with those from IBP, can be accounted for systematically with the Hilbert series.

The Hilbert series

In the following we discuss the Hilbert series (HS), also known as the Molien or Poincaré function, as a tool for writing down Lagrangian invariants in a conceptually clean and efficient way. The Hilbert series is a generating function that contains information about the number and structure of the invariants that can be constructed from a set of multiplets. The approach has been used in more formal contexts *e.g.* [130–132], although it has also been used to count lepton and quark flavour invariants [133, 134] as well as operators in the SMEFT [108]. Our aim here is to illustrate the essential components of the HS approach with examples.

The HS $\mathfrak{H}$ is a generating function that counts the number of operators with a certain field content, *i.e.*

$$\mathfrak{H}(\{\chi_j\}) = \sum_i c_i \mathcal{O}_i(\{\chi_j\}) \,, \tag{1.61}$$

where $c_i \in \mathbb{N}$ is the number of independent invariants with field content $\mathcal{O}_i$, a polynomial in the fields of the theory $\{\chi_j\}$. The c_i and $\mathcal{O}_i$ in the simplified case of a theory with a single field χ transforming under the compact Lie group G can be computed from the general formula for the HS:

$$\mathfrak{H}(\chi) = \int_G d\mu_G \exp\left[\sum_{r=1}^{\infty} \frac{\Delta(r)\chi^r \chi_R(z_j^r)}{r}\right] \,, \tag{1.62}$$

where $d\mu_G$ is Haar measure of the group, the invariant measure one can use to integrate over the manifold of G, and $\chi_R(z_j^r)$ is the character function associated with the representation R in which χ transforms under G. The character functions can be found using character generating functions [135] in general, but the functions relevant to the SM representations are listed in Appendix A.1 of Ref. [105]. The function

$$\Delta(r) = \begin{cases} 1 & \chi \text{ bosonic} \\ (-1)^{r+1} & \chi \text{ fermionic} \end{cases} \,, \tag{1.63}$$

accounts for the fact that χ is anticommuting in the fermionic case [135].

Even redundancies due to IBP and EOM relations can be incorporated into the HS technique. The space of invariants modulo EOM can be organised into representations of the conformal group [108, 109]. Irreducible representations of the conformal group involve a 'primary operator' $\mathcal{O}$ and its derivatives, called 'descendant operators': $(\mathcal{O}, \partial_\mu \mathcal{O}, \partial_\mu \partial_\nu \mathcal{O}, \ldots)$. The invariants can be constructed by decomposing tensor products of these irreps, which accounts for EOM redundancy, and then projecting out the primary operator, which deals with IBP relations. This alters the formula Eq. (1.62) slightly:

$$\mathfrak{H}(D,\chi) = d\mu_G \frac{1}{P(D, x_+, x_-)} \exp\left[\sum_{r=1}^{\infty} \frac{\Delta(r)\chi^r \chi_R(z_j^r)}{r D^{d_r}}\right] + \Delta\mathfrak{H}(D,\chi) \,, \tag{1.64}$$

where D is a spurion field representing the (covariant) derivative, d_r is the mass-dimension of the field χ_r and

$$P(D,x_+,x_-)=\frac{1}{(1-Dx_+x_-)\left(1-\frac{D}{x_+x_-}\right)\left(1-\frac{Dx_+}{x_-}\right)\left(1-\frac{Dx_-}{x_+}\right)}\,, \tag{1.65}$$

with $x_\pm$ the $\mathrm{SU}(2)_\pm$ integration variables. The function $\Delta\mathfrak{H}$ can be obtained from a general formula presented in Ref. [109]. It's role is to cancel unwanted terms (of mass-dimension $d\leq 4$) from the HS that come about because the character functions of the conformal group are not orthonormal [109].

We illustrate the use of Eq. (1.64) with a simple example: the independent invariants built out of the SM Higgs doublet H. The Higgs doublet transforms in the fundamental representation of $\mathrm{SU}(2)_L$ and carries hypercharge $Y=\frac{1}{2}$, for which the relevant Haar measures are [136]

$$\int_{\mathrm{SU}(2)}d\mu_{\mathrm{SU}(2)}=\frac{1}{2\pi i}\oint_{|x|=1}\frac{dx}{x}(1-x^2)\,,\quad \int_{\mathrm{U}(1)}d\mu_{\mathrm{U}(1)}=\frac{1}{2\pi i}\oint_{|y|=1}\frac{dy}{y}\,, \tag{1.66}$$

and the character functions are [105, 137]

$$\chi_{I=\frac{1}{2}}(x)=\frac{1}{x}+x\,,\quad \chi_{Y=\frac{1}{2}}(y)=y^{1/2}\,, \tag{1.67}$$

for $x,y\in\mathbb{C}$. This gives [109]

$$\begin{aligned}\mathfrak{H}(H,\tilde{H})=&\frac{1}{(2\pi i)^4}\oint_{|x_+|=1}dx_+\oint_{|x_-|=1}dx_-\cdot\oint_{|x|=1}\frac{dx}{x}(1-x^2)\cdot\oint_{|y|=1}\frac{dy}{y}\\&\cdot\exp\left[n_f\sum_{r=1}^{\infty}\frac{H^r}{rD}\left(\frac{1}{x^r}+x^r\right)y^{r/2}\chi^r_{(0,0)}\right]\cdot\exp\left[n_f\sum_{r=1}^{\infty}\frac{\tilde{H}^r}{rD}\left(\frac{1}{x^r}+x^r\right)y^{-r/2}\chi^r_{(0,0)}\right]\\&\cdot\frac{1}{P(D,x_+,x_-)}+(H^\dagger HD^2-D^4)\end{aligned} \tag{1.68}$$

for the Hilbert series, where we have accounted for H and it's conjugate $\tilde{H}$ separately, and included the possibility of n_f flavours. The last term in parentheses is the relevant part of $\Delta\mathfrak{H}$ in this case, and $\chi_{(0,0)}$ is the scalar character function:

$$\chi_{(0,0)}=DP(D,x_+,x_-)(1-D^2)\,. \tag{1.69}$$

The contour integrals can be done by expanding the integrand in H and $\tilde{H}$, and integrating up to the required order [130]. For this example, the first few terms in the HS are

$$\mathfrak{H}(H,\tilde{H})=\text{Fill this in}\,. \tag{1.70}$$

The HS approach has an attractive module structure. For example, if one wanted to count the number of invariants while not accounting for IBP and EOM redundancies, one need only remove the Lorentz integrals, character functions and $\Delta\mathfrak{H}$. Something that is perhaps less clear is that the HS can also be used to construct operators that are not invariants of the symmetry groups in G, but rather violate those symmetries in specific ways.

We work through this point with an even simpler example than the previous one: a scalar ϕ charged only under a U(1) symmetry, motivated by Ref. [105]. In this case, the HS is

$$\mathfrak{H}(\phi,\phi^*) = \sum_{n=0}^{\infty}(\phi^*\phi)^n \tag{1.71}$$

$$= \frac{1}{1-\phi^*\phi}\,, \tag{1.72}$$

where we treat $\phi^*\phi$ as a c-number less than one. This sum can be written as a contour integral, making a more clear connection[6] to Eq. (1.62):

$$\mathfrak{H}(\phi,\phi^*) = \frac{1}{2\pi i}\oint_{|z|=1}\frac{dz}{z}\frac{1}{(1-\phi z)(1-\phi^*/z)}\,. \tag{1.73}$$

This connection is made more clear by expanding:

$$\begin{aligned}\frac{1}{(1-\phi z)(1-\phi^* z)} = [1+\phi^*\phi+(\phi^*\phi)^2+\cdots] + z[\phi+\phi(\phi^*\phi)+\phi(\phi^*\phi)^2+\cdots] \\ + z^2[\phi^2+\phi^2(\phi\phi^*)+\cdots]+\cdots\end{aligned} \tag{1.74}$$

The invariants sit in the first term, and so are picked out by the contour integral after dividing through by z in Eq. (1.73). Importantly, the terms proportional to z in Eq. (1.74) violate the symmetry by one unit, and so these can be picked out by the contour integral if we divide by z^2 in Eq. (1.73), and similarly for any desired value of charge violation.

The HS provides information about the field content of the invariants and the number of independent operators, but does not tell us exactly how to construct the singlets. This is an important drawback of the approach, although even here there has been much recent progress using on-shell methods, *e.g.* [138–141].

[6] The integrand can also be written as an exponential like in Eq. (1.62) containing ϕ and ϕ^*:

$$\frac{1}{(1-\phi z)(1-\phi^*/z)} = \exp\left[\sum_{r=1}^{\infty}\frac{(\phi z)^r}{r}+\sum_{r=1}^{\infty}\left(\frac{\phi^*}{z}\right)^r\frac{1}{r}\right].$$

1.4 The flavour anomalies and their explanation

In recent years, measurements of a number of processes involving leptons have established a large set of significant and unresolved deviations from SM prediction. Many of these measurements involve semileptonic B-meson decays, and these can be placed into two broad classes:

Neutral-current These involve flavour-changing neutral-current (FCNC) $b \to s$ transitions and include branching-ratio measurements in final states with muons, anomalous angular observables in $B \to K^* \mu\mu$, and violations of μ–e LFU in $B \to K^{(*)} \ell\ell$ processes. This class corresponds to hundreds of discrepant measurements in total, and single-operator fits suggest a preference for new-physics at roughly 6σ, *e.g.* [14].

Charged-current These involve $b \to c\ell\nu$ transitions and shown apparent deviations from τ–μ and τ–e LFU. The main observables measured in this case are LFU ratios in $B \to D^{(*)}\ell\nu$, for which the combined deviation from the SM expectation is just over 3σ [21].

Excitingly there is a high-degree of self-consistency between the measurements, both within and across these two classes. That is, the measurements imply coherent and theoretically well-motivated patterns when interpreted in terms of deviations in four-fermion operator coefficients.

In addition to these classes, the most precise measurement of the anomalous magnetic moment of the muon $(g-2)_\mu$ [142], is in tension with the SM expectation [143] at roughly 3.5σ. More recently, a smaller discrepancy has also been measured in $(g-2)_e$ [144]. Taken together, these anomalies paint a picture of new-physics coupling to leptons in way that violates the LFU present in the SM. In the following we discuss the experimental situation relevant to each of these classes, and the extent to which new contributions to dimension-six operator coefficients can reconcile the discrepancies.

1.4.1 Neutral-current anomalies

The neutral-current anomalies represent a large family of measurements in tension with SM prediction with a common underlying $b \to s$ transition at the quark level and usually a $\mu^+\mu^-$ pair. The measurements come in three main categories: branching ratios, LFU ratios, and angular observables.

There are many discrepancies seen in branching ratio data at dimuon invariant masses below the charmonium threshold. Examples include the branching ratios for the semileptonic decays $B \to K^{(*)}\mu\mu$ [145] and $B_s \to \phi\mu\mu$ [146], the leptonic decay $B_s \to \mu\mu$ [147–150], and the hyperon channels $\Lambda_b \to \Lambda\mu\mu$ [151]. In all cases, the measured values tend to fall short of the respective SM expectations.

Semileptonic B decays like $B \to K^{(*)}\mu\mu$ had already been recognised as good probes of new physics even before the start of the LHC, *e.g.* [152]. This is because, being FCNC processes, they are additionally suppressed in the SM by off-diagonal CKM matrix elements, weak couplings, and a loop factor. The differential decay rate for $B^+ \to K^+\ell\ell$ is [153]

$$\begin{aligned}\frac{d\Gamma}{dq^2} = \frac{G_F^2\alpha^2|V_{tb}V_{ts}^*|^2}{128\pi^5}|k|\beta\Bigg[\frac{2}{3}|k|^2\beta^2|C_{10}f_+(q^2)|^2 + \frac{4m_\ell^2(m_B^2-m_K^2)^2}{q^2m_B^2}|C_{10}f_0(q^2)|^2 \\ + |k^2|\left(1-\frac{1}{3}\beta^2\right)\left|C_9 f_+(q^2) + 2C_7\frac{m_b+m_s}{m_B+m_K}f_T(q^2)\right|^2\Bigg],\end{aligned} \tag{1.75}$$

where k is the kaon momentum, $\beta = (1-4m_\ell^2q^{-2})^{1/2}$, and $f_{0,+,T}$ are the $B \to K$ scalar, vector and tensor form factors. The expression is representative of the structure of the whole class of relevant semileptonic decays. The strongest dependence is on the operator coefficients C_9 and C_{10} in the WET, defined as

$$\mathcal{O}_9 = (\bar{s}\gamma^\mu P_L b)(\bar{\mu}\gamma_\mu\mu)\,, \tag{1.76}$$

$$\mathcal{O}_{10} = (\bar{s}\gamma^\mu P_L b)(\bar{\mu}\gamma_\mu\gamma_5\mu)\,, \tag{1.77}$$

with the coefficients usually normalised such that

$$\mathcal{L} = \frac{4G_F}{\sqrt{2}}V_{tb}V_{ts}^*\frac{e^2}{16\pi^2}\sum_i C_i\mathcal{O}_i\,. \tag{1.78}$$

Experimentally, semileptonic process like $B \to K\mu\mu$ are difficult to separate from the corresponding background processes like $B \to K\psi(\to \mu\mu)$, where ψ represents any of the vector charmonium resonances. For this reason, kinematic regions close to the narrow charmonium resonances are excluded from experimental analyses. The most significant single deviation is in the semileptonic decay $B_s \to \phi\mu\mu$, for which the data depart from the SM prediction by more than 3σ in the $q^2 \in [1,5]$ GeV^2 bin [146]. A problematic feature of this and many of these channels is that the SM prediction is plagued by hadronic uncertainties, which can be difficult to calculate. We show the differential branching ratio for $B_s \to \phi\mu\mu$ measured by LHC*b* in Fig. 1.7, taken from Ref. [13], along with the SM predictions using different methods to deal with the form factors [10–12]. Both the large uncertainties on the theory side and the apparent suppression of the measured values are clear. The discrepancy with the SM is largest in the aforementioned q^2 bin.

The decay $B_s \to \mu\mu$ is cleaner than the semileptonic decays on the theory side: the final state is leptonic and the only non-perturbative physics needed is the B_s decay constant, which can be calculated to high precision on the lattice [154]. The measurements performed by ATLAS [150], LHC*b* [148, 149] and CMS [147] are shown in Fig. 1.8,

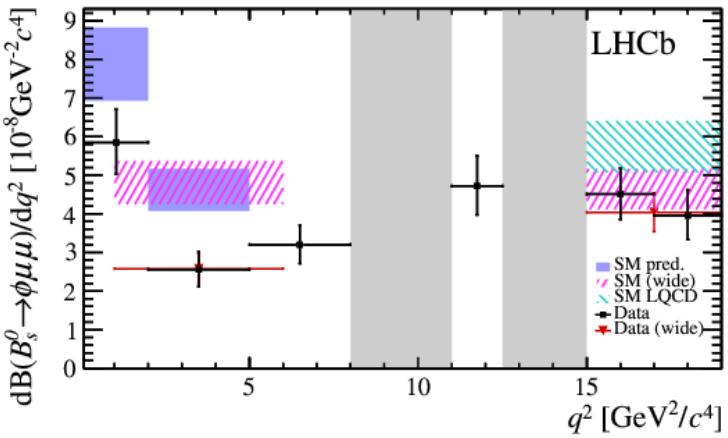

Figure 1.7: The figure shows the measured and predicted values for the differential branching ratio for $B_s \to \phi\mu\mu$ by bins of q^2. The data points are the LHC*b* measurements, while the coloured rectangles are the SM predictions with form factors calculated using light-cone sum rules [10, 11] and lattice QCD [12]. The greyed out regions correspond to charmonium resonances, exluded from the analysis as discussed in the main text. The LHC*b* data points are generally lower than the SM expectation, especially in the $q^2 \in [1,5]$ GeV^2 bin where the discrepancy is larger than 3σ. The plot is taken from Ref. [13].

along with correlated limits on $B^0 \to \mu\mu$. The combination of the measurements shown is taken from Ref. [14], and suggests a compatibility with the SM at close to 2σ. Currently, measurements of $B_s \to \mu\mu$ are statistically limited; the branching ratio in the SM is very small because it is chirality suppressed, but this also makes it a promising mode for measuring new-physics effects.

The large theoretical uncertainties featuring in the expressions for the decay rates $\Gamma[B \to K^{(*)}\mu\mu]$ can be tamed in a more direct way by constructing a ratio with the electronic mode $B \to K^{(*)}ee$, in which many sources of uncertainty cancel in the regime where new-physics effects are small [155–157]. Interestingly, the LHC*b* collaboration has measured a suppression in the ratios

$$R_{K^{(*)}} = \frac{\Gamma[B \to K^{(*)}\mu\mu]}{\Gamma[B \to K^{(*)}ee]} \tag{1.79}$$

in the $q^2 \in [1,6]$ GeV^2 bin. In the SM the prediction of the observables outside of the low-q^2 region is determined by physics which is wholly independent of the flavor of the lepton pair in the final state, making R_K and R_{K^*} finely sensitive to violations of LFU. LHC*b* finds [15]

$$R_K = 0.846\,^{+0.060+0.016}_{-0.054-0.014}\,, \tag{1.80}$$

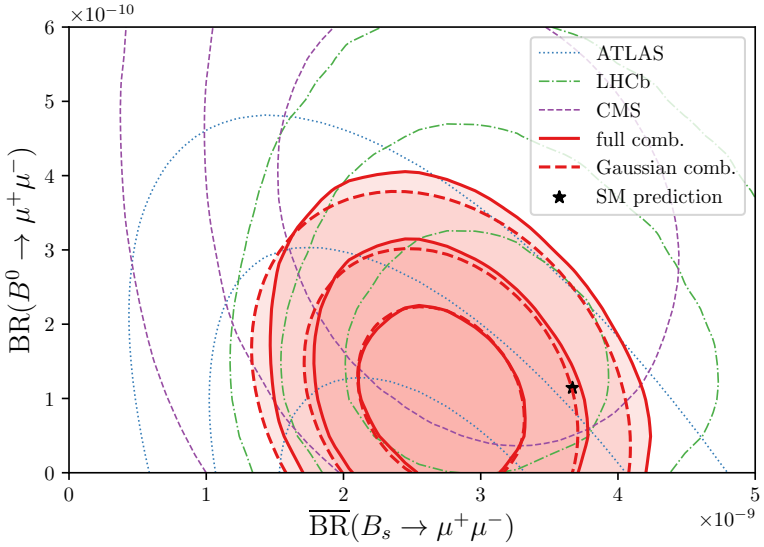

Figure 1.8: The figure shows the two-dimensional likelihood contours in $\mathrm{Br}(B^0 \to \mu\mu)$ and $\mathrm{Br}(B_s \to \mu\mu)$. The thin contours are individual measurements, while the thick contours are the combination. A Gaussian approximation to the combined fit is shown with thick dashed contours. For more details see Ref. [14], from where the figure is taken. The SM prediction (shown with a star) is compatible with the combined fit at 2σ.

for dilepton invariant mass squared range $q^2 \in [1.1, 6]\ \mathrm{GeV}^2$, while the SM demands $R_K^{\mathrm{SM}} = 1.0003 \pm 0.0001$ [158]. The analysis accounts for systematic differences in the reconstruction of muons and electrons by LHCb by first normalising the decay rates to the $B^+ \to K^+ J/\psi(\to \mu\mu/ee)$ rates. The measurement is then a double ratio in which many theoretical and experimental uncertainties cancel. The ratio R_K has also been measured by Belle [16] and BaBar [17] to be suppressed, although with larger uncertainties.

The K^* ratio has also been measured by LHCb [19] to show an approximately 2.5σ discrepancy in the central q^2 bin:

$$R_{K^*} = \begin{cases} 0.660\,^{+0.110}_{-0.070} \pm 0.024 & \text{for } 0.045\,\mathrm{GeV}^2 < q^2 < 1.1\,\mathrm{GeV}^2 \\ 0.685\,^{+0.113}_{-0.069} \pm 0.047 & \text{for } 1.1\,\mathrm{GeV}^2 < q^2 < 6\,\mathrm{GeV}^2 \end{cases} . \tag{1.81}$$

The Belle measurement [18] is consistent with the SM prediction at $\lesssim 2\sigma$:

$$R_{K^*} = \begin{cases} 0.90\,^{+0.27}_{-0.21} \pm 0.10 & \text{for } 0.1\,\mathrm{GeV}^2 < q^2 < 8\,\mathrm{GeV}^2 \\ 1.18\,^{+0.52}_{-0.32} \pm 0.10 & \text{for } 15\,\mathrm{GeV}^2 < q^2 < 19\,\mathrm{GeV}^2 \end{cases} . \tag{1.82}$$

Although the error bars are large, the central value is still suppressed with respect to the SM prediction in the low-q^2 region. A summary of the experimental situation relevant to R_K and R_{K^*} is presented in Fig. 1.9.

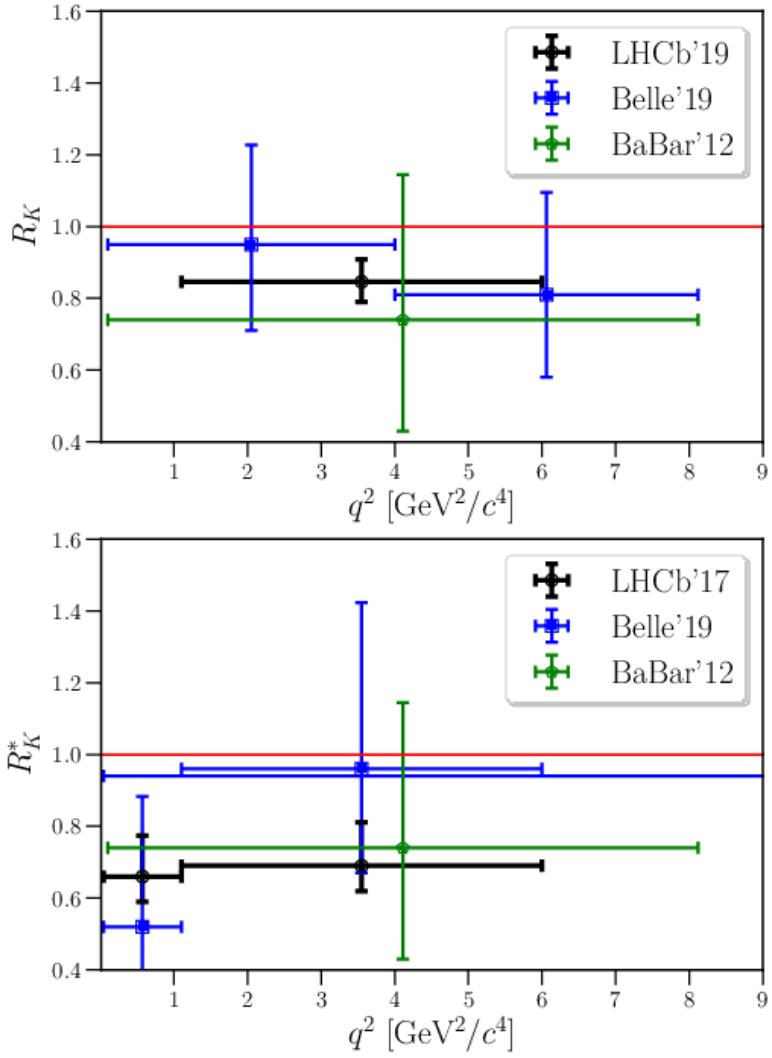

Figure 1.9: (top) The measurements of the LFU R_K by LHC*b* [15], Belle [16] and BaBar [17]. All measurements are suppressed relative to the SM prediction, shown in red. (bottom) The figure shows the experimental situation for R_{K^*} [17–19]. Like R_K, the measured values are found to be smaller than the SM value, shown in red. Both figures are taken from Ref. [20].

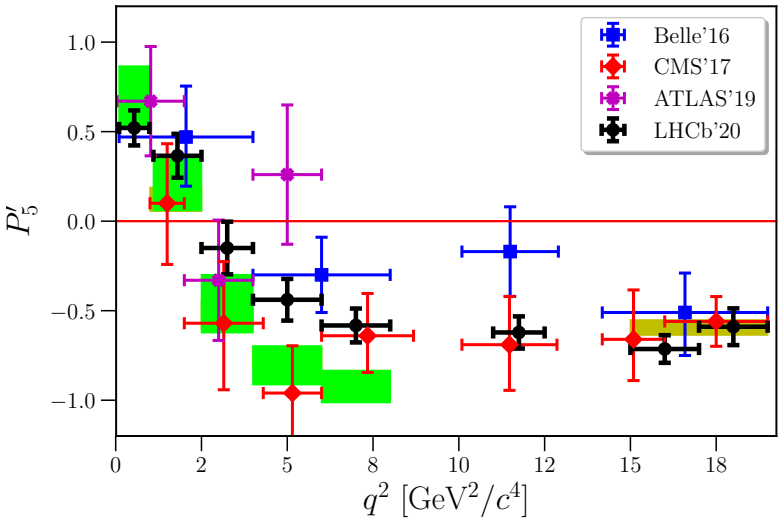

Figure 1.10: The figure shows the measured values of the P_5' angular observable in the decays $B \to K^*\mu\mu$ binned by q^2. With the exception of the CMS measurements, there is an enhancement with respect to the SM prediction (green) around $q^2 \sim 5\,\text{GeV}^2$. The plot is taken from Ref. [20].

The distribution of final-state particles in the semileptonic decays $B \to K^*\mu\mu$ define a number of angular observables, some of which have also been measured to be in disagreement with SM predictions. The P_5' asymmetry [159–161] is constructed as a ratio of angular observables to minimise from-factor uncertainties. Measurements show a significant deviation from the SM at around $q^2 \sim 5\,\text{GeV}^2$ [162–165] as shown in Fig. 1.10, although the CMS measurement [166] is consistent with the SM prediction [10, 11, 167, 168] in this region. The hadronic uncertainties are still sizeable in this case.

Fits

The picture of the neutral-current anomalies given above is still only a small cross-section of the several hundred observables that are in tension with the SM predictions. A large number of global-fit analyses have been conducted in which these anomalies are interpreted in terms of deviations in the operators C_9 and C_{10}, introduced above in Eq. (1.76). These analyses are all in mutual agreement, and generally find that a sizeable negative value for C_9 is preferred over the SM value at between 4 and 7σ [14, 169–171]. (This was first pointed out in Ref. [172], which analysed the 2013 data.) This wide range is largely due to differences in dealing with uncertainties in the semileptonic decays. Importantly, no large deviation in the electronic modes is necessary for a good fit. An example of one of the recent global fits [14] to C_9 and C_{10} is shown in Fig. 1.11. The

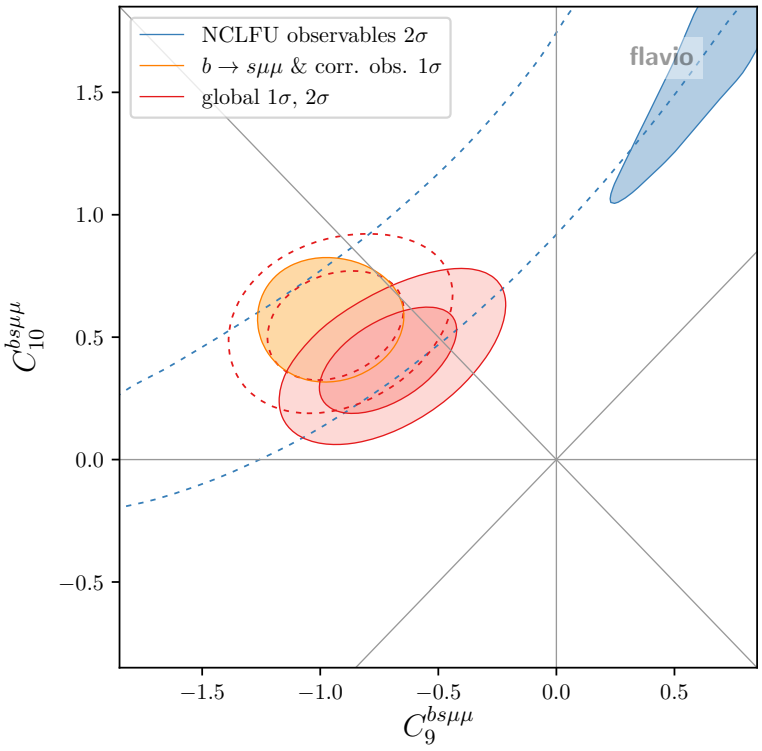

Figure 1.11: The figure shows the results of the global fit conducted in Ref. [14] in the C_9–C_{10} plane. The fit to just the LFU ratios is shown in blue, while that for the other $b \to s$ data is shown in yellow, with the combined fit shown in red. The $SU(2)_L$-invariant direction $C_9 = -C_{10}$ gives a good fit to the data, and any acceptible fit requires a sizeable negative value for C_9. The plot is taken from Ref. [14].

authors find the single-operator best-fit scenario to be in the $SU_L(2)$-invariant direction $C_9 = -C_{10}$, with $C_9 = -C_{10} = -0.53$ giving a pull from the SM of 6.6σ. We note that following the updated measurements of R_K [15] and R_{K^*} [18] presented at the 2019 Moriond conference, there is a slight tension between explaining the LFU ratios and the rest of the $b \to s$ data. We point the reader to Ref. [14] for a more detailed discussion on this point.

That much of the tension is driven by a deviation in C_9 also allows for an explanation of many of the anomalies in a way that does not require the introduction of new physics. The deviation in C_9 necessary to explain much of the anomalous $b \to s$ data can be mimicked by non-perturbative effects associated with loops of charm quarks, *e.g.* [13], and the data seem to be currently consistent with both hypotheses [173, 174]. Such effects cannot account for the violation of LFU seen in the ratios $R_{K^{(*)}}$, again highlighting their importance in understanding the potential role of new physics in

explaining the neutral-current anomalies.

1.4.2 Charged-current anomalies

The class of charged-current anomalies in the $b \to c$ transition consists of a smaller number of measurements and processes. The primary observables of interest are the LFU ratios

$$R_{D^{(*)}} = \frac{\mathrm{Br}[B \to D^{(*)}\tau\nu]}{\mathrm{Br}[B \to D^{(*)}\ell\nu]}\,, \tag{1.83}$$

where ℓ denotes one of the light leptons: $\ell \in \{e, \mu\}$. The ratio has been measured by BaBar [175, 176], Belle [177–180] and LHC*b* [181–183], with combined values from HFLAV given by [21]

$$R_D = 0.340 \pm 0.027 \pm 0.013 \quad \text{and} \quad R_{D^*} = 0.295 \pm 0.011 \pm 0.008\,. \tag{1.84}$$

These combinations are in tension with the SM predictions [184–187] as averaged by HFLAV:

$$R_D^{\mathrm{SM}} = 0.299 \pm 0.003 \quad \text{and} \quad R_{D^*}^{\mathrm{SM}} = 0.258 \pm 0.005 \tag{1.85}$$

at approximately 3σ. We note that BaBar and Belle use the average of the electronic and muonic modes in the denominator, while LHC*b* uses only the muonic mode. The tension was significantly decreased following the most recent Belle measurement presented at the Moriond 2019 conference [180]; this combined measurement is consistent with the SM prediction at 1.2σ. A summary of the measurements of $R_{D^{(*)}}$ is shown in Fig. 1.12. BaBar [176] and Belle [177] have measured the q^2 distributions of the tau-mode decay rate, which has proved to be a powerful model discriminator, *e.g.* [188].

Although the ratios $R_{D^{(*)}}$ are our primary concern in this work, we also introduce a number of other observables relevant to the charged current process. The first of these is the LFU ratio $R_{J/\psi}$:

$$R_{J/\psi} = \frac{\mathrm{Br}(B_c \to J/\psi\tau\nu)}{\mathrm{Br}(B_c \to J/\psi\mu\nu)}\,, \tag{1.86}$$

has recently been measured by LHC*b* to be $R_{J/\psi} = 0.71 \pm 0.17 \pm 0.18$ [189]. Although the ratio is also measured to be enhanced with respect to the SM prediction $R_{J/\psi}^{\mathrm{SM}} \approx 0.25$–$0.29$ [190–202], the central value of the measurement shows a very large effect that cannot be well-accommodated with BSM contributions [203], although the error bars are very large. The observable $f_L^{D^*}$, the longitudinal polarisation of the D^* in $B \to D^*\tau\nu$, also differs from the SM expectation by $\sim 1.6\sigma$:

$$f_L^{D^*} = 0.60 \pm 0.08 \pm 0.04, \tag{1.87}$$

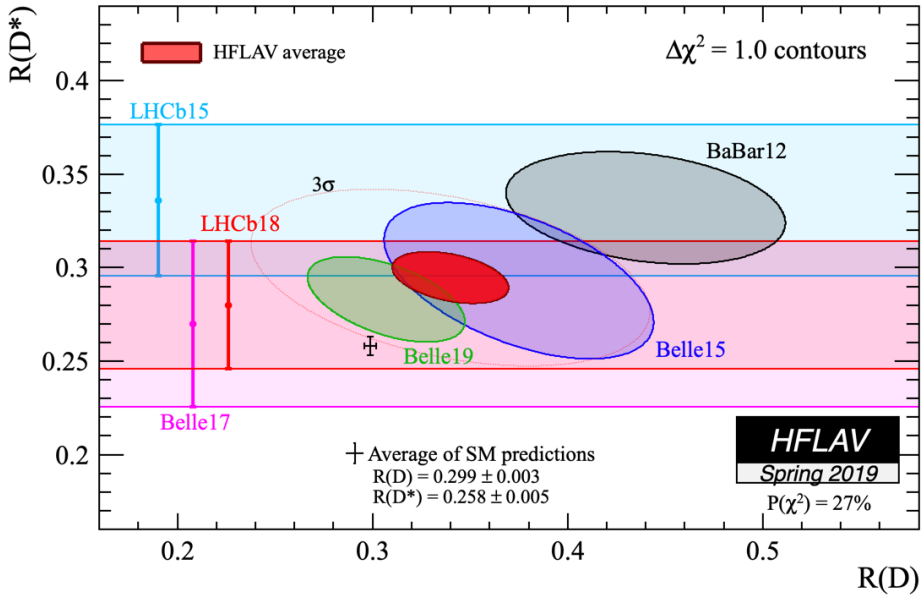

Figure 1.12: The figure shows the combined fit to the available R_D and R_{D^*} data from HFLAV [21]. The combination is shown in red, just over 3σ away from the SM prediction (black data point). Both ratios are measured to be enhanced compared to the SM value.

as measured by the Belle collaboration [204], and has been shown to have good discriminating power for BSM explanations of $R_{D^{(*)}}$. The third class of observables we consider are tau polarisation asymmetries [see Ref. [205] for a detailed discussion in the context of explaining $R_{D^{(*)}}$]. The polarisation asymmetry in the longitudinal direction of the τ in the D^* mode has also recently been measured by Belle [178]:

$$\mathcal{P}_\tau^* = -0.38 \pm 0.51^{+0.21}_{-0.16}. \tag{1.88}$$

Although the errors are large, the projected Belle II sensitivity at 50 ab^{-1} for the same observable in the D mode is estimated at about 3% [206], and we expect the $\mathcal{P}_\tau^*$ to be measured even more precisely at Belle II.

Fits

The charged-current $b \to c$ anomalies can be interpreted in terms of deviations from dimension-six operator coefficients in the WET. The pertinent Hamiltonian for $b \to$

$c\ell_r\nu_s$ is

$$H_{\text{eff}}^{b\to c} = \frac{4G_F}{\sqrt{2}}V_{cb}\sum_{rs}[(\delta^{rs}+C_{V_L}^{rs})\mathcal{O}_{V_L}^{rs}+C_{V_R}^{rs}\mathcal{O}_{V_R}^{rs}+C_{S_L}^{rs}\mathcal{O}_{S_L}^{rs}+C_{S_R}^{rs}\mathcal{O}_{S_R}^{rs}+C_T^{rs}\mathcal{O}_T^{rs}]+\text{h.c.} \quad (1.89)$$

where

$$\mathcal{O}_{V_X}^{rs} = (\bar{c}\gamma^\mu P_X b)(\bar{e}_r\gamma_\mu P_L\nu_s)\,,\ \mathcal{O}_{S_X}^{rs} = (\bar{c}P_X b)(\bar{e}_r P_L\nu_s)\,,\ \mathcal{O}_T^{rs} = (\bar{c}\sigma^{\mu\nu}P_X b)(\bar{e}_r\sigma_{\mu\nu}P_L\nu_s)\,, \quad (1.90)$$

with $X\in\{L,R\}$. The left-handed vector operator is the same one generated in the SM, while the scalar and tensor operators can provide large enhancements to the decay rate, since they lift the helicity-suppression of the decay.

1.4.3 Anomalous magnetic moment of the muon

Precise measurements of the deviation in the semi-classical value of the muon gyromagnetic ratio, $(g-2)_\mu$, have demonstrated an inconsistency. This is parameterised by the quantity

$$a_\mu \equiv \frac{(g-2)_\mu}{2}\,. \quad (1.91)$$

There is a persistent deviation between the SM prediction and the experimentally measured value [143, 207],

$$\Delta a_\mu = a_\mu^{\text{exp}} - a_\mu^{\text{SM}} = (286\pm 63\pm 43)\times 10^{-11}, \quad (1.92)$$

corresponding to a 3.6σ anomaly. The error values refer to the experimental and theoretical prediction errors, respectively. Similarly, recent experimental results have indicated a deviation from the SM for the electron anomalous magnetic moment, of 2.5σ significance [208]. The leading candidates to explain these anomalies involve flavour-dependent, loop-level, BSM effects [143].

1.4.4 Scalar and Vector leptoquarks

Nulla malesuada porttitor diam. Donec felis erat, congue non, volutpat at, tincidunt tristique, libero. Vivamus viverra fermentum felis. Donec nonummy pellentesque ante. Phasellus adipiscing semper elit. Proin fermentum massa ac quam. Sed diam turpis, molestie vitae, placerat a, molestie nec, leo. Maecenas lacinia. Nam ipsum ligula, eleifend at, accumsan nec, suscipit a, ipsum. Morbi blandit ligula feugiat magna. Nunc eleifend consequat lorem. Sed lacinia nulla vitae enim. Pellentesque tincidunt purus vel magna. Integer non enim. Praesent euismod nunc eu purus. Donec bibendum quam in tellus. Nullam cursus pulvinar lectus. Donec et mi. Nam vulputate metus eu enim. Vestibulum pellentesque felis eu massa.

Draft compiled on 2020/11/12 at 19:18:00

2

Model building from effective operators

2.1 Introduction

This is a test of *something with an apple* that I would like [25]. The following is $4a+5 = 13$ some inline math and `this` and we did in in Python.

$$\int_{-\infty}^{\infty} \frac{1}{(2\pi\hbar)^3}\phi(p)dp\,. \tag{2.1}$$

We need some sans serif **words** here too. Then we need to check **what** the bold looks like.

Draft compiled on 2020/11/12 at 19:18:00

3

Models of radiative neutrino mass

3.1 Introduction

This is a test of *something with an apple* that I would like [25]. The following is $4a+5 = 13$ some inline math and `this` and we did in in Python.

$$\int_{-\infty}^{\infty} \frac{1}{(2\pi\hbar)^3}\phi(p)dp\,. \tag{3.1}$$

We need some sans serif **words** here too. Then we need to check **what** the bold looks like.

Draft compiled on 2020/11/12 at 19:18:00

4

The S_1 leptoquark as an explanation of the flavour anomalies

This chapter is based on the publication 'Reconsidering the One Leptoquark scenario: flavour anomalies and neutrino mass,' written in collaboration with Yi Cai, Michael A. Schmidt, and Raymond R. Volkas [2]. We study the potential of the S_1 leptoquark to explain the flavour anomalies and the anomalous magnetic moment of the muon in a new region of parameter space.

4.1 Introduction

A common origin for $R_{D^{(*)}}$ and the anomalous $b \to s$ data is suggested naturally if the former is explained by the effects of the operator $(c^\dagger \bar{\sigma}_\mu b)(\tau^\dagger \bar{\sigma}^\mu \nu)$, related in its general structure by $\mathrm{SU}(2)_L$ invariance to the aforementioned four-fermion effective operator accounting for the $b \to s$ anomalies. A number of models exploring this idea have been suggested in the literature [209–223] (along with many others addressing one or the other anomaly, *e.g.* [188, 224–240]) and among these minimal explanations the Bauer–Neubert (BN) model [210] is one of notable simplicity and explanatory power: a TeV-scale scalar leptoquark protagonist mediating $\bar{B} \to D^{(*)} \tau \bar{\nu}$ at tree-level and the $b \to s$ decays through one-loop box diagrams. The leptoquark transforms under the SM gauge group like a right-handed down-type quark and its pattern of couplings to SM fermions can also reconcile the measured and predicted values of the anomalous

magnetic moment of the muon, another enduring tension.

5

Models of neutrino mass and the flavour anomalies

5.1 Introduction

Taken together, the anomalies studied in the previous chapter paint a picture of new physics interacting more strongly with the second and third generations of SM fermions, introducing lepton flavour non-universality and FCNC interactions at energies not significantly higher than the electroweak scale. Interestingly, many of these phenomenological motifs arise naturally in radiative models of neutrino mass, hinting towards the attractive possibility of a common explanation for both phenomena. Previous work has also considered radiative neutrino mass models whose particle content addresses R_K [223, 234, 241–243], $R_{D^{(*)}}$ [217, 223] and $(g-2)_\mu$ [223, 241–244]. In Refs. [217, 234] the flavour anomalies are explained through two light scalar or vector leptoquarks whose couplings to the SM Higgs doublet and fermions prohibit a consistent assignment of lepton number to the leptoquarks such that the symmetry is respected. Thus $\mathrm{U}(1)_L$ is explicitly broken by two units and the neutrinos gain mass at the one-loop level [245], apart from the imposition of any additional symmetries[1]. A general feature of such models is that large amounts of fine-tuning are required to suppress the neutrino mass to the required scale with at least one set of leptoquark–fermion couplings sizeable

[1] Mass generation in Ref. [244] occurs at the two-loop level because the Yukawa couplings of one of the leptoquarks to the left-chiral fermions is turned off.

enough to explain the anomalies.

6 The two-photon decay of a scalar-quirk bound state

We use $\mathfrak{f}$ to represent the scalar diquark.

6.1 Introduction

An excess of events containing two photons with invariant mass near 750 GeV has been observed in 13 TeV proton–proton collisions by the ATLAS and CMS collaborations [246, 247]. The cross section $\sigma(pp \to \gamma\gamma)$ is estimated to be

$$\sigma(pp \to \gamma\gamma) = \begin{cases} (10 \pm 3)\text{ fb} & \text{ATLAS} \\ (6 \pm 3)\text{ fb} & \text{CMS} \end{cases} \tag{6.1}$$

and there is no evidence of any accompanying excess in the dilepton channel [248]. If we interpret this excess as the two photon decay of a single new particle of mass m then ATLAS data provide a hint of a large width: $\Gamma/m \sim 0.06$, while CMS data prefer a narrow width. Naturally, further data collected at the LHC should provide a clearer picture as to the nature of this excess.

There has been vast interest in the possibility that the diphoton excess results from physics beyond the SM. Most discussion has focused on models where the excess is due to a new scalar particle which subsequently decays into two photons *e.g.* Ref. [249]. The possibility that the new scalar particle is a bound state of exotic charged fermions has

also been considered, *e.g.* Refs. [250–254]. Here we consider the case that the 750 GeV state is a non-relativistic bound state constituted by an exotic *scalar* particle χ and its antiparticle, charged under $\mathrm{SU}(3)_c$ as well as a new unbroken non-abelian gauge interaction. Having χ be a scalar rather than a fermion is not merely a matter of taste: In such a framework a fermionic χ would lead to the formation of bound states which (typically) decay to dileptons more often than to photons; a situation which is not favoured by the data.

The bound state, which we denote Π, can be produced through gluon–gluon fusion directly (*i.e.* at threshold $\sqrt{s_{gg}} \simeq M_\Pi$) or indirectly via $gg \to \chi^\dagger\chi \to \Pi + \textit{soft quanta}$ (*i.e.* above Π threshold: $\sqrt{s_{gg}} > M_\Pi$). The indirect production mechanism can dominate the production of the bound state, which is an interesting feature of this kind of theory.

6.2 The model

We take the new confining unbroken gauge interaction to be $\mathrm{SU}(N)$, and assume that, like $\mathrm{SU}(3)_c$, it is asymptotically free and confining at low energies. However, the new $\mathrm{SU}(N)$ dynamics is qualitatively different from QCD as all the matter particles [assumed to be in the fundamental representation of $\mathrm{SU}(N)$] are taken to be much heavier than the confinement scale, Λ_N. In fact we here consider only one such matter particle, χ, so that $M_\chi \gg \Lambda_N$ is assumed. In this circumstance a $\chi^\dagger\chi$ pair produced at the LHC above the threshold $2M_\chi$ but below $4M_\chi$ cannot fragment into two jets. The $\mathrm{SU}(N)$ string which connects them cannot break as there are no light $\mathrm{SU}(N)$-charged states available. This is in contrast to heavy quark production in QCD where light quarks can be produced out of the vacuum enabling the color string to break. The produced $\chi^\dagger\chi$ pair can be viewed as a highly excited bound state, which de-excites by $\mathrm{SU}(N)$-ball and soft glueball/pion emission [255].

With the new unbroken gauge interaction assumed to be $\mathrm{SU}(N)$ the gauge symmetry of the SM is extended to

$$\mathrm{SU}(3)_c \otimes \mathrm{SU}(2)_L \otimes \mathrm{U}(1)_Y \otimes \mathrm{SU}(N). \tag{6.2}$$

This kind of theory can arise naturally in models which feature large colour groups [256–258] and in models with leptonic colour [259–262] but was also considered earlier by Okun [263]. The notation *quirks* for heavy particles charged under an unbroken gauge symmetry (where $M_\chi \gg \Lambda_N$) was introduced in [255] where the relevant phenomenology was examined in some detail in a particular model[1]. For convenience we borrow their nomenclature and call the new quantum number *hue* and the massless gauge bosons *huons* ($\mathscr{H}$).

[1] Some other aspects of such models have been discussed over the years, including the possibility that the $\mathrm{SU}(N)$ confining scale is low ($\sim$ keV), a situation which leads to macroscopic strings [264].

The phenomenological signatures of the bound states (quirkonia) formed depend on whether the quirk is a fermion or boson. Here we assume that the quirk χ is a Lorentz scalar in light of previous work which indicated that bound states formed from a fermionic χ state would be expected to be observed at the LHC via decays of the spin-1 bound state into opposite-sign lepton pairs ($\ell^+\ell^-$) [255, 262]. In fact, this appears to be a serious difficulty in attempts to interpret the 750 GeV state as a bound state of fermionic quirk particles (such as those of Refs. [250–252]). The detailed consideration of a scalar χ appears to have been largely overlooked[2], perhaps due to the paucity of known elementary scalar particles. With the recent discovery of a Higgs-like scalar at 125 GeV [266, 267] it is perhaps worth examining signatures of scalar quirk particles. In fact, we point out here that the two photon decay is the most important experimental signature of bound states formed from electrically charged scalar quirks. Furthermore this explanation is only weakly constrained by current data and thus appears to be a simple and plausible option for the new physics suggested by the observed diphoton excess.

6.3 Explaining the excess

The scalar χ that we introduce transforms under the extended gauge group (Eq. 6.2) as

$$\chi \sim (\mathbf{3}, \mathbf{1}, Y; \mathbf{N}), \tag{6.3}$$

where we use the normalisation $Q = Y/2$. The possibility that χ also transforms non-trivially under $\mathrm{SU}(2)_L$ is interesting, however for the purposes of this letter we focus on the $\mathrm{SU}(2)_L$ singlet case for definiteness. Since two-photon decays of non-relativistic quirkonium will be assumed to be responsible for the diphoton excess observed at the LHC, the mass of χ will need to be around 375 GeV.

We have assumed that χ is charged under $\mathrm{SU}(3)_c$ so that it can be produced at tree-level through QCD-driven pair production. We present the production mechanisms in Fig. 6.1. To estimate the production cross section of the bound states, we first consider the indirect production mechanism which we expect to be dominant. Here, a $\chi^\dagger\chi$ pair is produced above threshold and de-excites emitting soft glueballs/pions and hueballs: $gg \to \chi^\dagger\chi \to \Pi + \textit{soft quanta}$. We first consider the case where the confinement scale of the new $\mathrm{SU}(N)$ interaction is similar to that of QCD. What happens in this case can be adapted from the discussion in [255], where a fermionic quirk charged under an unbroken SU(2) gauge interaction was considered. As already briefly discussed in the introduction, the $\chi^\dagger\chi$ pairs initially form a highly excited bound state, which subsequently de-excites in two stages. The first stage is the non-perturbative regime where the hue string is longer than Λ_N^{-1}. The second stage is characterised by a string scale

[2] The idea has been briefly mentioned in recent literature [253, 265].

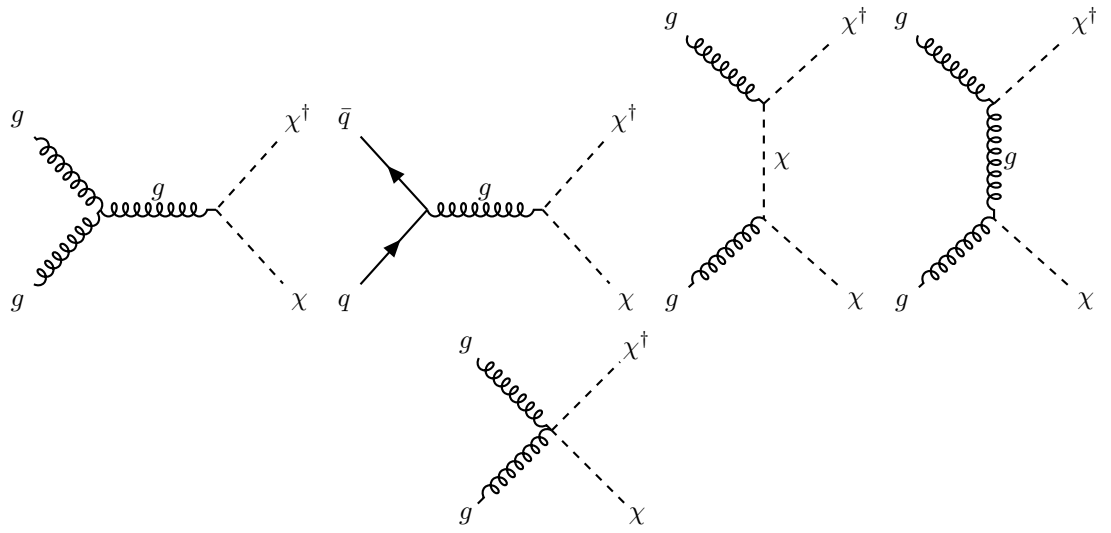

Figure 6.1: Tree-level pair production mechanisms for the scalar quirk χ.

significantly less than Λ_N^{-1}: the perturbative Coulomb region. Here the bound state can be characterised by the quantum numbers n and l. De-excitation continues until quirkonium is in a lowly excited state with $l \leq 1$ and n. Imagine first that de-excitation continued until the ground state ($n = 1, l = 0$) is reached. Given we are considering χ to be a scalar, the quirkonium ground state, Π, will have spin 0, and is thus expected to decay into SM gauge bosons and huons. The cross section $\sigma(pp \to \Pi \to \gamma\gamma)$ in this case is then

$$\sigma(pp \to \gamma\gamma) \approx \sigma(pp \to \chi^\dagger \chi) \times \mathrm{Br}(\Pi \to \gamma\gamma). \tag{6.4}$$

Since production is governed by QCD interactions, we can use the values of the pair production cross sections for stops/sbottoms in the limit of decoupled squarks and gluinos [268]. For a χ mass of 375 GeV

$$\sigma(pp \to \chi^\dagger \chi) \approx \begin{cases} 2.6N \text{ pb} & \text{at } 13 \text{ TeV} \\ 0.5N \text{ pb} & \text{at } 8 \text{ TeV} \end{cases}. \tag{6.5}$$

The branching fraction is to leading order

$$\mathrm{Br}(\Pi \to \gamma\gamma) \simeq \frac{3NQ^4\alpha^2}{\frac{2}{3}N\alpha_s^2 + \frac{3}{2}C_N\alpha_N^2 + 3NQ^4\alpha^2}, \tag{6.6}$$

where $C_N \equiv (N^2 - 1)/(2N)$, α_N is the new SU(N) interaction strength and we have neglected the small contribution of $\Pi \to Z\gamma/ZZ$ to the total width. Eq. (6.6) also neglects the decay to Higgs particles: $\Pi \to hh$, which arises from the Higgs potential

portal term $\lambda_\chi \chi^\dagger \chi \phi^\dagger \phi$. Theoretically this rate is unconstrained given the dependence on the unknown parameter λ_χ, but could potentially be important. However, limits from resonant Higgs boson pair production derived from 13 TeV data: $\sigma(pp \to X \to hh \to bbbb) \lesssim 50\,\text{fb}$ at $M_X \approx 750\,\text{GeV}$ [269, 270] imply that the Higgs decay channel must indeed be subdominant (*c.f.* $\Pi \to gg, \mathscr{H}\mathscr{H}$).

The renormalised gauge coupling constants in Eq. (6.6) are evaluated at the renormalisation scale $\mu \sim M_\Pi/2$. Taking for instance the specific case of $N = 2$, $\alpha_N = \alpha_s \simeq 0.10$ (at $\mu \sim M_\Pi/2$) gives

$$\sigma(pp \to \gamma\gamma) \approx 5 \left(\frac{Q}{1/2}\right)^4 \text{ fb at } 13\,\text{TeV}\,. \tag{6.7}$$

At $\sqrt{s} = 8\,\text{TeV}$ the cross section is around five times smaller. We present the cross section $\sigma(pp \to \Pi \to \gamma\gamma)$ for a range of masses M_Π and different combinations of Q and N in Fig. 6.2. The parameter choice $\alpha_N = \alpha_s$ and $\Lambda_N = \Lambda_{\text{QCD}}$ has been assumed. (The cross section is not highly sensitive to Λ_N, α_N so long as we are in the perturbative regime: $\Lambda_N \lesssim \Lambda_{\text{QCD}}$.) Evidently, for $N = 2$, a χ with electric charge $Q \approx 1/2$ is produced at approximately the right rate to explain the diphoton excess.

In practice de-excitation of the produced quirkonium does not always continue until the ground state is reached. In this case annihilations of excited states can also contribute. However those with $l = 0$ will decay in the same way as the ground state. The only difference is that the excited states will have a slightly larger mass (which we will estimate in a moment) due to the change in the binding energy. This detail could be important as it can effectively enlarge the observed width. Annihilation of excited states with non-zero orbital angular momentum could in principle also be important, however these are suppressed as the radial wavefunction vanishes at the origin: $R(0) = 0$ for $l \geq 1$. They are expected to de-excite predominately to $l = 0$ states rather than annihilate [255]. Nevertheless, for sufficiently large α_N the $l = 1$ annihilations: $\Pi \to \mu^+\mu^-$ and $\Pi \to e^+e^-$ could potentially be observable.

The $l = 0$ excited states can be characterized by the quantum number n with binding energies:

$$\frac{E_n}{M_\Pi} = -\frac{1}{8n^2}\left[\frac{4}{3}\bar{\alpha}_s + C_N\bar{\alpha}_N + Q^2\bar{\alpha}\right]^2 . \tag{6.8}$$

The above formula was adapted from known results with quarkonium, *e.g.* [250] (and of course also the hydrogen atom). The coupling constants $\bar{\alpha}_s$, $\bar{\alpha}_N$ and $\bar{\alpha}$ are evaluated at a renomalisation scale corresponding to the mean distance between the particles which is of order the Bohr radius: $a_0 = 4/[(4\bar{\alpha}_s/3 + C_N\bar{\alpha}_N + Q^2\bar{\alpha})M_\Pi]$. The bound state, described by the radial quantum number n has mass given by $M_\Pi(n) = 2M_\chi + E_n$. Considering as an example $N = 2$ and $\bar{\alpha}_N = \bar{\alpha}_s = 0.15$, $\bar{\alpha} = 1/137$ we find the mass difference between the $n = 1$ and $n = 2$ states to be $\Delta M = (E_1 - E_2) \approx 0.01 M_\Pi$. Larger mass splittings

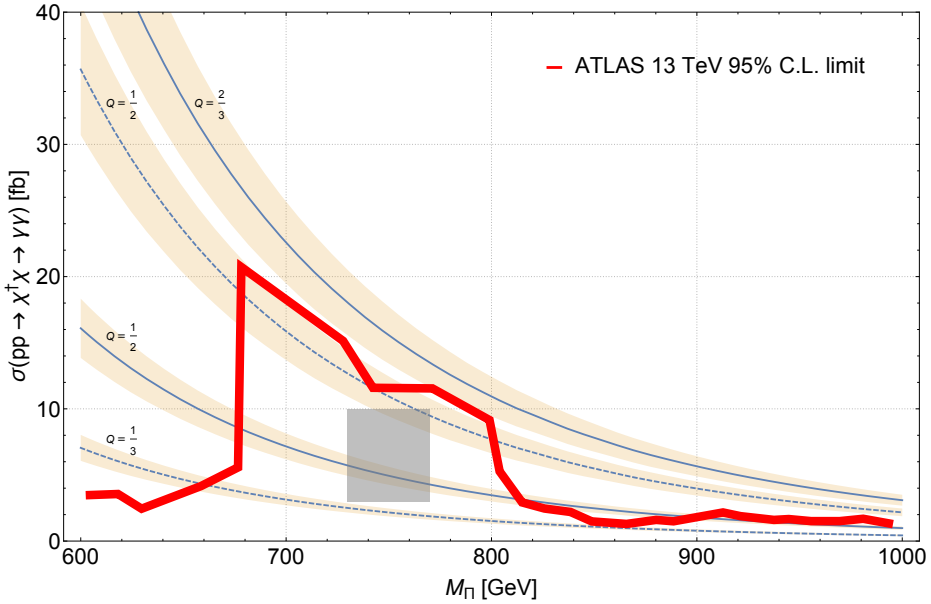

Figure 6.2: The cross section $\sigma(pp \to \Pi \to \gamma\gamma)$ at 13 TeV for a range of quirkonium masses M_Π and charge assignments. Solid lines denote choices of $N = 2$ and dashed lines choices of $N = 5$. The rectangle represents the $\sigma \in [3, 10]$ fb indicative region accommodated by the ATLAS and CMS data. The solid red line is the ATLAS 13 TeV exclusion limit. Uncertainties reflect error associated with the parton distribution functions.

will be possible[3] if $\bar{\alpha}_N > \bar{\alpha}_s$, although it has been shown in the context of fermionic quirk models that the phenomenology is substantially altered in this regime [251]. In particular, the hueballs can become so heavy that the decays of the bound state into hueballs is kinematically forbidden.

In the above calculation of the bound state production cross section, we considered only the *indirect* production following pair production of $\chi^\dagger\chi$ above threshold. The bound state can also be produced directly: $gg \to \Pi$, where $\sqrt{s_{gg}} \approx M_\Pi$. The cross section of the ground state direct resonance production is

$$\sigma(pp \to \Pi)_{\mathrm{DR}} \approx \frac{C_{gg} K_{gg} \Gamma(\Pi \to gg)}{s M_\Pi}, \tag{6.9}$$

[3] Additional possibilities arise if χ transforms non-trivially under $\mathrm{SU}(2)_L$, *i.e.* forming a representation N_L. The mass degeneracy of the multiplet will be broken at tree-level by Higgs potential terms along with electroweak radiative corrections. The net effect is that the predicted width of the $pp \to \gamma\gamma$ bump can be effectively larger as there are N_L distinct bound states, Π^i, (of differing masses) which can each contribute to the decay width. Although each state is expected to have a narrow width, when smeared by the detector resolution the effect can potentially be a broad feature.

where C_{gg} is the appropriate parton luminosity coefficient and K_{gg} is the gluon NLO QCD K-factor. For $\sqrt{s} = 13\,\text{TeV}$ we take $C_{gg} \approx 2137$ [249] and $K_{gg} = 1.6$ [271]. The partial width $\Gamma(\Pi \to gg)$ of the $n = 1, l = 0$ ground state is given by

$$\Gamma(\Pi \to gg) = \frac{4}{3} M_\Pi N \alpha_s^2 \frac{|R(0)|^2}{M_\Pi^3}, \tag{6.10}$$

where the radial wavefunction at the origin for the ground state is:

$$\frac{|R(0)|^2}{M_\Pi^3} = \frac{1}{16}\left[\frac{4}{3}\bar{\alpha}_s + C_N \bar{\alpha}_N + Q^2 \bar{\alpha}\right]^3. \tag{6.11}$$

Considering again the example of $N = 2$ and $\bar{\alpha}_N = \bar{\alpha}_s = 0.15$, $\bar{\alpha} = 1/137$ we find

$$\sigma(pp \to \Pi)_{DR} \approx 0.40\,\text{pb} \quad \text{at } 13\,\text{TeV}\,. \tag{6.12}$$

Evidently, the direct resonance production cross section is indeed expected to be subdominant, around 8% that of the indirect production cross section (Eq. 6.5)[4].

We now comment on the regime where Λ_N is smaller than Λ_{QCD}. In fact, if the SU(N) confining scale is only a little smaller than Λ_{QCD} then a light quark pair can form out of the vacuum, leading to a bound state of two QCD color singlet states: $\chi\bar{q}$ and $\chi^\dagger q$. These color singlet states would themselves be bound together by SU(N) gauge interactions to form the SU(N) singlet bound state. Since only SU(N) interactions bind the two composite states ($\chi\bar{q}$ and $\chi^\dagger q$), it follows that $\frac{4}{3}\bar{\alpha}_s + C_N\bar{\alpha}_N + Q^2\bar{\alpha} \to C_N\bar{\alpha}_N + (Q - Q_q)^2\bar{\alpha}$ in eqs. 6.8 and 6.11. Therefore if the confinement scale of SU(N) is smaller than that of QCD then the direct production rate becomes completely negligible relative to the indirect production mechanism. The rate of Π production is the same as that found earlier in Eq. 6.5, but the branching ratio to two photons is modified:

$$\text{Br}(\Pi \to \gamma\gamma) \simeq \frac{3NQ^4\alpha^2}{\frac{7}{3}N\alpha_s^2 + \frac{3}{2}C_N\alpha_N^2 + 3NQ^4\alpha^2}, \tag{6.13}$$

where, as before, we have neglected the small contribution of $\Pi \to Z\gamma/ZZ$ to the total width, and also the contribution from $\Pi \to hh$. In this regime somewhat larger values of Q can be accommodated, such as $Q = 5/6$ for $N = 2$ [5].

[4] If $\bar{\alpha}_N$ is sufficiently large, one can potentially have direct resonance production comparable or even dominating indirect production (such a scenario has been contemplated recently in [252, 253]). Naturally at such large $\bar{\alpha}_N$ the perturbative calculations become unreliable, and one would have to resort to non-perturbative techniques such as lattice computations.

[5] Although it is perhaps too early to speculate on the possible role of χ in a more elaborate framework, we nevertheless remark here that particles fitting its description are required for spontaneous symmetry breaking of extended Pati–Salam type unified theories [272].

Notice that in the $\Lambda_N < \Lambda_{\rm QCD}$ regime the size of the mass splittings between the excited states becomes small as $\frac{4}{3}\bar{\alpha}_s + C_N\bar{\alpha}_N + Q^2\bar{\alpha} \to C_N\bar{\alpha}_N + (Q-Q_q)^2\bar{\alpha}$ in Eq. 6.8. We therefore expect no effective width enhancement due to the excited state decays at the LHC in the small Λ_N regime. Of course a larger effective width is still possible if there are several nearly degenerate scalar quirk states, which, as briefly mentioned earlier, can arise if χ transforms nontrivially under $\mathrm{SU}(2)_L$.

Other signatures

While the two photon decay channel of the bound state should be the most important signature, the dominant decay is expected to be via $\Pi \to gg$ and $\Pi \to \mathscr{H}\mathscr{H}$. The former process is expected to lead to dijet production while the latter will be an invisible decay. The dijet cross section is easily estimated:

$$\sigma(pp \to jj) \approx \begin{cases} 2.6N \times \mathrm{Br}(\Pi \to gg)\ \mathrm{pb} & \text{at } 13\ \mathrm{TeV} \\ 0.5N \times \mathrm{Br}(\Pi \to gg)\ \mathrm{pb} & \text{at } 8\ \mathrm{TeV} \end{cases} . \tag{6.14}$$

The limit from 8 TeV data is $\sigma(pp \to jj) \lesssim 2.5$ pb [273, 274]. If gluons dominate the Π decays (i.e. $\mathrm{Br}(\Pi \to gg) \approx 1$) then this experimental limit is satisfied for $N \leq 5$. For sufficiently large α_N the invisible decay can be enhanced, thereby reducing $\mathrm{Br}(\Pi \to gg)$. In this circumstance the bound on N from dijet searches would weaken.

The invisible decays $\Pi \to \mathscr{H}\mathscr{H}$ are not expected to lead to an observable signal at leading order for much of the parameter space of interest[6]. However, the bremsstrahlung of a hard gluon from the initial state: $pp \to \Pi g \to \mathscr{H}\mathscr{H}g$ can lead to a jet plus missing transverse energy signature. Current data are not expected to give stringent limits from such decay channels, however this signature could become important when a larger data sample is collected. Note though that the rate will become negligible in the limit that α_N becomes small. Also, in the small Λ_N regime, where the bound state is formed from $\chi\bar{q}$ and $\chi^\dagger q$, the two-body decay $\Pi \to g\gamma$ (jet + photon) will also arise as in this case the scalar quirk pair is not necessarily in the color singlet configuration. The decay rate at leading order is substantial:

$$\frac{\Gamma(\Pi \to j\gamma)}{\Gamma(\Pi \to \gamma\gamma)} = \frac{8\alpha_s}{3\alpha Q^2} . \tag{6.15}$$

Nevertheless, we estimate that this is still consistent with current data [277], but would be expected to become important when a larger data sample is collected.

[6] Scalar quirk loops can mediate hueball decays into gluons and other SM bosons [255, 275, 276]. The decay rate is uncertain, depending on the non-perturbative hueball dynamics. However, if the hueballs are able to decay within the detector then they can lead to observable signatures including displaced vertices. This represents another possible collider signature of the model.

Another important signature of the model will be the $pp \to \Pi \to Z\gamma$ and $pp \to \Pi \to ZZ$ processes. The rates of these decays, relative to $\Pi \to \gamma\gamma$, are estimated to be:

$$\begin{aligned} \frac{\Gamma(\Pi \to Z\gamma)}{\Gamma(\Pi \to \gamma\gamma)} &= 2\tan^2\theta_W, \\ \frac{\Gamma(\Pi \to ZZ)}{\Gamma(\Pi \to \gamma\gamma)} &= \tan^4\theta_W. \end{aligned} \tag{6.16}$$

If χ transforms nontrivially under $SU(2)_L$ then deviations from these predicted rates arize along with the tree-level decay $\Pi \to W^+W^-$.

Conclusions

We have considered a charged scalar particle χ of mass around 375GeV charged under both $\mathrm{SU}(3)_c$ and a new confining gauge interaction (assigned to be $\mathrm{SU}(N)$ for definiteness). These interactions confine $\chi^\dagger\chi$ into non-relativistic bound states whose decays into photons can explain the 750 GeV diphoton excess observed at the LHC. Taking the new confining group to be SU(2), we found that the diphoton excess required χ to have electric charge approximately $Q \sim [\frac{1}{2}, 1]$. An important feature of our model is that the exotic particle χ has a mass much greater than the $\mathrm{SU}(N)$-confinement scale Λ_N. In the absence of light $\mathrm{SU}(N)$-charged matter fields this makes the dynamics of this new interaction qualitatively different to that of QCD: pair production of the scalars and the subsequent formation of the bound state dominates over direct bound state resonance production (at least in the perturbative regime where $\Lambda_N \lesssim \Lambda_{\mathrm{QCD}}$). Since χ is a Lorentz scalar, decays of $\chi^\dagger\chi$ bound states to lepton pairs are naturally suppressed, and thus constraints from dilepton searches at the LHC can be ameliorated. This explanation is quite weakly constrained by current searches and data from the forthcoming run at the LHC will be able to probe our scenario more fully. In particular, dijet, mono-jet, di-Higgs and jet + photon searches may be the most promising discovery channels.

Acknowledgements

This work was supported by the Australian Research Council. Feynman diagrams were generated using the Ti*k*Z-Feynman package for LaTeX [278].

Draft compiled on 2020/11/12 at 19:18:00

A Mathematical notation

Throughout the paper we choose to label representations by their dimension, which we typeset in bold. Fields are labelled by their transformation properties under the Lorentz group and the SM gauge group $\mathrm{SU}(3)_c \otimes \mathrm{SU}(2)_L \otimes \mathrm{U}(1)_Y$. All spinors are treated as two-component objects transforming as either $(\mathbf{2},\mathbf{1})$ (left-handed) or $(\mathbf{1},\mathbf{2})$ (right-handed) under the Lorentz group, written as $\mathrm{SU}(2)_+ \otimes \mathrm{SU}(2)_-$. The left-handed spinors carry undotted spinor indices $\alpha, \beta, \ldots \in \{1,2\}$, while the right-handed spinors carry dotted indices $\dot{\alpha}, \dot{\beta}, \ldots \in \{\dot{1},\dot{2}\}$. Wherever possible we attempt to conform to the conventions of Ref. [102] when working with spinor fields (see appendix G for the correspondence to four-component notation and appendix J for SM-fermion nomenclature). For objects carrying a single spacetime index V_μ we define

$$V_{\alpha\dot{\beta}} = \sigma^{\mu}_{\alpha\dot{\beta}} V_\mu \quad \text{and} \quad \bar{V}_{\dot{\alpha}\beta} = \bar{\sigma}^{\mu}_{\dot{\alpha}\beta} V_\mu. \tag{A.1}$$

Note that in this notation

$$\Box = \partial_\mu \partial^\mu = \tfrac{1}{2}\mathrm{Tr}[\partial\bar{\partial}] = \tfrac{1}{2}\mathrm{Tr}[\bar{\partial}\partial], \tag{A.2}$$

and we will often just use $\Box$ to represent the contraction of two covariant derivatives $D_\mu D^\mu$ where this is clear from context. For field-strength tensors, generically $X_{\mu\nu}$, we work with the irreducible representations (irreps) $X_{\alpha\beta}$ and $\bar{X}_{\dot{\alpha}\dot{\beta}}$, where

$$X_{\{\alpha\beta\}} = 2i[\sigma^{\mu\nu}]_\alpha^{\ \gamma} \epsilon_{\gamma\beta} X_{\mu\nu} \quad \text{and} \quad \bar{X}_{\{\dot{\alpha}\dot{\beta}\}} = 2i[\bar{\sigma}^{\mu\nu}]^{\dot{\gamma}}_{\ \dot{\beta}} \epsilon_{\dot{\alpha}\dot{\gamma}} X_{\mu\nu}, \tag{A.3}$$

or the alternate forms with one raised and one lowered index.

Indices for $\mathrm{SU}(2)_L$ (isospin) are taken from the middle of the Latin alphabet. These are kept lowercase for the fundamental representation for which $i, j, k, \ldots \in \{1, 2\}$ and the indices of the adjoint are capitalised $I, J, K, \ldots \in \{1, 2, 3\}$. Colour indices are taken from the beginning of the Latin alphabet and the same distinction between lowercase and uppercase letters is made. For both SU(2) and SU(3), a distinction between raised and lowered indices is maintained such that, for example, $(\psi^i)^\dagger = (\psi^\dagger)_i$ for an isodoublet field ψ. However, we often specialise to the case of only raised, symmetrised indices for SU(2), and use a tilde to denote a conjugate field whose $\mathrm{SU}(2)_L$ indices have been raised:

$$\tilde{\psi}^i \equiv \epsilon^{ij}\psi_j^\dagger. \tag{A.4}$$

We adopt this notation from the usual definition of $\tilde{H}$, and note that throughout the paper we freely interchange between $\tilde{\psi}^i$ and $\psi_i^\dagger$. For the sake of tidiness, we sometimes use parentheses $(\cdots)$ to indicate the contraction of suppressed indices. Curly braces are reserved to indicate symmetrised indices $\{\cdots\}$ and square brackets enclose antisymmetrised indices $[\cdots]$, but this notation is avoided when the permutation symmetry between indices is clear. We use τ^I and λ^A for the Pauli and Gell-Mann matrices, and normalise the non-abelian vector potentials of the SM such that

$$(W_{\alpha\dot{\beta}})^i{}_j = \frac{1}{2}(\tau^I)^i{}_j W^I_{\alpha\dot{\beta}} \quad \text{and} \quad (G_{\alpha\dot{\beta}})^a{}_b = \frac{1}{2}(\lambda^A)^a{}_b G^A_{\alpha\dot{\beta}}. \tag{A.5}$$

Flavour (or family) indices of the SM fermions are represented by the lowercase Latin letters $\{r, s, t, u, v, w\}$.

For the non-gauge degrees of freedom in the SM we capitalise isospin doublets (Q, L, H), while the left-handed isosinglets are written in lowercase with a bar featuring as a part of the name of the field ($\bar{u}$, $\bar{d}$, $\bar{e}$). The representations and hypercharges for the SM field content are summarised in Table A.1. Our definition of the SM gauge-covariant derivative is exemplified by

$$\bar{D}_{\dot{\alpha}\beta}Q_r^{\beta ai} = \left[\delta^a_b\delta^i_j(\bar{\partial}_{\dot{\alpha}\beta} + ig_1 Y_Q \bar{B}_{\dot{\alpha}\beta}) + ig_2\delta^a_b(\bar{W}_{\dot{\alpha}\beta})^i{}_j + ig_3\delta^i_j(\bar{G}_{\dot{\alpha}\beta})^a{}_b\right] Q_r^{\beta bj}\,. \tag{A.6}$$

Note that the derivative implicitly carries $\mathrm{SU}(2)_L$ and $\mathrm{SU}(3)_c$ indices [explicit on the right-hand side of Eq. (A.6)] which are suppressed on the left-hand side to reduce clutter. Where appropriate we show these indices explicitly.

We represent the SM quantum numbers of fields as a 3-tuple $(\mathbf{C}, \mathbf{I}, Y)_L$, with $\mathbf{C}$ and $\mathbf{I}$ the dimension of the colour and isospin representations, Y the hypercharge of the field, and L an (often omitted) label of the Lorentz representation: S (scalar), F (fermion) or V (vector), although sometimes we use the irrep, *e.g.* $(\mathbf{2}, \mathbf{1})$. We normalise the hypercharge such that $Q = I_3 + Y$. Finally, for exotic fields that contribute to dimension-six operators at tree-level, we try and adopt names consistent with Table 3 of Ref. [**?**].

Field	$\mathrm{SU}(3)_c \otimes \mathrm{SU}(2)_L \otimes \mathrm{U}(1)_Y$	$\mathrm{SU}(2)_+ \otimes \mathrm{SU}(2)_-$
$Q^{\alpha a i}$	$(\mathbf{3}, \mathbf{2}, \frac{1}{6})$	$(\mathbf{2}, \mathbf{1})$
$L^{\alpha i}$	$(\mathbf{1}, \mathbf{2}, -\frac{1}{2})$	$(\mathbf{2}, \mathbf{1})$
$\bar{u}_a^\alpha$	$(\bar{\mathbf{3}}, \mathbf{1}, -\frac{2}{3})$	$(\mathbf{2}, \mathbf{1})$
$\bar{d}_a^\alpha$	$(\bar{\mathbf{3}}, \mathbf{1}, \frac{1}{3})$	$(\mathbf{2}, \mathbf{1})$
$\bar{e}^\alpha$	$(\mathbf{1}, \mathbf{1}, 1)$	$(\mathbf{2}, \mathbf{1})$
$(G_{\alpha\beta})^a{}_b$	$(\mathbf{8}, \mathbf{1}, 0)$	$(\mathbf{3}, \mathbf{1})$
$(W_{\alpha\beta})^i{}_j$	$(\mathbf{1}, \mathbf{3}, 0)$	$(\mathbf{3}, \mathbf{1})$
$B_{\alpha\beta}$	$(\mathbf{1}, \mathbf{1}, 0)$	$(\mathbf{3}, \mathbf{1})$
H^i	$(\mathbf{1}, \mathbf{2}, \frac{1}{2})$	$(\mathbf{1}, \mathbf{1})$

Table A.1: The SM fields and their transformation properties under the SM gauge group G_{SM} and the Lorentz group. The final unbolded number in the 3-tuples of the G_{SM} column represents the $\mathrm{U}(1)_Y$ charge of the field, normalised such that $Q = I_3 + Y$. For the fermions a generational index has been suppressed.

Definition of Symbols and Acronyms

D

DFT density functional theory

L

lipsum Lorem Ipsum, a special type of fudge
  dolor No idea why
  ibit Sounds right, doesn't it?

P

π (π) Greek letter pi, Π does this work?

R

radial distribution function ($g(r)$)
RDF radial distribution function

Index

Bibliography

[1] R. Foot and J. Gargalionis, *Explaining the 750 GeV diphoton excess with a colored scalar charged under a new confining gauge interaction*, *Phys. Rev. D* **94** (2016), no. 1 011703, [arXiv:1604.06180].

[2] Y. Cai, J. Gargalionis, M. A. Schmidt, and R. R. Volkas, *Reconsidering the One Leptoquark solution: flavor anomalies and neutrino mass*, *JHEP* **10** (2017) 047, [arXiv:1704.05849].

[3] I. Bigaran, J. Gargalionis, and R. R. Volkas, *A near-minimal leptoquark model for reconciling flavour anomalies and generating radiative neutrino masses*, *JHEP* **10** (2019) 106, [arXiv:1906.01870].

[4] J. Gargalionis, I. Popa-Mateiu, and R. R. Volkas, *Radiative neutrino mass model from a mass dimension-11 $\Delta L = 2$ effective operator*, *JHEP* **03** (2020) 150, [arXiv:1912.12386].

[5] J. Gargalionis and R. R. Volkas, *Exploding operators for Majorana neutrino masses and beyond*, arXiv:2009.13537.

[6] I. Esteban, M. Gonzalez-Garcia, M. Maltoni, T. Schwetz, and A. Zhou, *The fate of hints: updated global analysis of three-flavor neutrino oscillations*, arXiv:2007.14792.

[7] "Nufit 5.0 (2020)." www.nu-fit.org. Accessed: 2020-09-03.

[8] **GERDA** Collaboration, M. Agostini et al., *Probing Majorana neutrinos with double-β decay*, *Science* **365** (2019) 1445, [arXiv:1909.02726].

[9] **DARWIN** Collaboration, F. Agostini et al., *Sensitivity of the DARWIN observatory to the neutrinoless double beta decay of ^{136}Xe*, arXiv:2003.13407.

[10] A. Bharucha, D. M. Straub, and R. Zwicky, *$B \to V\ell^+\ell^-$ in the Standard Model from light-cone sum rules*, *JHEP* **08** (2016) 098, [arXiv:1503.05534].

[11] W. Altmannshofer and D. M. Straub, *New physics in $b \to s$ transitions after LHC run 1*, *Eur. Phys. J. C* **75** (2015), no. 8 382, [arXiv:1411.3161].

[12] R. R. Horgan, Z. Liu, S. Meinel, and M. Wingate, *Calculation of $B^0 \to K^{*0}\mu^+\mu^-$ and $B_s^0 \to \phi\mu^+\mu^-$ observables using form factors from lattice QCD*, *Phys. Rev. Lett.* **112** (2014) 212003, [arXiv:1310.3887].

[13] T. Blake, M. Gersabeck, L. Hofer, S. Jäger, Z. Liu, and R. Zwicky, *Round table: Flavour anomalies in b ⟶ sl+l– processes*, *EPJ Web Conf.* **137** (2017) 01001, [arXiv:1703.10005].

[14] J. Aebischer, W. Altmannshofer, D. Guadagnoli, M. Reboud, P. Stangl, and D. M. Straub, *B-decay discrepancies after Moriond 2019*, *Eur. Phys. J. C* **80** (2020), no. 3 252, [arXiv:1903.10434].

[15] **LHCb** Collaboration, R. Aaij et al., *Search for lepton-universality violation in $B^+ \to K^+\ell^+\ell^-$ decays*, *Phys. Rev. Lett.* **122** (2019), no. 19 191801, [arXiv:1903.09252].

[16] **Belle** Collaboration, A. Abdesselam et al., *Test of lepton flavor universality in $B \to K\ell^+\ell^-$ decays*, arXiv:1908.01848.

[17] **BaBar** Collaboration, J. Lees et al., *Measurement of Branching Fractions and Rate Asymmetries in the Rare Decays $B \to K^{(*)}l^+l^-$*, *Phys. Rev. D* **86** (2012) 032012, [arXiv:1204.3933].

[18] **Belle** Collaboration, A. Abdesselam et al., *Test of lepton flavor universality in $B \to K^*\ell^+\ell^-$ decays at Belle*, arXiv:1904.02440.

[19] **LHCb** Collaboration, R. Aaij et al., *Test of lepton universality with $B^0 \to K^{*0}\ell^+\ell^-$ decays*, *JHEP* **08** (2017) 055, [arXiv:1705.05802].

[20] P. Koppenburg, Z. Dolezal, and M. Smizanska, *Rare decays of b hadrons*, *Scholarpedia* **11** (2016) 32643, [arXiv:1606.00999].

[21] **HFLAV** Collaboration, Y. S. Amhis et al., *Averages of b-hadron, c-hadron, and τ-lepton properties as of 2018*, arXiv:1909.12524. updated results and plots available at https://hflav.web.cern.ch/.

[22] W. Buchmuller and D. Wyler, *Effective Lagrangian Analysis of New Interactions and Flavor Conservation*, *Nucl. Phys. B* **268** (1986) 621–653.

[23] B. Grzadkowski, M. Iskrzynski, M. Misiak, and J. Rosiek, *Dimension-Six Terms in the Standard Model Lagrangian*, *JHEP* **10** (2010) 085, [arXiv:1008.4884].

[24] S. Glashow, *Partial Symmetries of Weak Interactions*, *Nucl. Phys.* **22** (1961) 579–588.

[25] S. Weinberg, *A Model of Leptons*, *Phys. Rev. Lett.* **19** (1967) 1264–1266.

[26] A. Salam, *Weak and Electromagnetic Interactions*, *Conf. Proc. C* **680519** (1968) 367–377.

[27] G. 't Hooft, *Renormalization of Massless Yang-Mills Fields*, *Nucl. Phys. B* **33** (1971) 173–199.

[28] S. Glashow, J. Iliopoulos, and L. Maiani, *Weak Interactions with Lepton-Hadron Symmetry*, *Phys. Rev. D* **2** (1970) 1285–1292.

[29] D. J. Gross and F. Wilczek, *Ultraviolet Behavior of Nonabelian Gauge Theories*, *Phys. Rev. Lett.* **30** (1973) 1343–1346.

[30] B. Pontecorvo, *Mesonium and anti-mesonium*, *Sov. Phys. JETP* **6** (1957) 429.

[31] Z. Maki, M. Nakagawa, and S. Sakata, *Remarks on the unified model of elementary particles*, *Prog. Theor. Phys.* **28** (1962) 870–880.

[32] J. N. Bahcall and R. K. Ulrich, *Solar models, neutrino experiments, and helioseismology*, *Rev. Mod. Phys.* **60** (Apr, 1988) 297–372.

[33] S. Turck-Chieze, S. Cahen, M. Casse, and C. Doom, *Revisiting the Standard Solar Model*, *APJ* **335** (Dec., 1988) 415.

[34] J. N. Bahcall and M. H. Pinsonneault, *Standard solar models, with and without helium diffusion, and the solar neutrino problem*, *Rev. Mod. Phys.* **64** (Oct, 1992) 885–926.

[35] J. N. Bahcall, M. H. Pinsonneault, and G. J. Wasserburg, *Solar models with helium and heavy-element diffusion*, *Rev. Mod. Phys.* **67** (Oct, 1995) 781–808.

[36] D. R. Morrison, *Review of solar models and solar neutrino experiments*, *Part. World* **3** (1992), no. 1 30–39.

[37] R. Davis, *Solar neutrinos. ii. experimental*, *Phys. Rev. Lett.* **12** (Mar, 1964) 303–305.

[38] **Kamiokande-II** Collaboration, K. Hirata et al., *Observation of B-8 Solar Neutrinos in the Kamiokande-II Detector*, *Phys. Rev. Lett.* **63** (1989) 16.

[39] **Kamiokande-II** Collaboration, K. Hirata et al., *Results from one thousand days of real time directional solar neutrino data*, *Phys. Rev. Lett.* **65** (1990) 1297–1300.

[40] **GALLEX** Collaboration, W. Hampel et al., *GALLEX solar neutrino observations: Results for GALLEX IV*, *Phys. Lett. B* **447** (1999) 127–133.

[41] **SAGE** Collaboration, J. Abdurashitov et al., *Measurement of the solar neutrino capture rate with gallium metal*, *Phys. Rev. C* **60** (1999) 055801, [astro-ph/9907113].

[42] **SNO** Collaboration, Q. Ahmad et al., *Measurement of the rate of $\nu_e + d \to p + p + e^-$ interactions produced by ^8B solar neutrinos at the Sudbury Neutrino Observatory*, *Phys. Rev. Lett.* **87** (2001) 071301, [nucl-ex/0106015].

[43] **SNO** Collaboration, Q. Ahmad et al., *Direct evidence for neutrino flavor transformation from neutral current interactions in the Sudbury Neutrino Observatory*, *Phys. Rev. Lett.* **89** (2002) 011301, [nucl-ex/0204008].

[44] **Kamiokande-II** Collaboration, K. Hirata et al., *Observation of a small atmospheric muon-neutrino / electron-neutrino ratio in Kamiokande*, *Phys. Lett. B* **280** (1992) 146–152.

[45] R. Becker-Szendy et al., *Neutrino measurements with the IMB detector*, *Nucl. Phys. B Proc. Suppl.* **38** (1995) 331–336.

[46] **Super-Kamiokande** Collaboration, Y. Fukuda et al., *Evidence for oscillation of atmospheric neutrinos*, *Phys. Rev. Lett.* **81** (1998) 1562–1567, [hep-ex/9807003].

[47] F. von Feilitzsch and N. Schmitz, eds., *Neutrino physics and astrophysics. Proceedings, 20th International Conference, Neutrino 2002, Munich, Germany, May 25-30, 2002*, vol. 118, 2003.

[48] M. Shiozawa, "Experimental results on atmospheric neutrinos in Super-Kamiokande-I." Neutrino 2002, 2002.

[49] **Super-Kamiokande** Collaboration, M. Smy, *Solar neutrino precision measurements using all 1496 days of Super-Kamiokande I data*, *Nucl. Phys. B Proc. Suppl.* **118** (2003) 25–32, [hep-ex/0208004].

[50] C. Giganti, S. Lavignac, and M. Zito, *Neutrino oscillations: The rise of the PMNS paradigm*, *Prog. Part. Nucl. Phys.* **98** (2018) 1–54, [arXiv:1710.00715].

[51] F. Capozzi, E. Di Valentino, E. Lisi, A. Marrone, A. Melchiorri, and A. Palazzo, *Global constraints on absolute neutrino masses and their ordering*, *Phys. Rev. D* **95** (2017), no. 9 096014, [arXiv:2003.08511]. [Addendum: Phys.Rev.D 101, 116013 (2020)].

[52] **KamLAND** Collaboration, K. Eguchi et al., *First results from KamLAND: Evidence for reactor anti-neutrino disappearance*, *Phys. Rev. Lett.* **90** (2003) 021802, [hep-ex/0212021].

[53] **T2K** Collaboration, K. Abe et al., *Measurements of neutrino oscillation in appearance and disappearance channels by the T2K experiment with 6.6×10^{20} protons on target*, *Phys. Rev. D* **91** (2015), no. 7 072010, [arXiv:1502.01550].

[54] **NOvA** Collaboration, P. Adamson et al., *Measurement of the neutrino mixing angle θ_{23} in NOvA*, *Phys. Rev. Lett.* **118** (2017), no. 15 151802, [arXiv:1701.05891].

[55] **Double Chooz** Collaboration, F. Ardellier et al., *Double Chooz: A Search for the neutrino mixing angle theta(13)*, hep-ex/0606025.

[56] **RENO** Collaboration, J. Ahn et al., *RENO: An Experiment for Neutrino Oscillation Parameter θ_{13} Using Reactor Neutrinos at Yonggwang*, arXiv:1003.1391.

[57] **Daya Bay** Collaboration, F. An et al., *The Detector System of The Daya Bay Reactor Neutrino Experiment*, *Nucl. Instrum. Meth. A* **811** (2016) 133–161, [arXiv:1508.03943].

[58] R. Shrock, *New Tests For, and Bounds On, Neutrino Masses and Lepton Mixing*, *Phys. Lett. B* **96** (1980) 159–164.

[59] **KATRIN** Collaboration, M. Aker et al., *Improved Upper Limit on the Neutrino Mass from a Direct Kinematic Method by KATRIN*, *Phys. Rev. Lett.* **123** (2019), no. 22 221802, [arXiv:1909.06048].

[60] **KATRIN** Collaboration, M. Aker et al., *First operation of the KATRIN experiment with tritium*, *Eur. Phys. J. C* **80** (2020), no. 3 264, [arXiv:1909.06069].

[61] J. Schechter and J. Valle, *Neutrinoless Double beta Decay in SU(2) x U(1) Theories*, *Phys. Rev. D* **25** (1982) 2951.

[62] E. Takasugi, *Can the Neutrinoless Double Beta Decay Take Place in the Case of Dirac Neutrinos?*, *Phys. Lett. B* **149** (1984) 372–376.

[63] M. Hirsch, S. Kovalenko, and I. Schmidt, *Extended black box theorem for lepton number and flavor violating processes*, *Phys. Lett. B* **642** (2006) 106–110, [hep-ph/0608207].

[64] M. J. Dolinski, A. W. Poon, and W. Rodejohann, *Neutrinoless Double-Beta Decay: Status and Prospects*, *Ann. Rev. Nucl. Part. Sci.* **69** (2019) 219–251, [arXiv:1902.04097].

[65] **Planck** Collaboration, N. Aghanim et al., *Planck 2018 results. VI. Cosmological parameters*, arXiv:1807.06209.

[66] P. Minkowski, *$\mu \to e\gamma$ at a rate of one out of 10^9 muon decays?*, *Physics Letters B* **67** (1977), no. 4 421 – 428.

[67] T. Yanagida, *Horizontal gauge symmetry and masses of neutrinos*, *Conf. Proc.* **C7902131** (1979) 95–99.

[68] M. Gell-Mann, P. Ramond, and R. Slansky, *Complex Spinors and Unified Theories*, *Conf. Proc.* **C790927** (1979) 315–321, [arXiv:1306.4669].

[69] R. N. Mohapatra and G. Senjanović, *Neutrino mass and spontaneous parity nonconservation*, *Phys. Rev. Lett.* **44** (Apr, 1980) 912–915.

[70] S. L. Glashow, *The Future of Elementary Particle Physics*, *NATO Sci. Ser. B* **61** (1980) 687.

[71] M. Magg and C. Wetterich, *Neutrino Mass Problem and Gauge Hierarchy*, *Phys. Lett.* **94B** (1980) 61–64.

[72] J. Schechter and J. W. F. Valle, *Neutrino masses in su(2) $\bigotimes$ u(1) theories*, *Phys. Rev. D* **22** (Nov, 1980) 2227–2235.

[73] G. Lazarides, Q. Shafi, and C. Wetterich, *Proton lifetime and fermion masses in an so(10) model*, *Nuclear Physics B* **181** (1981), no. 2 287 – 300.

[74] C. Wetterich, *Neutrino Masses and the Scale of B-L Violation*, *Nucl. Phys.* **B187** (1981) 343–375.

[75] R. N. Mohapatra and G. Senjanović, *Neutrino masses and mixings in gauge models with spontaneous parity violation*, *Phys. Rev. D* **23** (Jan, 1981) 165–180.

[76] R. Foot, H. Lew, X. G. He, and G. C. Joshi, *Seesaw Neutrino Masses Induced by a Triplet of Leptons*, *Z. Phys.* **C44** (1989) 441.

[77] A. Zee, *A Theory of Lepton Number Violation, Neutrino Majorana Mass, and Oscillation*, *Phys. Lett.* **93B** (1980) 389. [Erratum: Phys. Lett.95B,461(1980)].

[78] A. Zee, *Quantum Numbers of Majorana Neutrino Masses*, *Nucl. Phys.* **B264** (1986) 99–110.

[79] K. S. Babu, *Model of 'Calculable' Majorana Neutrino Masses*, *Phys. Lett.* **B203** (1988) 132–136.

[80] A. de Gouvea and J. Jenkins, *A Survey of Lepton Number Violation Via Effective Operators*, *Phys. Rev.* **D77** (2008) 013008, [arXiv:0708.1344].

[81] **ATLAS** Collaboration, G. Aad et al., *Search for doubly-charged Higgs bosons in like-sign dilepton final states at $\sqrt{s} = 7$ TeV with the ATLAS detector*, *Eur. Phys. J. C* **72** (2012) 2244, [arXiv:1210.5070].

[82] **ATLAS** Collaboration, G. Aad et al., *Search for anomalous production of prompt same-sign lepton pairs and pair-produced doubly charged Higgs bosons with $\sqrt{s} = 8$ TeV pp collisions using the ATLAS detector*, *JHEP* **03** (2015) 041, [arXiv:1412.0237].

[83] **ATLAS** Collaboration, M. Aaboud et al., *Search for doubly charged Higgs boson production in multi-lepton final states with the ATLAS detector using proton–proton collisions at $\sqrt{s} = 13$ TeV*, *Eur. Phys. J. C* **78** (2018), no. 3 199, [arXiv:1710.09748].

[84] **CMS** Collaboration, S. Chatrchyan et al., *A Search for a Doubly-Charged Higgs Boson in pp Collisions at $\sqrt{s} = 7$ TeV*, *Eur. Phys. J. C* **72** (2012) 2189, [arXiv:1207.2666].

[85] **CMS** Collaboration, *Search for a doubly-charged Higgs boson with $\sqrt{s} = 8$ TeV pp collisions at the CMS experiment*, .

[86] **CMS** Collaboration, *A search for doubly-charged Higgs boson production in three and four lepton final states at $\sqrt{s} = 13$ TeV*, .

[87] L. Wolfenstein, *A Theoretical Pattern for Neutrino Oscillations*, *Nucl. Phys. B* **175** (1980) 93–96.

[88] S. M. Boucenna, S. Morisi, and J. W. F. Valle, *The low-scale approach to neutrino masses*, *Adv. High Energy Phys.* **2014** (2014) 831598, [arXiv:1404.3751].

[89] Y. Cai, J. Herrero-García, M. A. Schmidt, A. Vicente, and R. R. Volkas, *From the trees to the forest: a review of radiative neutrino mass models*, *Front.in Phys.* **5** (2017) 63, [arXiv:1706.08524].

[90] Y. Farzan, S. Pascoli, and M. A. Schmidt, *Recipes and Ingredients for Neutrino Mass at Loop Level*, *JHEP* **03** (2013) 107, [arXiv:1208.2732].

[91] F. Bonnet, M. Hirsch, T. Ota, and W. Winter, *Systematic study of the d=5 Weinberg operator at one-loop order*, *JHEP* **07** (2012) 153, [arXiv:1204.5862].

[92] D. Aristizabal Sierra, A. Degee, L. Dorame, and M. Hirsch, *Systematic classification of two-loop realizations of the Weinberg operator*, *JHEP* **03** (2015) 040, [arXiv:1411.7038].

[93] R. Cepedello, R. M. Fonseca, and M. Hirsch, *Systematic classification of three-loop realizations of the Weinberg operator*, *JHEP* **10** (2018) 197, [arXiv:1807.00629].

[94] R. Cepedello, M. Hirsch, and J. Helo, *Loop neutrino masses from $d = 7$ operator*, *JHEP* **07** (2017) 079, [arXiv:1705.01489].

[95] K. S. Babu and C. N. Leung, *Classification of effective neutrino mass operators*, *Nucl. Phys.* **B619** (2001) 667–689, [hep-ph/0106054].

[96] P. W. Angel, N. L. Rodd, and R. R. Volkas, *Origin of neutrino masses at the lhc: $\Delta l = 2$ effective operators and their ultraviolet completions*, *Phys. Rev. D* **87** (Apr, 2013) 073007.

[97] Y. Cai, J. D. Clarke, M. A. Schmidt, and R. R. Volkas, *Testing Radiative Neutrino Mass Models at the LHC*, *JHEP* **02** (2015) 161, [arXiv:1410.0689].

[98] F. Bonnet, D. Hernandez, T. Ota, and W. Winter, *Neutrino masses from higher than d=5 effective operators*, *JHEP* **10** (2009) 076, [arXiv:0907.3143].

[99] G. Anamiati, O. Castillo-Felisola, R. M. Fonseca, J. C. Helo, and M. Hirsch, *High-dimensional neutrino masses*, *JHEP* **12** (2018) 066, [arXiv:1806.07264].

[100] C. Klein, M. Lindner, and S. Ohmer, *Minimal Radiative Neutrino Masses*, *JHEP* **03** (2019) 018, [arXiv:1901.03225].

[101] C. Klein, M. Lindner, and S. Vogl, *Radiative neutrino masses and successful $SU(5)$ unification*, *Phys. Rev. D* **100** (2019), no. 7 075024, [arXiv:1907.05328].

[102] H. K. Dreiner, H. E. Haber, and S. P. Martin, *Two-component spinor techniques and Feynman rules for quantum field theory and supersymmetry*, *Phys. Rept.* **494** (2010) 1–196, [arXiv:0812.1594].

[103] B. Henning, X. Lu, and H. Murayama, *How to use the Standard Model effective field theory*, *JHEP* **01** (2016) 023, [arXiv:1412.1837].

[104] I. Brivio and M. Trott, *The Standard Model as an Effective Field Theory*, *Phys. Rept.* **793** (2019) 1–98, [arXiv:1706.08945].

[105] L. Lehman and A. Martin, *Hilbert Series for Constructing Lagrangians: expanding the phenomenologist's toolbox*, *Phys. Rev.* **D91** (2015) 105014, [arXiv:1503.07537].

[106] B. Henning, X. Lu, T. Melia, and H. Murayama, *Hilbert series and operator bases with derivatives in effective field theories*, *Commun. Math. Phys.* **347** (2016), no. 2 363–388, [arXiv:1507.07240].

[107] L. Lehman and A. Martin, *Low-derivative operators of the Standard Model effective field theory via Hilbert series methods*, *JHEP* **02** (2016) 081, [arXiv:1510.00372].

[108] B. Henning, X. Lu, T. Melia, and H. Murayama, *2, 84, 30, 993, 560, 15456, 11962, 261485, ...: Higher dimension operators in the SM EFT*, *JHEP* **08** (2017) 016, [arXiv:1512.03433]. [Erratum: JHEP09,019(2019)].

[109] B. Henning, X. Lu, T. Melia, and H. Murayama, *Operator bases, S-matrices, and their partition functions*, *JHEP* **10** (2017) 199, [arXiv:1706.08520].

[110] A. Kobach, *Baryon Number, Lepton Number, and Operator Dimension in the Standard Model*, *Phys. Lett. B* **758** (2016) 455–457, [arXiv:1604.05726].

[111] J. Aebischer et al., *WCxf: an exchange format for Wilson coefficients beyond the Standard Model*, *Comput. Phys. Commun.* **232** (2018) 71–83, [arXiv:1712.05298].

[112] E. E. Jenkins, A. V. Manohar, and P. Stoffer, *Low-Energy Effective Field Theory below the Electroweak Scale: Operators and Matching*, *JHEP* **03** (2018) 016, [arXiv:1709.04486].

[113] J. Aebischer, M. Fael, C. Greub, and J. Virto, *B physics Beyond the Standard Model at One Loop: Complete Renormalization Group Evolution below the Electroweak Scale*, *JHEP* **09** (2017) 158, [arXiv:1704.06639].

[114] E. E. Jenkins, A. V. Manohar, and P. Stoffer, *Low-Energy Effective Field Theory below the Electroweak Scale: Anomalous Dimensions*, *JHEP* **01** (2018) 084, [arXiv:1711.05270].

[115] J. Aebischer, A. Crivellin, M. Fael, and C. Greub, *Matching of gauge invariant dimension-six operators for $b \to s$ and $b \to c$ transitions*, *JHEP* **05** (2016) 037, [arXiv:1512.02830].

[116] G. Buchalla, A. J. Buras, and M. E. Lautenbacher, *Weak decays beyond leading logarithms*, *Rev. Mod. Phys.* **68** (1996) 1125–1144, [hep-ph/9512380].

[117] C. Arzt, *Reduced effective Lagrangians*, *Phys. Lett. B* **342** (1995) 189–195, [hep-ph/9304230].

[118] H. Georgi, *On-shell effective field theory*, *Nucl. Phys. B* **361** (1991) 339–350.

[119] J. Gasser and H. Leutwyler, *Chiral Perturbation Theory to One Loop*, *Annals Phys.* **158** (1984) 142.

[120] J. Gasser and H. Leutwyler, *Chiral Perturbation Theory: Expansions in the Mass of the Strange Quark*, *Nucl. Phys. B* **250** (1985) 465–516.

[121] A. De Rujula, M. Gavela, P. Hernandez, and E. Masso, *The Selfcouplings of vector bosons: Does LEP-1 obviate LEP-2?*, *Nucl. Phys. B* **384** (1992) 3–58.

[122] J. Chisholm, *Change of variables in quantum field theories*, *Nuclear Physics* **26** (1961), no. 3 469 – 479.

[123] S. Kamefuchi, L. O'Raifeartaigh, and A. Salam, *Change of variables and equivalence theorems in quantum field theories*, *Nucl. Phys.* **28** (1961) 529–549.

[124] P. Divakaran, *Equivalence theorems and point transformations in field theory*, *Nuclear Physics* **42** (1963) 235–246.

[125] M. Bergere and Y.-M. P. Lam, *Equivalence Theorem and Faddeev-Popov Ghosts*, *Phys. Rev. D* **13** (1976) 3247–3255.

[126] H. Sharatchandra, *The equivalence theorem is subtle*, *Annals of Physics* **116** (1978), no. 2 408 – 418.

[127] A. Salam and J. Strathdee, *Equivalent formulations of massive vector field theories*, *Phys. Rev. D* **2** (Dec, 1970) 2869–2876.

[128] R. Kallosh and I. Tyutin, *The Equivalence theorem and gauge invariance in renormalizable theories*, *Yad. Fiz.* **17** (1973) 190–209.

[129] H. Lehmann, K. Symanzik, and W. Zimmermann, *On the formulation of quantized field theories*, *Nuovo Cim.* **1** (1955) 205–225.

[130] P. Pouliot, *Molien function for duality*, *JHEP* **01** (1999) 021, [hep-th/9812015].

[131] S. Benvenuti, B. Feng, A. Hanany, and Y.-H. He, *Counting BPS Operators in Gauge Theories: Quivers, Syzygies and Plethystics*, *JHEP* **11** (2007) 050, [hep-th/0608050].

[132] F. Dolan, *Counting BPS operators in N=4 SYM*, *Nucl. Phys. B* **790** (2008) 432–464, [arXiv:0704.1038].

[133] A. Hanany, E. E. Jenkins, A. V. Manohar, and G. Torri, *Hilbert Series for Flavor Invariants of the Standard Model*, *JHEP* **03** (2011) 096, [arXiv:1010.3161].

[134] E. E. Jenkins and A. V. Manohar, *Algebraic Structure of Lepton and Quark Flavor Invariants and CP Violation*, *JHEP* **10** (2009) 094, [arXiv:0907.4763].

[135] A. Hanany and R. Kalveks, *Highest Weight Generating Functions for Hilbert Series*, *JHEP* **10** (2014) 152, [arXiv:1408.4690].

[136] A. Hanany, N. Mekareeya, and G. Torri, *The Hilbert Series of Adjoint SQCD*, *Nucl. Phys. B* **825** (2010) 52–97, [arXiv:0812.2315].

[137] R. Feger and T. W. Kephart, *LieART—A Mathematica application for Lie algebras and representation theory*, *Comput. Phys. Commun.* **192** (2015) 166–195, [arXiv:1206.6379].

[138] T. Ma, J. Shu, and M.-L. Xiao, *Standard Model Effective Field Theory from On-shell Amplitudes*, arXiv:1902.06752.

[139] B. Henning and T. Melia, *Constructing effective field theories via their harmonics*, *Phys. Rev. D* **100** (2019), no. 1 016015, [arXiv:1902.06754].

[140] H.-L. Li, Z. Ren, J. Shu, M.-L. Xiao, J.-H. Yu, and Y.-H. Zheng, *Complete Set of Dimension-8 Operators in the Standard Model Effective Field Theory*, arXiv:2005.00008.

[141] H.-L. Li, Z. Ren, M.-L. Xiao, J.-H. Yu, and Y.-H. Zheng, *Complete Set of Dimension-9 Operators in the Standard Model Effective Field Theory*, arXiv:2007.07899.

[142] **Muon g-2** Collaboration, G. Bennett et al., *Final Report of the Muon E821 Anomalous Magnetic Moment Measurement at BNL*, *Phys. Rev. D* **73** (2006) 072003, [hep-ex/0602035].

[143] T. Blum, A. Denig, I. Logashenko, E. de Rafael, B. L. Roberts, T. Teubner, and G. Venanzoni, *The Muon (g-2) Theory Value: Present and Future*, arXiv:1311.2198.

[144] R. H. Parker, C. Yu, W. Zhong, B. Estey, and H. Müller, *Measurement of the fine-structure constant as a test of the standard model*, *Science* **360** (Apr, 2018) 191–195.

[145] **LHCb** Collaboration, R. Aaij et al., *Differential branching fractions and isospin asymmetries of $B \to K^{(*)}\mu^+\mu^-$ decays*, *JHEP* **06** (2014) 133, [arXiv:1403.8044].

[146] **LHCb** Collaboration, R. Aaij et al., *Angular analysis and differential branching fraction of the decay $B_s^0 \to \phi\mu^+\mu^-$*, *JHEP* **09** (2015) 179, [arXiv:1506.08777].

[147] **CMS Collaboration** Collaboration, *Measurement of properties of Bs0 to mu+mu- decays and search for B0 to mu+mu- with the CMS experiment*, Tech. Rep. CMS-PAS-BPH-16-004, CERN, Geneva, 2019.

[148] **LHCb** Collaboration, R. Aaij et al., *First Evidence for the Decay $B_s^0 \to \mu^+\mu^-$*, *Phys. Rev. Lett.* **110** (2013), no. 2 021801, [arXiv:1211.2674].

[149] **LHCb** Collaboration, R. Aaij et al., *Measurement of the $B_s^0 \to \mu^+\mu^-$ branching fraction and effective lifetime and search for $B^0 \to \mu^+\mu^-$ decays*, *Phys. Rev. Lett.* **118** (2017), no. 19 191801, [arXiv:1703.05747].

[150] **ATLAS** Collaboration, M. Aaboud et al., *Study of the rare decays of B_s^0 and B^0 mesons into muon pairs using data collected during 2015 and 2016 with the ATLAS detector*, *JHEP* **04** (2019) 098, [arXiv:1812.03017].

[151] **LHCb** Collaboration, R. Aaij et al., *Differential branching fraction and angular analysis of $\Lambda_b^0 \to \Lambda\mu^+\mu^-$ decays*, *JHEP* **06** (2015) 115, [arXiv:1503.07138]. [Erratum: JHEP 09, 145 (2018)].

[152] F. Kruger, L. M. Sehgal, N. Sinha, and R. Sinha, *Angular distribution and CP asymmetries in the decays $\bar{B} \to K^-\pi^+e^-e^+$ and $\bar{B} \to \pi^-\pi^+e^-e^+$*, *Phys. Rev. D* **61** (2000) 114028, [hep-ph/9907386]. [Erratum: Phys.Rev.D 63, 019901 (2001)].

[153] U. Egede and J. Serrano, *Rare b-hadron decays*, *Comptes Rendus Physique* **21** (2020), no. 1 93–106.

[154] C. Bobeth, M. Gorbahn, T. Hermann, M. Misiak, E. Stamou, and M. Steinhauser, *$B_{s,d} \to l^+l^-$ in the Standard Model with Reduced Theoretical Uncertainty*, *Phys. Rev. Lett.* **112** (2014) 101801, [arXiv:1311.0903].

[155] G. Hiller and F. Krüger, *More model-independent analysis of $b \to s$ processes*, *Phys. Rev.* **D69** (2004) 074020, [hep-ph/0310219].

[156] B. Capdevila, A. Crivellin, S. Descotes-Genon, J. Matias, and J. Virto, *Patterns of New Physics in $b \to s\ell^+\ell^-$ transitions in the light of recent data*, arXiv:1704.05340.

[157] B. Capdevila, S. Descotes-Genon, J. Matias, and J. Virto, *Assessing lepton-flavour non-universality from $B \to K^*\ell\ell$ angular analyses*, *JHEP* **10** (2016) 075, [arXiv:1605.03156].

[158] C. Bobeth, G. Hiller, and G. Piranishvili, *Angular distributions of $\bar{B} \to \bar{K}\ell^+\ell^-$ decays*, *JHEP* **12** (2007) 040, [arXiv:0709.4174].

[159] A. Ali, T. Mannel, and T. Morozumi, *Forward backward asymmetry of dilepton angular distribution in the decay b —> s l+ l-*, *Phys. Lett. B* **273** (1991) 505–512.

[160] U. Egede, T. Hurth, J. Matias, M. Ramon, and W. Reece, *New observables in the decay mode $\bar{B}_d \to \bar{K}^{*0}l^+l^-$*, *JHEP* **11** (2008) 032, [arXiv:0807.2589].

[161] S. Descotes-Genon, T. Hurth, J. Matias, and J. Virto, *Optimizing the basis of $B \to K^* ll$ observables in the full kinematic range*, *JHEP* **05** (2013) 137, [arXiv:1303.5794].

[162] **LHCb** Collaboration, R. Aaij et al., *Measurement of Form-Factor-Independent Observables in the Decay $B^0 \to K^{*0}\mu^+\mu^-$*, *Phys. Rev. Lett.* **111** (2013) 191801, [arXiv:1308.1707].

[163] **LHCb** Collaboration, R. Aaij et al., *Measurement of CP-Averaged Observables in the $B^0 \to K^{*0}\mu^+\mu^-$ Decay*, *Phys. Rev. Lett.* **125** (2020), no. 1 011802, [arXiv:2003.04831].

[164] **Belle** Collaboration, S. Wehle et al., *Lepton-Flavor-Dependent Angular Analysis of $B \to K^*\ell^+\ell^-$*, *Phys. Rev. Lett.* **118** (2017), no. 11 111801, [arXiv:1612.05014].

[165] **ATLAS** Collaboration, M. Aaboud et al., *Angular analysis of $B^0_d \to K^*\mu^+\mu^-$ decays in pp collisions at $\sqrt{s} = 8$ TeV with the ATLAS detector*, *JHEP* **10** (2018) 047, [arXiv:1805.04000].

[166] **CMS** Collaboration, A. M. Sirunyan et al., *Measurement of angular parameters from the decay $\mathrm{B}^0 \to \mathrm{K}^{*0}\mu^+\mu^-$ in proton-proton collisions at $\sqrt{s} = 8$ TeV*, *Phys. Lett. B* **781** (2018) 517–541, [arXiv:1710.02846].

[167] S. Descotes-Genon, L. Hofer, J. Matias, and J. Virto, *On the impact of power corrections in the prediction of $B \to K^*\mu^+\mu^-$ observables*, *JHEP* **12** (2014) 125, [arXiv:1407.8526].

[168] A. Khodjamirian, T. Mannel, A. Pivovarov, and Y.-M. Wang, *Charm-loop effect in $B \to K^{(*)}\ell^+\ell^-$ and $B \to K^*\gamma$*, *JHEP* **09** (2010) 089, [arXiv:1006.4945].

[169] M. Algueró, B. Capdevila, A. Crivellin, S. Descotes-Genon, P. Masjuan, J. Matias, M. Novoa Brunet, and J. Virto, *Emerging patterns of New Physics with and without Lepton Flavour Universal contributions*, *Eur. Phys. J. C* **79** (2019), no. 8 714, [arXiv:1903.09578]. [Addendum: Eur.Phys.J.C 80, 511 (2020)].

[170] A. Arbey, T. Hurth, F. Mahmoudi, D. M. Santos, and S. Neshatpour, *Update on the $b \longrightarrow s$ anomalies*, *Phys. Rev. D* **100** (2019), no. 1 015045, [arXiv:1904.08399].

[171] M. Ciuchini, A. M. Coutinho, M. Fedele, E. Franco, A. Paul, L. Silvestrini, and M. Valli, *New Physics in $b \to s\ell^+\ell^-$ confronts new data on Lepton Universality*, *Eur. Phys. J. C* **79** (2019), no. 8 719, [arXiv:1903.09632].

[172] S. Descotes-Genon, J. Matias, and J. Virto, *Understanding the $B \to K^*\mu^+\mu^-$ Anomaly*, *Phys. Rev. D* **88** (2013) 074002, [arXiv:1307.5683].

[173] W. Altmannshofer and D. M. Straub, *Implications of $b \to s$ measurements*, in *50th Rencontres de Moriond on EW Interactions and Unified Theories*, pp. 333–338, 3, 2015. arXiv:1503.06199.

[174] S. Descotes-Genon, L. Hofer, J. Matias, and J. Virto, *Global analysis of $b \to s\ell\ell$ anomalies*, *JHEP* **06** (2016) 092, [arXiv:1510.04239].

[175] **BaBar** Collaboration, J. Lees et al., *Evidence for an excess of $\bar{B} \to D^{(*)}\tau^-\bar{\nu}_\tau$ decays*, *Phys. Rev. Lett.* **109** (2012) 101802, [arXiv:1205.5442].

[176] **BaBar** Collaboration, J. Lees et al., *Measurement of an Excess of $\bar{B} \to D^{(*)}\tau^-\bar{\nu}_\tau$ Decays and Implications for Charged Higgs Bosons*, *Phys. Rev. D* **88** (2013), no. 7 072012, [arXiv:1303.0571].

[177] **Belle** Collaboration, M. Huschle et al., *Measurement of the branching ratio of $\bar{B} \to D^{(*)}\tau^-\bar{\nu}_\tau$ relative to $\bar{B} \to D^{(*)}\ell^-\bar{\nu}_\ell$ decays with hadronic tagging at Belle*, *Phys. Rev. D* **92** (2015), no. 7 072014, [arXiv:1507.03233].

[178] **Belle** Collaboration, S. Hirose et al., *Measurement of the τ lepton polarization and $R(D^*)$ in the decay $\bar{B} \to D^*\tau^-\bar{\nu}_\tau$*, *Phys. Rev. Lett.* **118** (2017), no. 21 211801, [arXiv:1612.00529].

[179] **Belle** Collaboration, S. Hirose et al., *Measurement of the τ lepton polarization and $R(D^*)$ in the decay $\bar{B} \to D^*\tau^-\bar{\nu}_\tau$ with one-prong hadronic τ decays at Belle*, *Phys. Rev. D* **97** (2018), no. 1 012004, [arXiv:1709.00129].

[180] **Belle** Collaboration, A. Abdesselam et al., *Measurement of $\mathcal{R}(D)$ and $\mathcal{R}(D^*)$ with a semileptonic tagging method*, arXiv:1904.08794.

[181] **LHCb** Collaboration, R. Aaij et al., *Measurement of the ratio of branching fractions $\mathcal{B}(\bar{B}^0 \to D^{*+}\tau^-\bar{\nu}_\tau)/\mathcal{B}(\bar{B}^0 \to D^{*+}\mu^-\bar{\nu}_\mu)$*, *Phys. Rev. Lett.* **115** (2015), no. 11 111803, [arXiv:1506.08614]. [Erratum: Phys.Rev.Lett. 115, 159901 (2015)].

[182] **LHCb** Collaboration, R. Aaij et al., *Measurement of the ratio of the $B^0 \to D^{*-}\tau^+\nu_\tau$ and $B^0 \to D^{*-}\mu^+\nu_\mu$ branching fractions using three-prong τ-lepton decays*, *Phys. Rev. Lett.* **120** (2018), no. 17 171802, [arXiv:1708.08856].

[183] **LHCb** Collaboration, R. Aaij et al., *Test of Lepton Flavor Universality by the measurement of the $B^0 \to D^{*-}\tau^+\nu_\tau$ branching fraction using three-prong τ decays*, *Phys. Rev. D* **97** (2018), no. 7 072013, [arXiv:1711.02505].

[184] D. Bigi and P. Gambino, *Revisiting $B \to D\ell\nu$*, *Phys. Rev. D* **94** (2016), no. 9 094008, [arXiv:1606.08030].

[185] F. U. Bernlochner, Z. Ligeti, M. Papucci, and D. J. Robinson, *Combined analysis of semileptonic B decays to D and D^*: $R(D^{(*)})$, $|V_{cb}|$, and new physics*, *Phys. Rev. D* **95** (2017), no. 11 115008, [arXiv:1703.05330]. [Erratum: Phys.Rev.D 97, 059902 (2018)].

[186] D. Bigi, P. Gambino, and S. Schacht, *$R(D^*)$, $|V_{cb}|$, and the Heavy Quark Symmetry relations between form factors*, *JHEP* **11** (2017) 061, [arXiv:1707.09509].

[187] S. Jaiswal, S. Nandi, and S. K. Patra, *Extraction of $|V_{cb}|$ from $B \to D^{(*)}\ell\nu_\ell$ and the Standard Model predictions of $R(D^{(*)})$*, *JHEP* **12** (2017) 060, [arXiv:1707.09977].

[188] M. Freytsis, Z. Ligeti, and J. T. Ruderman, *Flavor models for $\bar{B} \to D^{(*)}\tau\bar{\nu}$*, *Phys. Rev. D* **92** (2015), no. 5 054018, [arXiv:1506.08896].

[189] **LHCb** Collaboration, R. Aaij et al., *Measurement of the ratio of branching fractions $\mathcal{B}(B_c^+ \to J/\psi\tau^+\nu_\tau)/\mathcal{B}(B_c^+ \to J/\psi\mu^+\nu_\mu)$*, *Phys. Rev. Lett.* **120** (2018), no. 12 121801, [arXiv:1711.05623].

[190] A. Yu. Anisimov, I. M. Narodetsky, C. Semay, and B. Silvestre-Brac, *The B_c meson lifetime in the light front constituent quark model*, *Phys. Lett.* **B452** (1999) 129–136, [hep-ph/9812514].

[191] V. V. Kiselev, *Exclusive decays and lifetime of B_c meson in QCD sum rules*, hep-ph/0211021.

[192] M. A. Ivanov, J. G. Korner, and P. Santorelli, *Exclusive semileptonic and nonleptonic decays of the B_c meson*, *Phys. Rev.* **D73** (2006) 054024, [hep-ph/0602050].

[193] E. Hernandez, J. Nieves, and J. M. Verde-Velasco, *Study of exclusive semileptonic and non-leptonic decays of B_c in a nonrelativistic quark model*, *Phys. Rev.* **D74** (2006) 074008, [hep-ph/0607150].

[194] T. Huang and F. Zuo, *Semileptonic B_c decays and charmonium distribution amplitude*, *Eur. Phys. J.* **C51** (2007) 833–839, [hep-ph/0702147].

[195] W. Wang, Y.-L. Shen, and C.-D. Lu, *Covariant Light-Front Approach for B(c) transition form factors*, *Phys. Rev.* **D79** (2009) 054012, [arXiv:0811.3748].

[196] A. Issadykov and M. A. Ivanov, *The decays $B_c \to J/\psi + \bar{\ell}\nu_\ell$ and $B_c \to J/\psi + \pi(K)$ in covariant confined quark model*, *Phys. Lett.* **B783** (2018) 178–182, [arXiv:1804.00472].

[197] W.-F. Wang, Y.-Y. Fan, and Z.-J. Xiao, *Semileptonic decays $B_c \to (\eta_c, J/\Psi)lv$ in the perturbative QCD approach*, *Chin. Phys.* **C37** (2013) 093102, [arXiv:1212.5903].

[198] A. K. Alok, D. Kumar, J. Kumar, S. Kumbhakar, and S. U. Sankar, *New physics solutions for R_D and R_{D^*}*, *JHEP* **09** (2018) 152, [arXiv:1710.04127].

[199] A. Azatov, D. Bardhan, D. Ghosh, F. Sgarlata, and E. Venturini, *Anatomy of $b \to c\tau\nu$ anomalies*, *JHEP* **11** (2018) 187, [arXiv:1805.03209].

[200] X.-Q. Hu, S.-P. Jin, and Z.-J. Xiao, *Semileptonic decays $B_c \to (\eta_c, J/\psi) l\bar{\nu}_l$ in the "PQCD + Lattice" approach*, arXiv:1904.07530.

[201] D. Leljak, B. Melic, and M. Patra, *On lepton flavour universality in semileptonic $B_c \to \eta_c, J/\psi$ decays*, arXiv:1901.08368.

[202] K. Azizi, Y. Sarac, and H. Sundu, *Lepton flavour universality violation in semileptonic tree level weak transitions*, arXiv:1904.08267.

[203] C. Murgui, A. Peñuelas, M. Jung, and A. Pich, *Global fit to $b \to c\tau\nu$ transitions*, arXiv:1904.09311.

[204] **Belle** Collaboration, A. Abdesselam et al., *Measurement of the D^{*-} polarization in the decay $B^0 \to D^{*-}\tau^+\nu_\tau$*, in *10th International Workshop on the CKM Unitarity Triangle (CKM 2018) Heidelberg, Germany, September 17-21, 2018*, 2019. arXiv:1903.03102.

[205] P. Asadi, M. R. Buckley, and D. Shih, *Asymmetry Observables and the Origin of $R_{D^{(*)}}$ Anomalies*, *Phys. Rev.* **D99** (2019), no. 3 035015, [arXiv:1810.06597].

[206] R. Alonso, J. Martin Camalich, and S. Westhoff, *Tau properties in $B \to D\tau\nu$ from visible final-state kinematics*, *Phys. Rev.* **D95** (2017), no. 9 093006, [arXiv:1702.02773].

[207] **Muon g-2** Collaboration, A. Chapelain, *The Muon g-2 experiment at Fermilab*, *EPJ Web Conf.* **137** (2017) 08001, [arXiv:1701.02807].

[208] R. Parker, C. Yu, W. Zhong, B. Estey, and H. Mãeller, *Measurement of the fine-structure constant as a test of the standard model*, *Science* **360** (04, 2018) 191–195.

[209] R. Alonso, B. Grinstein, and J. Martin Camalich, *Lepton universality violation and lepton flavor conservation in B-meson decays*, *JHEP* **10** (2015) 184, [arXiv:1505.05164].

[210] M. Bauer and M. Neubert, *Minimal Leptoquark Explanation for the $R_{D^{(*)}}$, R_K, and $(g-2)_\mu$ Anomalies*, *Phys. Rev. Lett.* **116** (2016), no. 14 141802, [arXiv:1511.01900].

[211] D. Bečirević, N. Košnik, O. Sumensari, and R. Zukanovich Funchal, *Palatable Leptoquark Scenarios for Lepton Flavor Violation in Exclusive $b \to s\ell_1\ell_2$ modes*, *JHEP* **11** (2016) 035, [arXiv:1608.07583].

[212] D. Bečirević, S. Fajfer, N. Košnik, and O. Sumensari, *Leptoquark model to explain the B-physics anomalies, R_K and R_D*, *Phys. Rev.* **D94** (2016), no. 11 115021, [arXiv:1608.08501].

[213] S. M. Boucenna, A. Celis, J. Fuentes-Martin, A. Vicente, and J. Virto, *Non-abelian gauge extensions for B-decay anomalies*, *Phys. Lett.* **B760** (2016) 214–219, [arXiv:1604.03088].

[214] S. M. Boucenna, A. Celis, J. Fuentes-Martin, A. Vicente, and J. Virto, *Phenomenology of an $SU(2) \times SU(2) \times U(1)$ model with lepton-flavour non-universality*, *JHEP* **12** (2016) 059, [arXiv:1608.01349].

[215] L. Calibbi, A. Crivellin, and T. Ota, *Effective Field Theory Approach to $b \to s\ell\ell^{(\prime)}$, $B \to K(*)\nu\bar{\nu}$ and $B \to D(*)\tau\nu$ with Third Generation Couplings*, *Phys. Rev. Lett.* **115** (2015) 181801, [arXiv:1506.02661].

[216] A. Crivellin, D. Müller, and T. Ota, *Simultaneous Explanation of $R(D^{(*)})$ and $b \to s\mu^+\mu^-$: The Last Scalar Leptoquarks Standing*, arXiv:1703.09226.

[217] F. F. Deppisch, S. Kulkarni, H. Päs, and E. Schumacher, *Leptoquark patterns unifying neutrino masses, flavor anomalies, and the diphoton excess*, *Phys. Rev.* **D94** (2016), no. 1 013003, [arXiv:1603.07672].

[218] N. G. Deshpande and X.-G. He, *Consequences of R-parity violating interactions for anomalies in $\bar{B} \to D^{(*)}\tau\bar{\nu}$ and $b \to s\mu^+\mu^-$*, *Eur. Phys. J.* **C77** (2017), no. 2 134, [arXiv:1608.04817].

[219] S. Fajfer and N. Košnik, *Vector leptoquark resolution of R_K and $R_{D^{(*)}}$ puzzles*, *Phys. Lett.* **B755** (2016) 270–274, [arXiv:1511.06024].

[220] F. Feruglio, P. Paradisi, and A. Pattori, *Revisiting Lepton Flavor Universality in B Decays*, *Phys. Rev. Lett.* **118** (2017), no. 1 011801, [arXiv:1606.00524].

[221] F. Feruglio, P. Paradisi, and A. Pattori, *On the Importance of Electroweak Corrections for B Anomalies*, arXiv:1705.00929.

[222] E. Megias, M. Quiros, and L. Salas, *Lepton-flavor universality violation in $R_{D^{(*)}}$ and R_K from warped space*, arXiv:1703.06019.

[223] O. Popov and G. A. White, *One Leptoquark to unify them? Neutrino masses and unification in the light of $(g-2)_\mu$, $R_{D^{(*)}}$ and R_K anomalies*, arXiv:1611.04566.

[224] D. Bečirević, S. Fajfer, and N. Košnik, *Lepton flavor nonuniversality in $b \to s\ell^+\ell^-$ processes*, *Phys. Rev.* **D92** (2015), no. 1 014016, [arXiv:1503.09024].

[225] D. Bečirević and O. Sumensari, *A leptoquark model to accommodate $R_K^{\rm exp} < R_K^{\rm SM}$ and $R_{K^*}^{\rm exp} < R_{K^*}^{\rm SM}$*, arXiv:1704.05835.

[226] A. J. Buras and J. Girrbach, *Left-handed Z' and Z FCNC quark couplings facing new $b \to s\mu^+\mu^-$ data*, *JHEP* **12** (2013) 009, [arXiv:1309.2466].

[227] R. Gauld, F. Goertz, and U. Haisch, *On minimal Z' explanations of the $B \to K^*\mu^+\mu^-$ anomaly*, *Phys. Rev.* **D89** (2014) 015005, [arXiv:1308.1959].

[228] S. L. Glashow, D. Guadagnoli, and K. Lane, *Lepton Flavor Violation in B Decays?*, *Phys. Rev. Lett.* **114** (2015) 091801, [arXiv:1411.0565].

[229] B. Gripaios, M. Nardecchia, and S. A. Renner, *Composite leptoquarks and anomalies in B-meson decays*, *JHEP* **05** (2015) 006, [arXiv:1412.1791].

[230] G. Hiller and M. Schmaltz, *Diagnosing lepton-nonuniversality in $b \to s\ell\ell$*, *JHEP* **02** (2015) 055, [arXiv:1411.4773].

[231] G. Hiller and M. Schmaltz, *R_K and future $b \to s\ell\ell$ physics beyond the standard model opportunities*, *Phys. Rev.* **D90** (2014) 054014, [arXiv:1408.1627].

[232] F. Mahmoudi, S. Neshatpour, and J. Virto, *$B \to K^*\mu^+\mu^-$ optimised observables in the MSSM*, *Eur. Phys. J.* **C74** (2014), no. 6 2927, [arXiv:1401.2145].

[233] E. Megias, G. Panico, O. Pujolas, and M. Quiros, *A Natural origin for the LHCb anomalies*, *JHEP* **09** (2016) 118, [arXiv:1608.02362].

[234] H. Päs and E. Schumacher, *Common origin of R_K and neutrino masses*, *Phys. Rev.* **D92** (2015), no. 11 114025, [arXiv:1510.08757].

[235] S. Sahoo and R. Mohanta, *Leptoquark effects on $b \to s\nu\bar{\nu}$ and $B \to K\ell^+\ell^-$ decay processes*, *New J. Phys.* **18** (2016), no. 1 013032, [arXiv:1509.06248].

[236] S. Sahoo and R. Mohanta, *Study of the rare semileptonic decays $B_d^0 \to K^*\ell^+\ell^-$ in scalar leptoquark model*, *Phys. Rev.* **D93** (2016), no. 3 034018, [arXiv:1507.02070].

[237] Y. Sakaki, M. Tanaka, A. Tayduganov, and R. Watanabe, *Testing leptoquark models in $\bar{B} \to D^{(*)}\tau\bar{\nu}$*, *Phys. Rev.* **D88** (2013), no. 9 094012, [arXiv:1309.0301].

[238] D. Aristizabal Sierra, F. Staub, and A. Vicente, *Shedding light on the $b \to s$ anomalies with a dark sector*, *Phys. Rev.* **D92** (2015), no. 1 015001, [arXiv:1503.06077].

[239] I. de Medeiros Varzielas and G. Hiller, *Clues for flavor from rare lepton and quark decays*, *JHEP* **06** (2015) 072, [arXiv:1503.01084].

[240] S. de Boer and G. Hiller, *Flavor and new physics opportunities with rare charm decays into leptons*, *Phys. Rev.* **D93** (2016), no. 7 074001, [arXiv:1510.00311].

[241] K. Cheung, T. Nomura, and H. Okada, *Testable radiative neutrino mass model without additional symmetries and explanation for the $b \to s\ell^+\ell^-$ anomaly*, *Phys. Rev.* **D94** (2016), no. 11 115024, [arXiv:1610.02322].

[242] K. Cheung, T. Nomura, and H. Okada, *A Three-loop Neutrino Model with Leptoquark Triplet Scalars*, *Phys. Lett.* **B768** (2017) 359–364, [arXiv:1701.01080].

[243] K. Cheung, T. Nomura, and H. Okada, *Three-loop neutrino mass model with a colored triplet scalar*, *Phys. Rev.* **D95** (2017), no. 1 015026, [arXiv:1610.04986].

[244] K. S. Babu and J. Julio, *Two-Loop Neutrino Mass Generation through Leptoquarks*, *Nucl. Phys.* **B841** (2010) 130–156, [arXiv:1006.1092].

[245] D. Aristizabal Sierra, M. Hirsch, and S. G. Kovalenko, *Leptoquarks: Neutrino masses and accelerator phenomenology*, *Phys. Rev.* **D77** (2008) 055011, [arXiv:0710.5699].

[246] *Search for resonances decaying to photon pairs in 3.2 fb^{-1} of pp collisions at $\sqrt{s} = 13$ TeV with the ATLAS detector*, Tech. Rep. ATLAS-CONF-2015-081, CERN, Geneva, Dec, 2015.

[247] **CMS** Collaboration, *Search for new physics in high mass diphoton events in proton-proton collisions at 13TeV*, .

[248] *Search for new phenomena in the dilepton final state using proton-proton collisions at $\sqrt{s} = 13$ TeV with the ATLAS detector*, Tech. Rep. ATLAS-CONF-2015-070, CERN, Geneva, Dec, 2015.

[249] R. Franceschini, G. F. Giudice, J. F. Kamenik, M. McCullough, A. Pomarol, R. Rattazzi, M. Redi, F. Riva, A. Strumia, and R. Torre, *What is the $\gamma\gamma$ resonance at 750 GeV?*, *JHEP* **03** (2016) 144, [arXiv:1512.04933].

[250] Y. Kats and M. J. Strassler, *Resonances from QCD bound states and the 750 GeV diphoton excess*, *JHEP* **05** (2016) 092, [arXiv:1602.08819]. [Erratum: JHEP 07, 044 (2016)].

[251] D. Curtin and C. B. Verhaaren, *Quirky Explanations for the Diphoton Excess*, *Phys. Rev. D* **93** (2016), no. 5 055011, [arXiv:1512.05753].

[252] J. F. Kamenik and M. Redi, *Back to 1974: The Q-onium*, *Phys. Lett. B* **760** (2016) 158–163, [arXiv:1603.07719].

[253] P. Ko, C. Yu, and T.-C. Yuan, *Probing a new strongly interacting sector via composite diboson resonances*, *Phys. Rev. D* **95** (2017), no. 11 115034, [arXiv:1603.08802].

[254] N. D. Barrie, A. Kobakhidze, S. Liang, M. Talia, and L. Wu, *Heavy Leptonium as the Origin of the 750 GeV Diphoton Excess*, arXiv:1604.02803.

[255] E. D. Carlson, L. J. Hall, U. Sarid, and J. W. Burton, *Cornering color SU(5)*, *Phys. Rev. D* **44** (1991) 1555–1568.

[256] R. Foot, O. F. Hernandez, and T. G. Rizzo, *SU(5)-c COLOR MODEL SIGNATURES AT HADRON COLLIDERS*, *Phys. Lett. B* **246** (1990) 183–187.

[257] R. Foot, *Top quark forward-backward asymmetry from SU(N_c) color*, *Phys. Rev. D* **83** (2011) 114013, [arXiv:1103.1940].

[258] T. Gherghetta, N. Nagata, and M. Shifman, *A Visible QCD Axion from an Enlarged Color Group*, *Phys. Rev. D* **93** (2016), no. 11 115010, [arXiv:1604.01127].

[259] R. Foot and H. Lew, *QUARK - LEPTON SYMMETRIC MODEL*, *Phys. Rev. D* **41** (1990) 3502.

[260] R. Foot, H. Lew, and R. Volkas, *Phenomenology of quark - lepton symmetric models*, *Phys. Rev. D* **44** (1991) 1531–1546.

[261] R. Foot and R. Volkas, *Generalised leptonic colour*, *Phys. Lett. B* **645** (2007) 345–350, [hep-ph/0607047].

[262] J. D. Clarke, R. Foot, and R. R. Volkas, *Quark-lepton symmetric model at the LHC*, *Phys. Rev. D* **85** (2012) 074012, [arXiv:1112.3405].

[263] L. Okun, *THETA PARTICLES*, *Nucl. Phys. B* **173** (1980) 1–12.

[264] J. Kang and M. A. Luty, *Macroscopic Strings and 'Quirks' at Colliders*, *JHEP* **11** (2009) 065, [arXiv:0805.4642].

[265] P. Agrawal, J. Fan, B. Heidenreich, M. Reece, and M. Strassler, *Experimental Considerations Motivated by the Diphoton Excess at the LHC*, *JHEP* **06** (2016) 082, [arXiv:1512.05775].

[266] **ATLAS** Collaboration, G. Aad et al., *Observation of a new particle in the search for the Standard Model Higgs boson with the ATLAS detector at the LHC*, *Phys. Lett. B* **716** (2012) 1–29, [arXiv:1207.7214].

[267] **CMS** Collaboration, S. Chatrchyan et al., *Observation of a New Boson at a Mass of 125 GeV with the CMS Experiment at the LHC*, *Phys. Lett. B* **716** (2012) 30–61, [arXiv:1207.7235].

[268] C. Borschensky, M. Krämer, A. Kulesza, M. Mangano, S. Padhi, T. Plehn, and X. Portell, *Squark and gluino production cross sections in pp collisions at $\sqrt{s}$ = 13, 14, 33 and 100 TeV*, *Eur. Phys. J. C* **74** (2014), no. 12 3174, [arXiv:1407.5066].

[269] *Search for pair production of Higgs bosons in the $b\bar{b}b\bar{b}$ final state using proton-proton collisions at $\sqrt{s} = 13$ TeV with the ATLAS detector*, Tech. Rep. ATLAS-CONF-2016-017, CERN, Geneva, Mar, 2016.

[270] **CMS Collaboration** Collaboration, *Search for resonant pair production of Higgs bosons decaying to two bottom quark-antiquark pairs in proton-proton collisions at 13 TeV*, Tech. Rep. CMS-PAS-HIG-16-002, CERN, Geneva, 2016.

[271] R. Harlander and P. Kant, *Higgs production and decay: Analytic results at next-to-leading order QCD*, *JHEP* **12** (2005) 015, [hep-ph/0509189].

[272] R. Foot, H. Lew, and R. Volkas, *Models of extended Pati-Salam gauge symmetry*, *Phys. Rev. D* **44** (1991) 859. [Erratum: Phys.Rev.D 47, 1272 (1993)].

[273] **ATLAS** Collaboration, G. Aad et al., *Search for new phenomena in the dijet mass distribution using $p - p$ collision data at $\sqrt{s} = 8$ TeV with the ATLAS detector*, *Phys. Rev. D* **91** (2015), no. 5 052007, [arXiv:1407.1376].

[274] **CMS** Collaboration, V. Khachatryan et al., *Search for narrow resonances decaying to dijets in proton-proton collisions at $\sqrt{(s)} = 13$ TeV*, *Phys. Rev. Lett.* **116** (2016), no. 7 071801, [arXiv:1512.01224].

[275] J. E. Juknevich, D. Melnikov, and M. J. Strassler, *A Pure-Glue Hidden Valley I. States and Decays*, *JHEP* **07** (2009) 055, [arXiv:0903.0883].

[276] J. E. Juknevich, *Pure-glue hidden valleys through the Higgs portal*, *JHEP* **08** (2010) 121, [arXiv:0911.5616].

[277] **ATLAS** Collaboration, G. Aad et al., *Search for new phenomena with photon+jet events in proton-proton collisions at $\sqrt{s} = 13$ TeV with the ATLAS detector*, *JHEP* **03** (2016) 041, [arXiv:1512.05910].

[278] J. Ellis, *TikZ-Feynman: Feynman diagrams with TikZ*, *Comput. Phys. Commun.* **210** (2017) 103–123, [arXiv:1601.05437].